INVESTIGATION INTO THE PERFORMANCE OF A TWIN-SCREW COMPRESSOR FOR HELIUM COMPRESSION

By

Tasha L. Williams

A DISSERTATION

Submitted to
Michigan State University
in partial fulfillment of the requirements
for the degree of

Mechanical Engineering – Doctor of Philosophy

2022

ABSTRACT

INVESTIGATION INTO THE PERFORMANCE OF A TWIN-SCREW COMPRESSOR FOR HELIUM COMPRESSION

By

Tasha L. Williams

The screw compressor is a rotary positive displacement compressor, capable of compressing gas, vapors, and refrigerants. It is commonly used in various applications, including building and architecture, food, chemical process, pharmaceutical, metallurgical industries, refrigeration, air conditioning, vehicle superchargers and in cryogenic helium compression applications. The main characteristics that make the screw compressor attractive include high rotational speed, compactness, ability to maintain high efficiency over a wide range of operating conditions, long service life, and good reliability.

An oil-flooded twin screw compressor is selected for investigation in the present work due to its reliability, large capacity, and capability to handle helium's high heat of compression. Oil-flooded screw compressors refers to the oil being injected into the compression process and mixed with helium. The benefits of injected oil are cooling the helium, creating sealing between rotors, lubrication, and higher performance. In helium systems, the loss of power within the compression system is roughly two-thirds. With such a high loss in power, it is imperative to understand the need for investigating the design and thermodynamic parameters that impact the overall performance of these machines.

Initially, a review of different types of compressors is carried out to determine the best suited compressor for helium compression in this current work. A numerical model was created to simulate the compression process of the screw compressor. The model consists of three segments: rotor curve generation, thermodynamic analysis, and performance prediction. The geometric data are a necessary input for the thermodynamic analysis; however, the thermodynamic analysis segment can be used for any rotor geometry. The thermodynamic analysis outputs the thermodynamic parameters as a function of the male rotation angle of helium and oil. The performance prediction

determines characteristics of performance such as the volumetric and isothermal efficiencies. The model was validated using a commercial software, which was developed on the basis of extensive screw compressor data. The model predicted performance with reasonable accuracy varying at extreme case with a maximum of a 13% difference. Using the numerical model, the oil analysis in this thesis determined that the compressor performance is highly dependent on oil injection parameters. The isothermal efficiency spanned from 49.9% to 56.5% when adjusting the mass flow rate and oil injection position of the oil. Experimental results determined that the discharge temperature has the biggest impact on compressor performance.

ACKNOWLEDGEMENTS

I would like to thank Dr. Wei Liao, Dr. Norbert Mueller, and Dr. Peter Knudsen for agreeing to participate in my guidance committee and for their helpful suggestions and comments to improve this work. Specially, I want to express my sincere gratitude to my supervisor, Dr. Abraham Engeda, for his invaluable advice, continuous support, and patience during my Ph.D. study. I want to thank Matthew Cambio and the compressor team at Trane Technologies for the support and opportunities I was given to further my research.

I am thankful for the support and engaging conversations from the turbomachinery lab group, including Casey Palanca, Ahmed Helmy,and Mekuannint Mesfin. Last but not least, I want to thank my family, friends, and all those who have been apart of my support system. I could not have completed this dissertation without your continuous encouragement and support.

TABLE OF CONTENTS

LIST OF TABLES

LIST OF FIGURES

CHAPTER 1

INTRODUCTION AND RESEARCH OBJECTIVES

A gas compressor is a device used to increase pressure and provide thermodynamic availability to systems. As the pressure increases isothermally, the entropy decreases, which results in more availability. Thermodynamic availability is the maximum useful work which can be extracted from a system. Compressors are widely used in many different fields such as cryogenics, gas turbines, manufacturing, industrial refrigeration, and more. There are different types of gas compressors, available in a range of capacities.

This study focuses on twin screw compressors' in cryogenic refrigerator applications. Previous research has focused on screw compressors rotor design, mass flow rate of injected oil, built-in-volume ratio, tip speed of rotors, and many other factors. In large helium refrigeration systems, 1 W of cooling at 4.5 K demands 250 W of input power and 1 W of cooling at 2K demands at least 750 W of input power [1]. Smaller system losses can be much higher. A majority of the unit losses occur in the compression system, which indicates that there is ample opportunity for improvement. This study aims to evaluate key parameters such as helium-oil thermal equilibrium conditions and oil injection location in the compression process to understand the effect they have on the performance of the oil-flooded screw compressors used for helium refrigeration and liquefaction systems. The expected outcome of this research is an improved fundamental understanding of the key performance parameters for oil-flooded twin screw compressors: namely, the volumetric and isothermal efficiencies.

1.1 Classification of Gas Compressors

Gas compressors generally fall under two categories, positive displacement compressors and dynamic compressors with various types in each shown in Fig. 1.1. A positive displacement compressor is one that decreases the volume of the gas by moving a mechanical part. A dynamic compressor is one that imparts kinetic energy to the fluid, then converts it into potential energy,

thereby increasing the pressure. In this research study we will focus on the rotary screw compressor, which falls under the positive displacement type category.

While commercial rotary screw compressors are commonly used for compressed air, HVAC, and industrial refrigeration systems, in the context of this study, these compressors will be used for helium refrigeration systems. Before the 1980s, reciprocating compressors were generally used for helium refrigeration. However, since then, oil-flooded rotary screw compressors have mostly replaced reciprocating compressors. A brief comparison of reciprocating and screw compressors is discussed to understand the adoption of screw compressors in refrigeration applications.

1.1.1 Reciprocating Compressors

Reciprocating compressors are used in helium refrigeration to increase the pressure of the gas. The reciprocating compressor consist of a piston, cylinder, and valves. Gas enters the cylinder with the movement of the piston and inlet valve. Within the cylinder the gas is compressed. Once gas reaches a desired pressure, the compression process is finished. After compression, the gas is then discharged from the cylinder. When gas is discharged the process is repeated. While

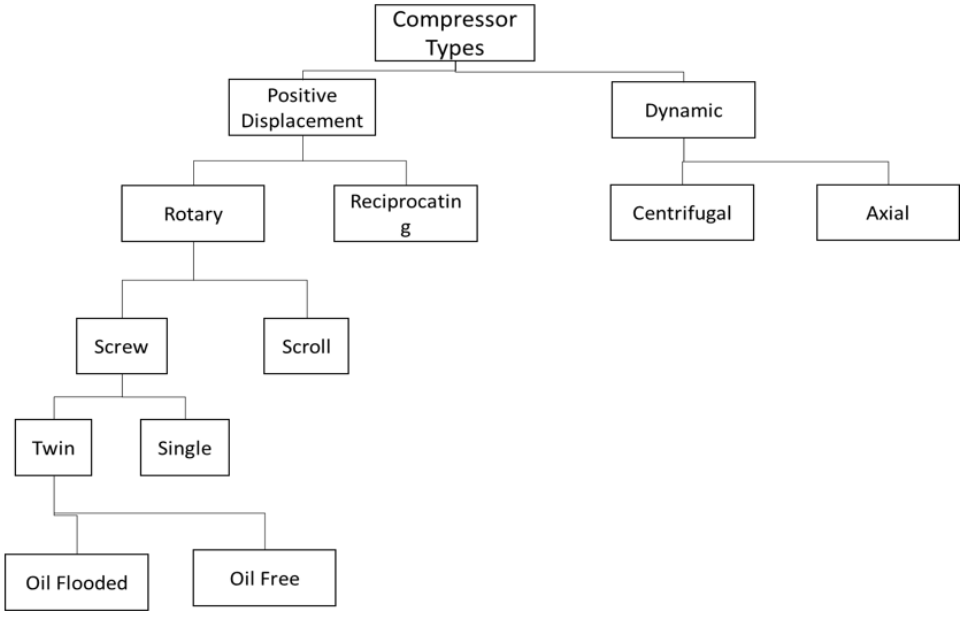

Figure 1.1: Gas Compressor Types

Table 1.1: Reciprocating and Rotary Screw Compressor Characteristics

Compressor Type	**Reciprocating**	**Twin Screw**
Volumetric Flow Rate	102-104 cfm	102-103 cfm
Compression ratio	1.5-7	2-15
Max Discharge Pressure	100 (trunk design)	26
Isentropic Efficiency	60-85%	50-80%
Volumetric Efficiency	60-95%	85-95%
Oil injection	Not possible	Yes
BVR	Varies	Fixed or varied
Use for Helium service	Yes	Yes

reciprocating compressors can have a higher efficiency than rotary screw compressors, they have a lower reliability due to seal wear and parts associated with inlet and discharge port actuation. Mean time before maintenance (MTBM) for this type of compressor is typically on the order of thousands of hours. Reciprocating compressors are better suited for lower flow applications requiring higher single stage pressure ratios [2]. While reciprocating compressors are used in industry, the rotary screw compressor has been adopted and is widely used today primarily due to its high reliability, low vibration, and reasonable efficiency.

1.1.2 Rotary Screw Compressors

The rotary screw compressor creates availability by reducing the entropy and producing high pressure helium through compression. Rotary screw compressors, as compared to reciprocating compressors have been found to be generally more robust and reliable than reciprocating compressors, being less sensitive to liquid phases mixed with the gas, solid contaminates, and requiring less maintenance. Since the 1980s, the rotary screw compressor has been adopted as a replacement for reciprocating compressors in many helium systems. Also a rotary screw compressor discharges the gas in a more continuous, less pulsating manner, due to the rotation of the rotors. Table 1 shows a comparison between the two compressor types.

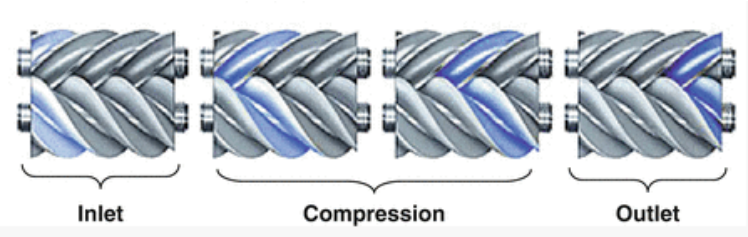

Figure 1.2: Imagery of how the fluid moves through compressor

1.2 Single and Twin Screw Compressor

There are two types of rotary screw compressors, namely, single screw compressors and twin screw compressors. The twin rotary screw, sometimes referred to as "twin screw" compressor, was invented in the 1930s by Alfred Lysholm followed by the single screw compressor in the early 1960s. The twin screw compressor is composed of a helical female and male rotor that are meshed together to create compression within the flute and lobe. The screw compressor undergoes three stages: suction, compression, and discharge. At suction, gas enters the lobes and fills the opening volume. Compression follows the suction stage; this is where the current chamber is no longer exposed to the inlet port and the male lobe reduces the volume in the female flute. This is conceptually similar to the piston cylinder reducing the volume in a reciprocating compressor except that the gas is translating as it is being compressed. Lastly, the compressed gas is discharged when the gas exits the compressor to the downstream piping. The compressor delivers a relatively even gas flow to the discharge because of the rotational motion.

1.2.1 Single Screw Compressor

The single screw compressor is composed of a main rotor and two gate rotors as seen in Fig.1.3. The main rotor is motor driven and the teeth of the gate rotors traps the gas within the flutes. There are lower bearing loads in the single screw compressor due to the balanced axial load on the main rotor. As with the twin screw compressor, the single screw compressor and the twin screw compressor alike can be oil free or oil flooded.

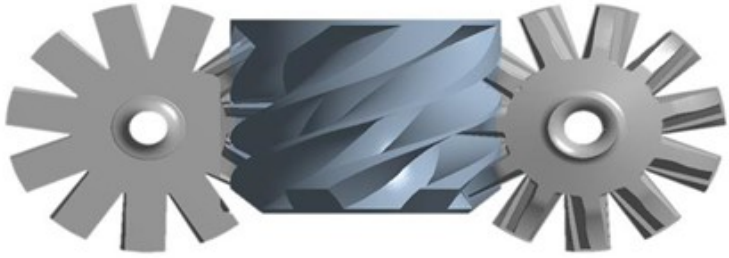

Figure 1.3: Single Screw Comp

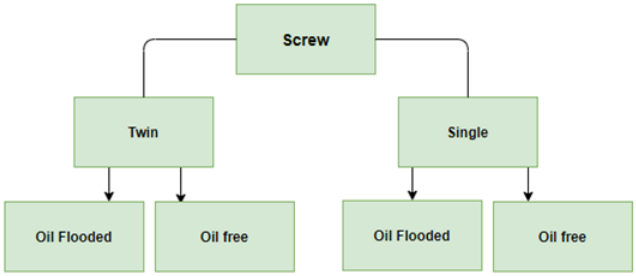

Figure 1.4: Screw Compressors Classifications

1.3 Oil Free and Oil Flooded Twin Screw Compressor

There are two different types of rotary screw compressors: oil-flooded (wet) and oil-free (dry). Each are used for different applications. Sealing, lubrication, and cooling are the three aspects common to these compressors, and they are handled differently in the design between oil-flooded and oil-free types. Proper sealing is required to achieve an efficient compression process by minimizing leakage of high pressure gas back to a lower pressure internally within the screw compressor. Lubrication is necessary for the bearings and prevents wear and excessive heating if the rotors are in contact. Cooling of the gas limits the discharge temperature, preventing seizure of rotating elements in close contact. Oil-flooded and oil-free screw compressor design address these aspects in different manners.

1.3.1 Oil Free Screw Compressors

Though referred to as oil free, this compressor uses oil in the gear box. In oil free screw compressors, oil is contained in an isolated compartment, which is separate from the compression chamber. The

following sections will outline the differing sealing, lubrication, and cooling designs between oil-free and oil-flooded screw compressors.

Sealing

In oil-free screw compressors, shaft seals are used for sealing.

Lubrication

In the design of dry screw compressors, female and male rotors are arranged not to touch. Timing gears are used to decrease contact while still achieving tight tolerances between rotors and casing, thereby eliminating the need for lubrication in the compression chamber. However, the bearings and gears must be lubricated.

Cooling

As mentioned previously, oil is utilized in the dry screw compressors for two purposes: lubrication and cooling of rotors. In order to cool rotors within this compressor, oil runs through a passage in the center of the rotors [3].

Oil free screw compressors compression gas process is completely free of oil and contamination within the compression chamber. This allows the compressor to handle any gas. Dry compressors are widely used in applications that are sensitive to contamination. They have uses in the following areas: food and beverage processing, the pharmaceutical industry, waste water treatment, and many more. While dry screw compressors are useful, these machine are limited in performance thermodynamically and mechanically due to the restricted pressure ratios and normal temperature ranges for selected materials. Typically, this machine discharge pressure can range from 50psig to 250psig and discharge temperatures up to 225°C. There is a fixed temperature ratio dictated by the pressure ratio and effective polytropic coefficient. The temperature limits the discharge pressure for a given suction pressure, suction temperature and polytropic coefficient. This relationship can be seen in Eq.1.1. In dry compressors, the discharge temperature is largely determined by the ratio of specific heats (Eq.1.2) for a given pressure ratio.

$$T_2/T_1 = (P_2/P_1)^{\varphi} \tag{1.1}$$

Figure 1.5: Oil Free Screw compressor

$$\varphi = C_p/C_v \tag{1.2}$$

$$\varphi = (k-1)/k \tag{1.3}$$

1.3.2 Oil Flooded Screw Compressors

In oil flooded (wet) screw compressors oil is injected into the compression chamber, which provides cooling, sealing, and lubrication during the compression process. In contrast to the dry screw compressor, wet screw compressors are not sensitive to contaminants. In wet screw compressors, cooling, sealing, and lubrication is accomplished within the compression chamber due to the presence of oil, which eliminates the need for rotor cooling passages, shaft seals, and timing gears. In oil flooded twin screw compressors the male rotor drives the female rotor. Due to the injection of oil, a mixture of oil and gas exist at the discharge of the compressor. The oil and gas mixture is discharged to a bulk oil separator, which is used to separate oil from the pressurized gas after the mixture leaves the compressor.

In wet screw compressors, higher pressure ratios are available due to the capability of oil to adsorb a large portion of the heat of compression from the gas. Also, oil occupies a relatively small

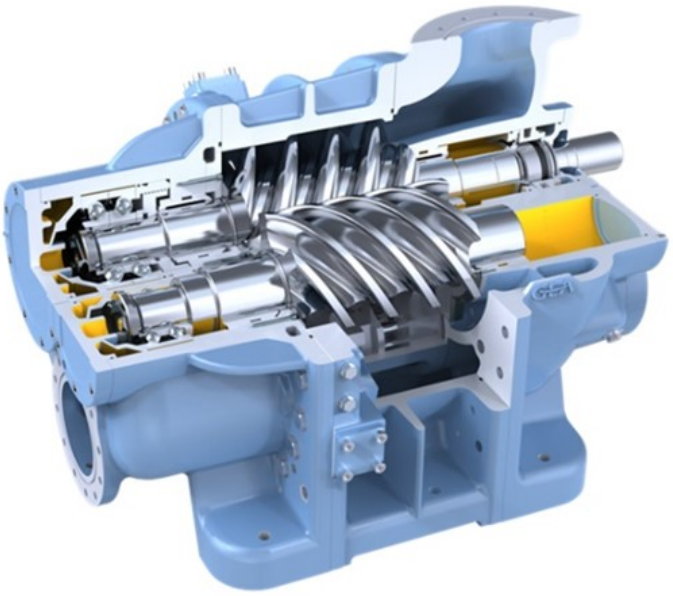

Figure 1.6: Oil Flooded Screw compressor

portion of the compression volume; and as a non-condensible liquid, it can be readily separated from the gas using conventional means.

Oil flooded screw compressors can also attain high pressure ratios in a single stage, which isn't possible in dry screw compressors [3]. The reduction of the heat of compression allows the discharge pressure (or pressure ratio) to be increased. As such, wet screw compressors tend to be more robust and reliable.

1.4 Pressure Ratio and Built-in Volume Ratio

The screw compressor performance in this study will be defined using the isentropic and volumetric efficiency. Isentropic efficiency is defined as the ratio of the power required if the gas undergoes a reversible isothermal compression to the actual shaft power required by the compressor [3]. The volumetric efficiency is defined as the ratio of the actual delivered mass flow rate of gas to the theoretical mass flow achievable at the suction condition and the volumetric displacement rate of the compressor [3]. There are many parameters that affect the performance of a screw compressor: e.g., working fluid, pressure ratio, built-in volume ratio (BVR), suction pressure, rotational speed, oil injection amount and location, and rotor geometry. The pressure

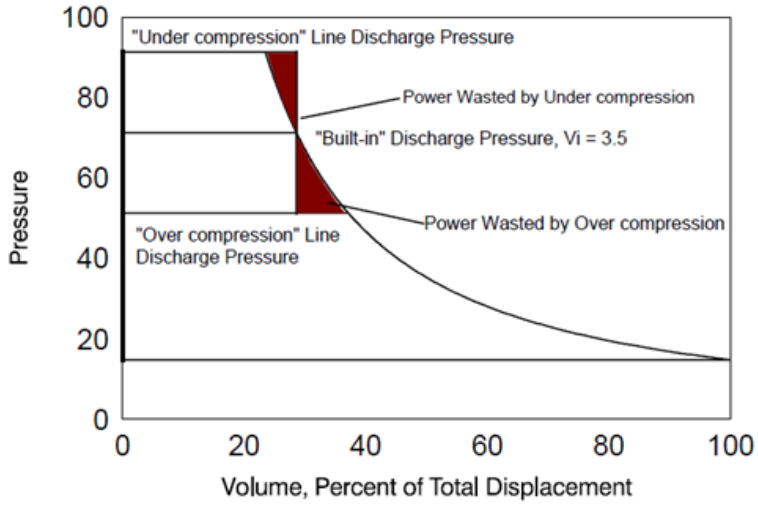

Figure 1.7: Over-Under Compression PV graph

ratio, $\frac{P_2}{P_1}$, is typically defined as the discharge pressure P_2 divided by the suction pressure,P_1, so that it is never less than unity. As the pressure ratio increases above an optimum, the performance decreases. The suction pressure is limited by mechanical loading (deflection) on the rotors and the installed motor size. The higher the pressure difference the higher the potential for the needed oil flow and greater work of compression [4]. The built-in volume ratio (BVR) $\frac{V_1}{V_2}$ is the ratio of the volume at suction V_1 divided by the volume just prior to the opening of the discharge V_2.

The internal pressure ratio is related to the BVR according to, $\frac{P_2}{P_1} = \frac{(}{V_1}V_2)^k$, where, k is the effective polytropic exponent. The internal pressure ratio for a given BVR determines whether the internal pressure at just prior to discharging is less than, equal to, or greater than the pressure in the discharge piping. These three conditions are referred to as when the internal compression process is under-compressed, matched, or over-compressed, respectively. The thermodynamic optimum is for the internal compression ratio to equal the overall pressure ratio. If the discharge pressure is higher than the needed downstream operational discharge pressure, then over-compression losses occur Fig. 1.7. If the discharge pressure is lower than operational discharge, then under-compression losses occur Fig. 1.7.

The losses are seen on the pressure-volume (p-V) diagram on the compression process. For most applications the operating process conditions will change over time. If the compressor design

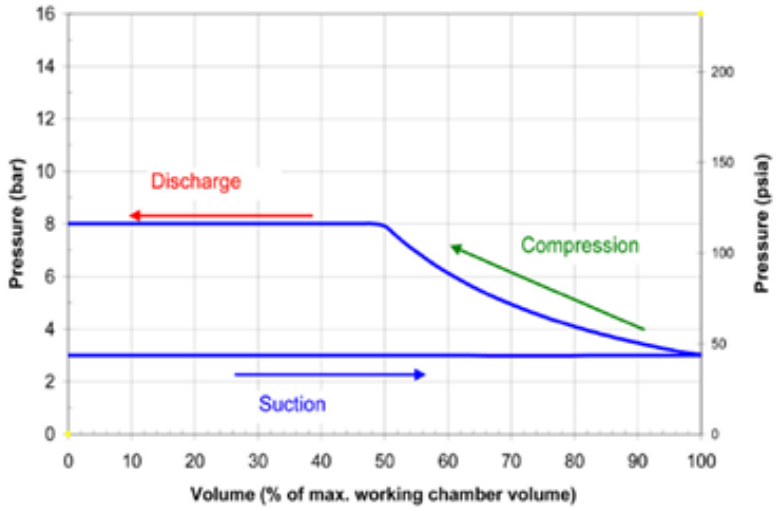

Figure 1.8: Ideal pressure - volume diagram for a screw compressor with well suited BVR

allows for adjustment of the BVR, then in principle, the compression process can be matched and p-v losses minimized. As such, the ideal efficiency can be achieved by adjusting the BVR. If the BVR cannot be adjusted while the compressor is operating, under-compression is typically chosen to avoid over-compression to ensure mechanical damage is not incurred. For a fixed BVR, to account for the change in operation conditions, a BVR that does not result in over-compression is chosen for a wide range of operating conditions [5]. The BVR can be changed by moving or changing the size of the radial or axial discharge port. There are several types of mechanisms that can be used within the screw compressor to vary capacity or built-in volume ratio, namely, slide valve/slide stop, round slide valve, plug valves, and variable frequency drive.

1.5 Twin Screw Compressor and Application Areas

The screw compressor was invented in 1935 by a Swedish engineer Alf Lysholm-Holman at The Ljumgstrom Steam Company, now named Scenska Rotor Maskiner (SRM). SRM tested many male female rotor combinations and profiles; eventually, a symmetric circular profile with four male lobes and six female flutes (4+6) rotor combination was selected. Rotor combinations are described using male rotor lobe number plus female rotor flute number notation e.g. 3+6 would indicate 3 male lobes and 6 female flutes. Over time advancements in rotor design and oil-injection took

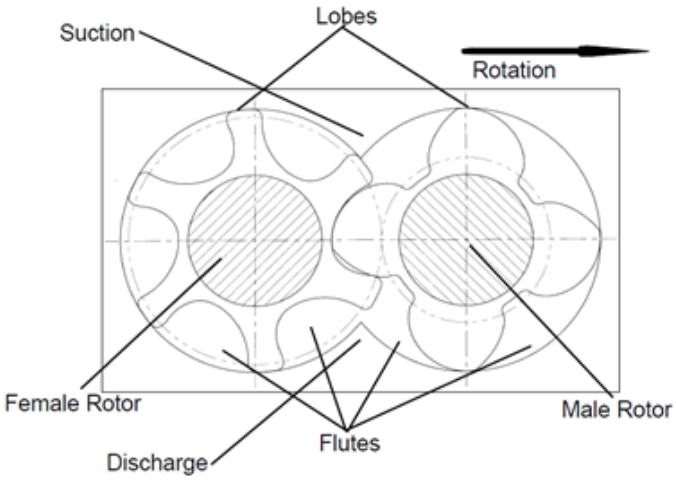

Figure 1.9: Common rotor terminology [Rotary Screw Compression Process]

place with advancements in manufacturing. Modern milling machines allowed for the rotors to be produced with the required tolerances in a repeatable manner, thereby reducing the manufacturing cost. Extensive research has been done on the design on the rotors' profiles, resulting in higher efficiency but increasing their manufacturing complexity. Very small tolerances and clearances are achievable today e.g., 3 µm and 12 µm, respectfully [6].

The oil free and oil flooded rotary screw compressor can be found in applications involving process refrigeration, cryogenics, process gas, gas boosters, vapor recovery systems, hydrogen service, building systems, pharmaceutical, metallurgical, and natural gas. The oil-flooded screw compressor is particularly well suited to several of these uses because it is capable of a high suction pressure (up to 450 psig), high pressure ratio (up to 20), variety of gas options, higher discharge temperature, and has wide operating ranges. An oil-free compressor is well suited for constant volume flow at low pressure ratios. In this study the oil-injected rotary screw compressor is evaluated as it is used in Helium refrigeration (cryogenics).

Screw compressors have become widely used in various applications in the last few decades. They have relatively high volume gas flow with high reliability and reasonable efficiency. They have superior performance when compressing fluids at power inputs in the range of 10 kW – 1.5 MW. For lower compressor input power, reciprocating or other positive displacement compressors are selected and at higher power inputs centrifugal or axial compressors are selected. The rapid

expansion of screw compressors in various industries over the past four decades is due to their relatively high rotational speeds compared to other types of positive displacement machines which make them compact, their ability to maintain high efficiencies over a wide range of operating pressures and flow rates and their long service life and high reliability.

1.6 Objectives of the Dissertation

In this work, the oil-flooded twin screw compressor configurations with Helium as the working fluid will be studied under ambient conditions. No attempt will be made to design a new compressor. The goals of this work will be accomplished systematically by the following tasks:

1. Review literature of previous similar and related works.
2. Review and develop the theoretical bases and governing equations of the screw compressor.
3. Review and develop all aerodynamic and mechanical losses of the screw compressor.
4. Develop a 1-D performance prediction code
5. Experimental investigation of a screw compressor.
6. Calibration of Numerical Tool.
7. Develop and propose changes to improve volumetric and isothermal efficiency

In any compressor applications, it is often essential that a designer, developer, or user has a good knowledge of the compressor performance prediction, the effect of different types of rotor profiles, and other compressor geometry on performance. Since the compressor experiences a broad range of design and operating conditions, a designer, developer, or user must acquire the skills to deal with these challenges. This work develops and presents a performance prediction numerical code and thermodynamic paramters impacts on isothermal and volumetric efficiency. The specific details of the above tasks will consist of:

- Using Helium as a working fluid under ambient conditions to develop a code for predicting the performance of oil-flooded twin screw compressors in the power rating range. The code will account for a few important loss and leakages.
- The code will be based on theory with semi-empirical models for the heat transfer and leakage models
- The code after being verified can be used to determine the performance of any given profile with supplied geometrical curves using helium as the working fluid.

The research of the screw compressor can involve many factors. The goal of this research study is to understand key thermodynamic parameters that affect the isothermal and volumetric efficiencies of oil-flooded screw compressors. A better understanding of the degree to which the helium and oil are in equilibrium is investigated, as well as questions, how long does it take to reach equilibrium, and how does it affect the isothermal efficiency? Expected outcomes of this study are increased knowledge regarding the volumetric and isothermal efficiency for oil-flooded screw compressors, particularly those using helium.

1.7 Outline of Thesis

This dissertation is comprised of eight chapters. The first chapter introduces the screw compressor and research objectives. Chapter two provides a background to rotary screw compressors in order to gain insight on the gaps with helium refrigeration and understand how several thermodynamic parameters impact the performance of compressors within other applications. Chapter three discusses the screw compressor rotor profile generation, important geometric characteristics, and a 1-D mathematical model. Methods used to determine rotor profile and geometry curves are outlined in these chapters and are used as required inputs within the numerical model. Additionally, the 1-D model uses conservation laws, heat transfer model, limited leakage model, and thermodynamic relations to model the entire compression process from suction to discharge. The numerical model is presented in chapter four. The layout, input, outputs, and functions of the

numerical model are described here. The numerical model uses the mathematical model outlined in chapter three. Chapter six describes the experimental setup, equipment used, and test matrix. Chapter seven discusses the experimental results and ways to improve performance. Lastly, chapter 8 provides the conclusions of this study and presents future work.

CHAPTER 2

LITERATURE REVIEW OF SCREW COMPRESSORS AND HELIUM COMPRESSION

In the 1930s Alfred Lysholm developed the first screw compressor [7]. The screw compressor was applied to industrial applications by the late 1950s. The screw compressor was developed using the concept of gear theory [8, 9]. The invention of the screw compressor provided a decrease in size and cost of compressors. Oil -looded twin screw compressors allowed for a wide range of operating conditions permitting pressure ratios up to 15, nominal pressure difference, up to 15 bar, and max. pressure difference, 40 bar. While much research has been done on screw compressors since the 1930s, scientific knowledge is limited. Scientific knowledge of screw compressors used in helium applications is even more limited. Very little literature is available in this field. Most of the information we have regarding operation of screw compressors utilizes air or a typical refrigerant for the working fluid. Notably, compressors using air or refrigerant have variability in results; however, the general idea of parameters should be the same. In this chapter, several parameters that have an effect on performance will be discussed from published literature.

- Screw compressor design
- Geometric design and characteristics
- Design optimization
- Computational models
- Pressure ratio and build-in volume
- Compressor speed
- Oil injection
- Gas and oil heat transfer
- Leakages

Table 2.1: Literature Review

Author	Topic	Results
Ganni [10]	Pressure Ratio (PR) and Built-in volume ratio (BVR)	For given PR, there is a BVR that produces an optimum performance
Seshaiah [11]	Pressure Ratio	Testing determined that increase in PR reduces the volumetric efficiency and increases the adiabatic efficiency
Kishi [12]	Compressor speed and oil mass flow rate	• Volumetric efficiency increases as RPM increases • Heat transfer between oil and gas increases as the amount of oil increases
Wu [13]	Oil injection location	The isentropic efficiency is negatively impacted when injecting oil into discharge end bearing
He [14]	Compressor speed and oil mass flow rate	• Discharge temperature, volumetric efficiency, and adiabatic efficiency increases as speed increases • Volumetric and adiabatic efficiency increases as oil mass flow rate increase
Stosic [15]	Oil injection mass ratio, oil droplet diameter, oil viscosity, oil temperature, and oil injection position	• Oil temperature has a strong impact on the discharge temperatures • As the oil inlet port angle increases the isothermal an volumetric efficiency decreases
Hammerl [16]	Nozzle design, oil injection location, and droplet size	Flat spray requires more energy to operate and reduces volumetric efficiency
Fleming [17]	Leakages	• The contact line, rotor tip sealing line, and compression start blow hole has the largest impact on the volumetric efficiency • The rotor tip sealing line, contact line, blow, and discharge end face leakage paths has largest impact on isentropic efficiency

2.1 Screw compressor design

This section examines screw compressor design. Screw compressor design has been practiced for many years and incorporates profile generation and geometric characteristic design. The basis of rotor profile generation originated from helical gears. Over the years, design of screw compressors have been optimized to produce better performing systems.

Profile Generation

Stosic [18] presented a technique that generates the secondary arc curves numerically using given primary arcs curves. This is commonly referred to as the envelope method. Using the method, the given profile can be either the male or the female. Additionally, the rack generation method is presented and can be used to produce the primary profile curves. Very little information regarding profile generation existed in English prior to this paper before this time. This provided a way to design a large number of profiles quickly. The meshing line is typically an output after a rotor profile is generated. Zaytsev [19, 20] reversed this process by using the meshing line to define the rotor profile analytically. This method formed a rotor profile successfully when several design conditions are met. Using this process, the contact line length and blow hole area can be optimized.

Geometric characteristic design

Geometric characteristics of rotor profiles are important in determining screw compressor performance. Each geometric curve has a different impact on the overall performance. The geometric characteristics are defined using area curves.Methods to determine these values are discussed. The calculation geometric characteristics such as: volume curves, sealing line length, flute area, and blow hole area are defined analytically by Zhang and Hamilton [21]. These characteristics are evaluated based on a provided rotor profile. Singh and Bowman [22] observed the influence of rotor profile, number of lobes, rotor length to diameter ratio, wrap angle, discharge port size, and tip speed on the screw compressor performance. A computer program was used to determine the compressor performance when adjusting various parameters. It was determined that opening the discharge port earlier (decreasing built-in pressure ratio) could lead to improved performance. This performance boost is dependent on the operating conditions and rotor profile. Sjoholm paper

reviews various parameters that impact the screw compressor.

Design optimization

As screw compressor design knowledge knowledge expands, the design is optimized. Manufacturing advancements allowed for better rotor production as well. Tang [23] published a paper that studies the contact line length and blow hole area of different rotor profiles on performance. Both design characteristics change with rotor profile changes. In this paper, the blow hole was optimized by changing the shapes of the curved sides of the curvilinear triangle. The compressor volumetric and indicated efficiencies increased as a result of the smaller blow hole area. Stosic [24] uses a computer package to determine the best compressor for various conditions. You [25] studied the different geometrical characteristics of rotors to understand their impact on compressor efficiencies, rotor deflection of female, bearing loads, and contact forces of rotors to determine the optimum profile. This studied showed that the best profile is dependent on the application and operating conditions.

2.2 Computational models

A model is a a representation of a physical process and is (usually) comprised of mathematical relationships to describe the physics using fundamental principles (e.g., conservation of energy) and/or empirically derived relationships. It is often implemented into a programming language to obtain numerical results (although this is not a prerequisite for the model itself). Several authors have produced rotor profile generation and performance prediction models. Singh and Patel [26,27] presented a computer program that has the capability to generate several rotor profiles quickly, determine geometric curves, and predict compressor performance. The profile shape can consist of any known profile segment type such as circular arc, straight line, polynomial curve fit, and data fit curves. Intersection and tangent points are determined within the program for each curve and the total profile is created. Additionally, the program produces cavity area curve, volume curve, blow hole area, seal-line length, and discharge port area. The curves produced were used to predict the performance. The performance was within good agreement with test data. From

this model, the impact of various capacity and power losses is shown. Fujiwara [28, 29] created a computer model that predicted the performance of the oil injected screw compressor numerically. Perfect gas laws were adopted and effects of internal leakage, heat exchange between oil and gas, and suction and discharge port flow resistances are incorporated within the model. Various geometric parameters such as; blow hole area, interlobe clearance, and wrap angle, were adjusted to observe performance effects. As interlobe clearance and blow hole areas were increased, the performance decreased. The wrap angle experienced very little variation for volumetric efficiency however the adiabatic efficiency slightly increased as the wrap angle increased. A numerical computer program was created to develop rotor profiles and accessory geometric plots by Zhou [30]. Xing [31] designed a software package called SCCAD that includes rotor profile generation, geometrical data thermodynamic model, rotor forces, deflection of rotors, and cutter shape. An analytical thermodynamic model for screw compressors was presented by Sauls [32, 33] to fain more insight on the leakage. A clearance analysis derived from drawing data was used to determine cold and hot clearances. Performance predictions are more accurate as a result of clearance analysis.

2.3 Pressure ratio and build-in volume

The pressure ratio is the discharge pressure divided by the suction pressure. The build in volume ratio (BVR) is the maximum volume divided by the volume just before the discharge port opens. These two parameters have a relationship that directly impacts the performance as mentioned in the previous chapter. Research that supports this claim is discussed in this section. Ganni et.al [10] reported the findings of The Spallation Neutron Source (SNS) compressor testing in their presentation. The testing was done using 1st and 2nd stage compressors varying both BVR and pressure ratio to understand the effects on efficiency. SNS' tests showed that there is a BVR that optimizes the efficiency for a given operating system pressure ratio and given stage machine (i.e., 1st or 2nd) that results in an optimum efficiency. Also, it confirms the result from the SSCL compressor performance testing that there is a pressure ratio that optimizes the efficiency for a given BVR and a given stage. This research provides a guideline that helps determine the BVR

needed by knowing the operating conditions of the system. Seshaiah [11] evaluated theoretically and experimentally the performance over a span of pressure ratios. The compressor testing was accomplished using Argon, Nitrogen, Air, and Helium. Theoretical and experimental results were within reasonable agreement. Both showed a decrease in volumetric efficiency as the pressure ratio increased. Adversely, the adiabatic efficiency and specific power increases as the pressure ratio increases. The outcomes were attributed to the changes in leakage and mass flow rate.

2.4 Compressor speed

Compressor speed is defined by the revolutions per minute (RPM) of the motor. Typically screw compressors are often coupled directly to a motor and therefore run at a single speed. With the use of a drive screw compressors can be run with various speeds. The former approach is simpler and more practical than using a drive gear reduction to operate at higher speeds. For the same size screws, in general, the increase in the RPM decreases the amount of leakage within the compression cycle because the leakage time is reduced. The advantages of adjusting the speed is often associated with the compressor capacity however, the screw compressor performance is affected as well.

Stosic [34] reviewed three different capacity control methods: shaft speed, slide valve, and suction throttling. This was modeled using an air and refrigeration compressor. The flow, power, and specific power are the observed performance parameters. When ranging the speed from 2000 to 6000 rpm the flow power increased dramatically for the air compressor. Kishi et.al [12] completed a study to understand the RPM influence has on the performance through theoretical analysis and experimentation. Overall, the RPM was increased from 3000 to 4500 and the volumetric efficiency increased from roughly 83% to 86%. The max tip speed is limited by discharge port losses and the lowest tip speed is restricted by internal leakage [35]. The influence of compressor speed measured experimentally by He [14]. In this study the speed ranged from 1000 to 3000 rpm. As speed increased; the discharge temperature, volumetric efficiency, and adiabatic efficiency increased.

2.5 Oil injection

Within a screw compressor, oil has several purposes: lubricating rotating parts like bearings and seals, absorbing the heat of compression, decreasing vibrations, and sealing [36]. Typically 30% is required for the lubrication of the bearings while the other 70% is used for cooling the gas in helium screw compressors. Numerous researchers have conducted studies on screw compressors to better understand the effect oil injection has on the compressor. Such scholarship has explored the impact that oil injection method, temperature, nozzle shape, and mass flow rate, and oil injection position has on the performance of screw compressors. This previous research provides insight and direction for ways to increase the efficiency of the compressor. The influence of compressor oil injection flow rate was measured experimentally by He [14]. In this study the oil mass flow rate ranged from 27-87 L/min. As oil mass flow rate increased, the volumetric and adiabatic efficiencies increased up to a point and then had roughly constant values. However, the discharge temperature decreased and the rate of change reduced as the oil mass flow rates reached higher amounts. An experiment was conducted by Peng [37] to understand oil distribution within the working chamber using a PIV system. In the working chamber, an oil film was always present on the rotor surface, droplets were floating around, and large amounts of foamed oil is formed.

Stosic [15, 38, 39] developed a mathematical model and conducted an experiment to better understand the effects that the oil injection mass ratio ($\frac{m_o}{m_g}$) , oil droplet diameter, oil viscosity, oil temperature, and oil injection position has on the performance of the screw compressor. The mass ratio varied from 0 to 8, the oil droplet diameters used was 0, 100, 500, and 1000µm, the oil viscosity ranged from 1 to 5, oil injection temperature varied from 293 to 373, and the oil inlet position went from 0 to 270. From the mathematical simulation results several observations were made [38, 39] :

- For droplet sizes up to 100 micrometers oil and gas temperatures are the same. For larger droplets (0.5mm), the oil and gas temperature difference is small (less than 30°C).
- Oil temperature has a strong impact on the temperature of the gas exiting

- Lower oil-to-gas mass ratios affect the compressor process more than a higher ratio which leads to possibility of optimization for the oil to gas ratio and oil temperatures.
- Varying the oil types slightly affect gas discharge temperature while considerably affected the power and volumetric efficiencies
- As the oil inlet port angle increases the isothermal and volumetric efficiency decreases
- Compressor oil outlet temperatures are influenced by the oil mass flowrate and an optimum was found
- The results showed that reducing the oil mass ratio reduces the power consumption.

Due to different size droplet sizes within the screw compressor and uncertainty of the droplet motion within the chamber, oil and gas temperatures cannot be assumed to be the same. These differences effect the heat transfer conditions. An experiment was conducted in order to verify the results obtained from the mathematical model using a Trudbenik screw compressor. A standard and modified compressor was used. The oil injection mass flow ratio and nozzle were adjusted on the modified compressor. This was done to create better oil atomization, decrease the oil injection mass flow rate, and overall increase air to oil heat transfer. Atomization is converting a substance into very fine particles or droplets. Oil atomization is an important parameter in increasing the heat transfer. As the heat transfer increases, the compressor performance increases. From the experimental and computer simulation, the position and orientation of the nozzle resulted in a better isothermal efficiency and lower delivery efficiency.

Hammerl et.al [16] studied the influence that nozzle design, injection location, and droplet size has on compressor performance. The experiment attempted to increase the efficiency of a screw compressor by using oil atomization. Flat spray and hollow cone shaped nozzles were used in this experiment. Injection of the oil was positioned at the suction port to increase the time the oil and air are in contact to get a better homogenous distribution of the oil. Atomization is tested using low system pressure and high pressure generated from a hydraulic pump. Mathematically, it is

understood that the droplet diameter size has a direct effect on heat transfer between the oil and air. The smaller the oil diameter of a droplet, the bigger the surface area of the oil droplet.

The experiment yielded no improvements in efficiency and actually had a negative impact on the performance of the screw compressor, using both low and high pressures for atomization. While, there is a longer contact time (from injection location), the oil being injected at the suction port caused hydraulic losses from churn losses. Additionally, the flat spray nozzle requires more energy to operate and reduces the volumetric efficiency. Wu et.al conducted an experimental study to analyze how injecting oil at different locations could have an impact on the performance of the screw compressor. Along with Hammerl, Wu et.al research shows that injecting oil into the suction port of the compressor results negatively [13]. Additionally, it was seen that injecting oil into the discharge end bearing also negatively impacts the isentropic efficiency due to the high temperature heating up working fluid and the volumetric efficiency marginally increases due to positive effects the oil has on sealing leakage paths. When oil enters rotor cavity versus the suction, the negative effect reduces. Furthermore, when temperature of oil injected is reduced the performance is increased. In order to achieve a cooler temperature of oil, an oil-cooler is needed. Lower oil temperature does not really change the volumetric efficiency but reduces the power consumption of the compressor and overall increases the total efficiency at certain conditions.

The effect of oil mass ratio (mh/mo) on efficiency was explored experimentally by Kishi [12]. The helium to oil mass ratio was varied by increasing the amount of oil injected. However, it is known that large amounts of oil injected into the compressor can result in increased compression power and bearing failure which limits the amount the oil can be increased. The study used low and high stage machines with 4.4 and 3.8 pressure ratios respectfully and a low density lubricating oil. The mass flow ratio used was 0.03-0.04, overall the oil quantity was increased almost two times the normal amount. The study determined that increasing the amount of oil used increases the volumetric efficiency. The oil mass flow rate can also be seen to have a direct influence on the performance. As the oil mass flow rate increases the volumetric and adiabatic efficiency also increases [39]. It has also been observed that the volumetric flow rate decreases with the increase in

pressure ratio and oil temperature [10]. This is due to oil viscosity decreasing at higher temperatures and pressure increase which leads to higher leakage.

In addition to above research mentioned, Fujiwara and Osada [40] created a mathematical model using heat transfer and flow coefficients attained from experimental data. De Paepe et.al [41] explored the effect of oil atomization on an oil injected screw compressor using several atomizers ranging in size. It was found from this study that using atomization increases the effectiveness of heat transfer however there was not much improvement in performance. Also, he determined that oil coming from the bearing has a negative influence on the performance and lowering oil temperature has a stronger influence on performance, confirming Stosic [39] observations. Various research shows that the performance of the compressor has a strong dependence on the oil injection conditions specifically temperature, injection method, location, and oil velocity.

2.6 Gas and oil heat transfer

As mentioned in the previous section, the oil conditions has a large influence on the compressor performance. The heat transfer between the gas and oil is directly related to oil conditions. According to Ganni [10] , understanding the heat transfer between oil and gas is key to maximizing the efficiency of the compressor. Heat transfer models are presented with most scholars using the same heat transfer relationship with minor variations. Singh and Bowman [22] presented a heat transfer model that determines the hat transfer coefficient implying various assumptions. Droplet trajectories are calculated with particle flight time ending when the oil particle comes in contact solid rotor boundaries. The model assumes droplets are injected radially with uniform spacing.

2.7 Leakages

Within the screw compressor internal leakages are a source of capacity loss and inefficiency. Leakages can be described as compressed high-pressure fluid flowing back into low pressure regions. Leakages are inherently present due to geometric clearances that must exist [20] and design flaws. Clearances are necessary to account for manufacturing limitations, tolerance build

up, and displacement caused by load pressures and temperatures [42]. Leakages greatly affect both the volumetric and isentropic efficiencies by reducing the mass flow rate delivered [24] without a commensurate reduction in input power. In an effort to make screw compressors more efficient, it is imperative that the location and particular cause of leakage paths are identified. Each leakage paths varies with the rotational angle. Understanding the causes of particular leakage paths can lead to the minimization of leaks and increase overall efficiency in the design of clearances. In their work on leakages, Fleming et.al [43] identified six leakage paths

- Contact Line: when the gas flows back to suction from the cavity through the contact line.

  The contact line leakage path is one of the most important leakage path due to the largest influence on the volumetric efficiency. Depending on the size of the wrap angle, the cavity can leak from high pressure to current cavity at beginning of compression, from current cavity to low pressure cavity at the end of compression process. The contact line length area can be found at any time by multiplying the contact line length by the average clearance between rotors.

- Rotor Tip: when the fluid goes from the leading cavity or discharge to the trailing cavity.

  This is the leakage between female and male rotor tips and the housing bore.

- Rotor Blow Hole: is a small triangular leakage found at the junction of male and female rotor tips and housing cusp.

  The high pressure side of female and male rotor tips has a greater influence on the performance due to the leak being present during the entire compression process. The high pressure side can be referred to as just blow hole and is when leakage path is exposed to the discharge pressure of the compressor [44]. The blow hole has a huge impact on the overall performance and was reduced by 90% by the development of the “A” profile versus the original semi-circle profile [45] as compared to the original SRM profile .

- Compression Start Blow Hole: The compression start blow hole leakage is characterized by fluid leaking into trailing suction cavity from the cavity where compression has just begun. The compression start blow hole is a triangle formed on the low pressure side of the male and female rotor tips. The blow hole or "leakage triangle" is created between the female tips, male tips, and housing cusp. This leaks allows for leakage between nearby threads. The blow hole consist of low pressure and high pressure sides. The low pressure side leakage triangle or blow hole can be referred to as the compression start blow hole. Leakage occurs when gas located in leading high pressure cavity leaks back to suction at the beginning of compression. The compression start blow hole leakage is present for a small range however it can reduce the volumetric efficiency by roughly one percent [44].

- Discharge End Face: The discharge end face leakage is where the fluid leaks from discharge back to suction.

  - Leakage from leading cavity to trailing cavity.
  - Leakage from discharge chamber to chamber during beginning of compression process.
  - Leakage from discharge to suction

  Out of the three leakages mentioned above, not all of them exist for the entire compression and discharge process. The three leakages are all collected together into the total discharge end face leakage.

- Suction End Face: Clearance between the end plate and the rotor end face at the discharge end [44]

  The compressed gas can leak back to suction at the start of the compression process across the suction rotor end face. The suction clearance is biggest clearance within the screw compressor and is designed to compensate for axial thermal expansion of the rotors.

According to Fleming [43] research each leakage path has a different effect on the volumetric and isentropic efficiencies because of variance in mass flow rates delivered. Aside from the rotor blow

hole leakage, all other leakage paths are affected by the load due to pressure induced mechanical loading on the rotor, housing, and bearings.

Fleming et.al [17] did a study on leakage within the screw compressor and developed a mathematical model of the compressor thermo-fluid process. The model was verified using measured data. Fleming thermodynamic modeled was used to determine how each leakage path effects the volumetric efficiency and isentropic indicated efficiencies. From this information, the compression start blow hole was found to have the smallest leakage while also having the largest flow area. This is because this area only last for 30-40°of the male rotation at the start of compression when the pressure difference is low. Using the model, the net flowrates were determined for each leakage path by setting each leakage to zero and comparing to model results with normal leakages. This approach is used to determine the change in efficiency between ideal and real conditions. The contact line, rotor tip sealing lines, and compression start blow hole had the largest impact on the volumetric efficiency. On the other hand, the rotor tip sealing lines, contact line, blow hole, and discharge end face leakages paths had the biggest impact on the isentropic efficiency. With the compression start blow hole and suction end face barely affecting the isentropic efficiency. These finding can be found in Fig.2.2. The suction end face exist only at the beginning of compression when pressures are very low resulting in a lower effect on the isentropic efficiency. The suction end face affects the volumetric efficiency more because of the larger clearance at suction. While the suction at clearance is relatively large the discharge clearance is much smaller and does not affect the volumetric efficiency much. It was also found that the pressure ratio has the biggest impact on the contact line because the maximum pressure difference is found at this path. With increased speed the leakage rates are decreased increasing both volumetric and isentropic efficiencies.

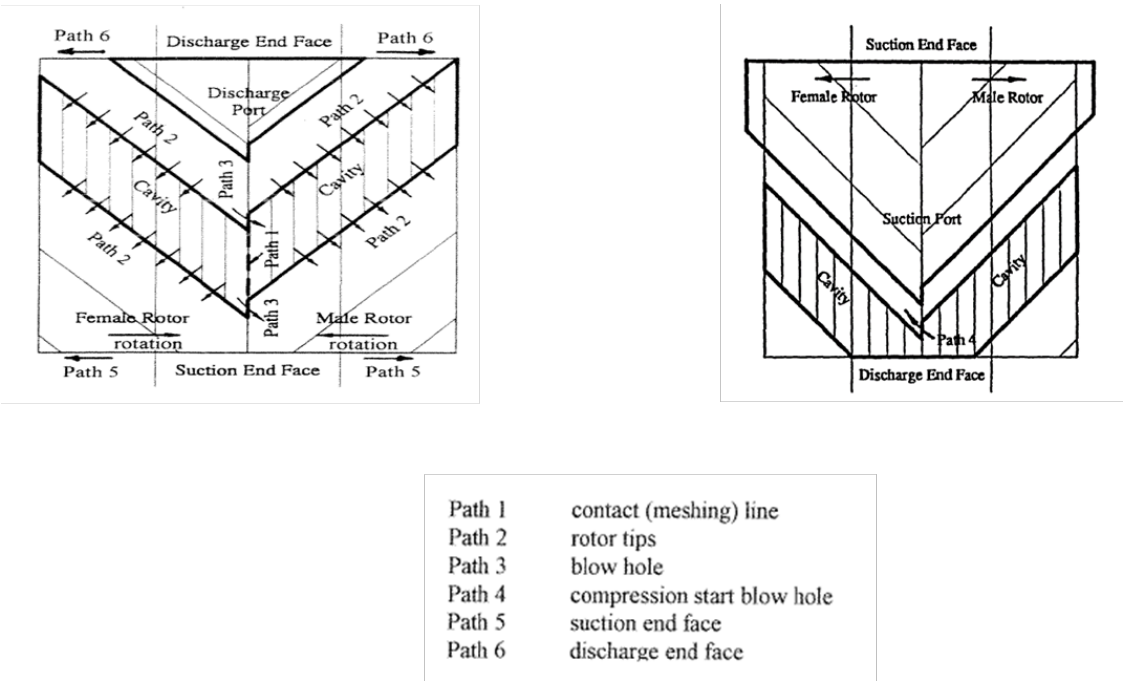

Figure 2.1: Leakage paths identified by Fleming [42]

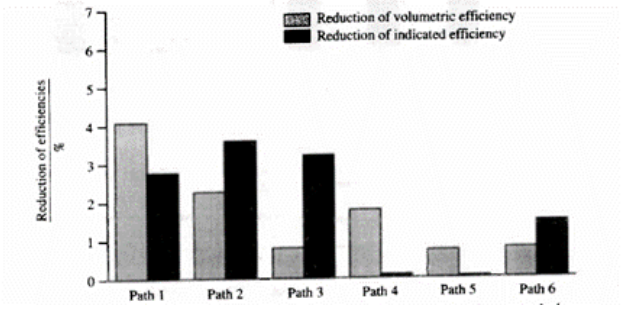

Figure 2.2: Reduced efficiencies - leakage compared with zero leakage path by path (3000rpm) [43]

CHAPTER 3

A 1−D DESIGN AND MODELLING

3.1 Geometry and profile generation of twin oil−flooded screw compressor

Geometry characteristics of the compressor provide the required input data for the thermodynamic numerical model. Rotor design has been an important area of improvement for the screw compressor over the years and has been optimized by several researchers [18, 21, 46]. The geometrical characteristics that influence the performance are the cross-sectional area, cavity volume, suction and discharge ports, axial and radial discharge ports, leakage paths (Contact line, rotor tip, blow holes, compression start blow hole, suction end face, and discharge end face), injection port, and by-pass port. In this chapter, the geometry characteristics and profile will be discussed. Geometric curves will be obtained as a function of the male rotation angle and used directly as an input for the numerical model.

The geometry of the rotors within the compressor mimics a helical screw along the length of the rotor [47]. Differences between helical gears and rotors are that the rotors must maintain a sealing line and low contact forces. The two helical rotors are enclosed within a casing and meshed together. Individual working chambers are created between any two consecutive lobes. As the rotors rotate, the volume of gas in between each lobe is reduced and the seal along the rotor lengths is maintained. When the volume decreases, the pressure increases. The volume is a function of the position going from zero to maximum volume and back to zero. The volume is maximum when the entire length between the lobes is unobstructed by the meshing contact with the other rotor [45]. It has a minimum value of zero when there is full meshing contact with the second rotor at the end face [45]. The maximum volume occurs at suction within each chamber, and volume is reduced to roughly zero at discharge.

Rotor profile generation within a screw compressor consist of designing primary profile curves and producing a corresponding profile curve from it [48] . The male rotor profile is typically

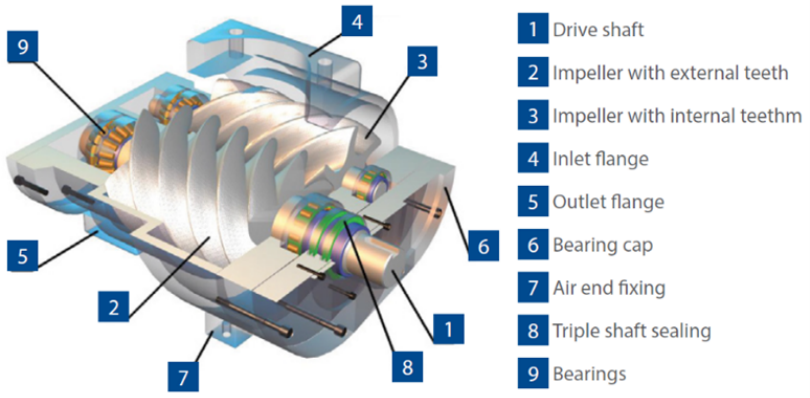

Figure 3.1: Components of the Screw Compressor

designed first, and the female rotor profile is created from the male rotor profile or vice versa. Circles, ellipses, parabola, and hyperbolae are common curves with circles being the most common. The original profile developed by Asl Lysholm consisted of all circular arcs [49]. Stosic states that the hyperbola profile is the best replacement for the circle because it gives the best ratio of the rotor displacement and seal line length [45]. To increase the screw compressor performance, a large cross section area, small sealing line, and small blow hole area must be used. The cross section area impacts the flow rate for the same size and speed. When the leakages are reduced along with increasing the cross section area, the volumetric and adiabatic efficiencies are increased. Further rotor designs can be investigated to reduce internal friction and contact stress. Friction is caused by relative motion between the contacting rotor surfaces. Lowering the contact stress reduces the amount of lubricant needed [49].

The screw compressor comes in different profile configurations. The original and most common profile is the semicircle (symmetric circular) 4+6 profile. The 4 and 6 represent the number of male and the female lobes respectively. This is common practice for identifying the number of lobes for any given rotor profile. Over the years, screw compressor profiles have developed significantly as seen in Fig.3.2 to reduce the amount of leakages and increase the cross section area, the left represents male rotor profiles and the right represents female. The profile configuration and the rotor design work conjointly. The sealing line, blow hole area, and lobe number rely on the compressor load. Fewer number of lobes leads to higher flow area and higher pressure difference [49]. Five

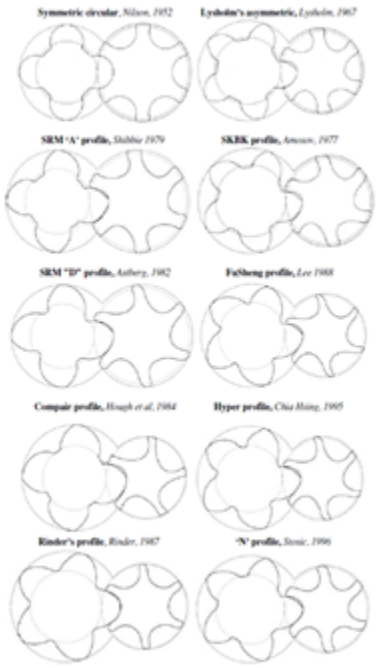

Figure 3.2: Popular Screw Compressor Rotor Profiles

male lobes can be used to increase the compressor pressure ratios, especially if combined with larger helix angle [45]. Stosic states that the 4 + 5 lobe combination is the best combination for oil-flooded applications with moderate pressure ratios [49]. Ease of manufacturing is also considered when designing the rotors.

The profile of rotors can be produced using several methods such as envelope method, rack generated method, and point generation. One basis for rotor generation is the envelope method. Rack generation uses a rotor infinite radius to acquire a secondary arc. The approach to generating curves using imaginary rotors is used in rack generation. Equations used to define rotor profile can be simplified by defining arcs using an independent coordinate system and/or using one coordinate system for all curves [45]. The configuration and rotor parameters must be defined before the rotor geometry can be generated.

3.1.1 Envelope Method

The envelope method states that two surfaces are in mesh if each generates or envelops the other under a specified relative motion [49]. The envelope method is used to calculate mathematically the mating rotor profile from a given rotor profile and was explained by Litvin [47] . The analysis done by Tang [44] will be used to explain the envelope method mathematical procedures. In order to begin, the coordinate system must be well understood as depicted in Fig.3.3. $O_1X_1Y_1$ and $O_2X_2Y_2$ are static coordinate systems with $o_1x_1y_1$ and $o_2x_2y_2$ being the male and female rotating coordinate systems respectfully. Both coordinate systems are independent of the other. o_1 is the center of the male and o_2 is the center of the female. The static and rotational coordinate systems coincide with one another at the start position. The male and female rotate by angle φ_1 and φ_2, respectfully, in opposite directions.

Transform equations of the coordinates between the two rotational coordinates systems and transmission ratio, i, are shown in Eqs.(3.1), (3.2) and (3.3), respectfully. k = 1-(1/i) and A is the distance between the male center and female center.

$$\begin{cases} x_1(\varphi_1) = -x_2 \cos k\varphi_1 - y_2 \sin \varphi_1 + A \cos \varphi_1 \\ y_1(\varphi_1) = -x_2 \sin \varphi_1 - y_2 \cos k\varphi_1 + A \sin \varphi_1 \end{cases} \tag{3.1}$$

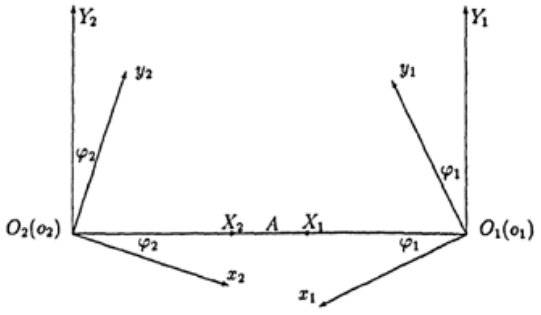

Figure 3.3: Coordinate System for analysis

$$\begin{cases} x_2(\varphi_1) = -x_1 \cos k\varphi_1 - y_1 \sin \varphi_1 + A \cos \varphi_1 \\ y_2(\varphi_1) = -x_1 \sin \varphi_1 + y_1 \cos k\varphi_1 + A \sin \varphi_1 \end{cases} \tag{3.2}$$

$$i = \frac{\varphi_2}{\varphi_1} = \frac{\omega_2}{\omega_1} = \frac{z_2}{z_1} \tag{3.3}$$

where,

z_2 Number of female flutes

z_1 Number of male lobes

ω_1 Rotational angular speed of male ω_2 Rotational angular speed of female

A given profile can be defined as a parametric equation as seen in Eq. (3.4). When Eq. (3.4) is substituted back in the transform Eq.(3.1) or (3.2), the mating profile is acquired in the $o_2x_2y_2$ coordinate system, seen in Eq. 3.5. These equations produce a set of curves, which is the envelope that can be obtained for any given profile. While the male profile is used here, the female profile can be given, and the male can be determined [50].

$$\begin{aligned} x_1 &= x_1(t) \\ y_1 &= y_1(t) \end{aligned} \tag{3.4}$$

$$\begin{aligned} x_2 &= x_2(t, \varphi_1) \\ y_2 &= y_2(t, \varphi_1) \end{aligned} \tag{3.5}$$

There is a contact point that exists between the envelope and the given profile. At this point the two curves have a common tangent. At any point in the envelope the slope of the tangent can be calculated by taking the derivative of Eq. (3.5). The slope of the tangent at any point in the given curve can be calculated also by taking the derivative of Eq. 3.4. Equating the two derivative produces the envelope condition, seen in Eq. 3.6.

$$\frac{\partial x_2}{\partial t}\frac{\partial y_2}{\partial \varphi_2} - \frac{\partial x_2}{\partial \varphi_2}\frac{\partial y_2}{\partial t} = 0 \tag{3.6}$$

The envelope condition provides the relationship between the parameter, t, and the female rotation angle. This can be characterized by Eq.(3.7).

$$f(t, \varphi_1) = 0 \tag{3.7}$$

Along with the envelope condition equations, the derivative of the profiles, Eqs. (3.8) and (3.9), rotational to static system transformation, and static to rotational system transformation equations are commonly used.

$$\begin{cases} \frac{dx_1}{dt} = -\frac{dx_2}{dt}\cos k\varphi_1 - \frac{dy_2}{dt}\sin k\varphi_1 \\ \frac{dy_1}{dt} = -\frac{dx_2}{dt}\sin k\varphi_1 - \frac{dy_2}{dt}\cos k\varphi_1 \end{cases} \tag{3.8}$$

$$\begin{cases} \frac{dx_2}{dt} = -\frac{dx_1}{dt}\cos k\varphi_1 - \frac{dy_1}{dt}\sin k\varphi_1 \\ \frac{dy_2}{dt} = -\frac{dx_1}{dt}\sin k\varphi_1 + \frac{dy_1}{dt}\cos k\varphi_1 \end{cases} \tag{3.9}$$

3.1.2 Rack Generation

The rack generation method is different from the envelope method because both female and male profiles are generated using a rack profile and conjugated to the rack. The rack is a profile of infinite radius. The infinite radius is composed of several arcs, elipses, ect. The concave side of the rack is used to form the male profile and the convex is used for the female rotor. Once one profile is generated, the envelope method can be used to find the other. However, both male and female profiles can be found using a given rack. The method for designing a rack explicitly by Wu [51] was used in this research to produce a 5+6 rotor profile. A combination of circular arcs, trochiods, ellipses, and lines were used in this approach to construct the full rack with each curve having independent adjustable parameters. This allows for greater flexibility within rotor generation.

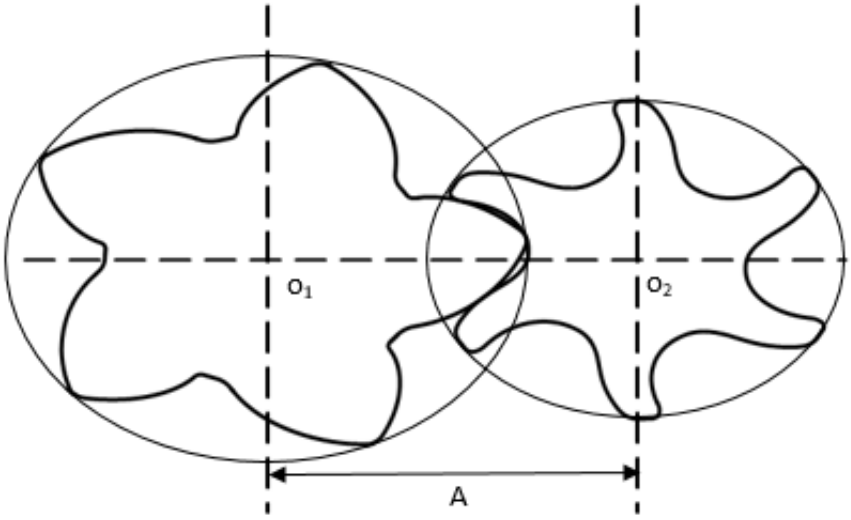

Figure 3.4: Rotor profile

Table 3.1: Rotor Geometry Characteristics

Number of male lobes	m_1	5
Number of female flutes	m_2	6
Distance between rotor axes	A	90 mm
Length of rotors	L	205.9 mm
Wrap angle	φ	299.622 °
Pitch Helix Angle	β	46.0 °

The 5+6 rotor profile generated using method presented by Wu and information provided in Table. 3.1 is shown in Fig.3.4 .

3.2 Modeling various graphical performance curves for twin oil–flooded screw compressor

Geometrical characteristics are solely based on profile of rotors and essential to modeling the internal compression process to help understand the performance. A large number of separate points are needed for the generated rotor profile in order to numerically calculate important geometrical characteristics, such as cross-sectional area. Geometrical characteristics include cross-sectional area, cavity volume, port areas, leakage paths, etc. Each characteristic will be defined in this section.

3.2.1 Cross-sectional Area and Cavity Volume

The cross-sectional area is the area bounded by the rotor end profiles and the hosing bores and changes based on the rotational angle of the male rotor [52]. The cross-sectional area is found by integrating parametric curves in Eq. (3.4). The cross-sectional area, can be graphed versus the male rotation angle Fig. 3.6. To analytically determine the cross sectional area Eq. (3.10) can be used. Adding A_{01} and A_{02} together gives the maximum cross-sectional area Fig. 3.5.

$$A(\varphi) = \frac{1}{2}\oint xdy - ydx = \frac{1}{2}\sum\int_{y_{i,min}}^{y_{i,max}} x_i dy_i - \frac{1}{2}\sum\int_{x_{i,min}}^{x_{i,max}} y_i dx_i \tag{3.10}$$

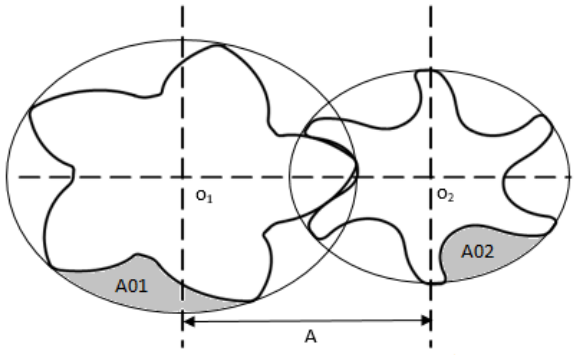

Figure 3.5: Cross section of screw rotors

The cavity volume is the volume enclosed within the female lobe, male lobes, housing, and end planes of the compressor. The volume curve is defined by the cavity volume and the male rotor angle. There are a number of ways to determine the volume curve present by different researchers [21, 46, 53] . Singh [53] introduced an analytical method that uses the relationship between the analytical volume and boundary surface. Zhang [21] presented a method that determines the volume by integrating the cross sectional area where the cross sectional area is determined analytically. Similarly, Margolis [46] laid out an approach to calculate the volume curve from a calculated area.

In this study, the cavity volume is found using Zhang [21] approach. Integrating the cross sectional area generates the cavity volume. The rotational angle is transformed to rotor length along the rotor axis for integration. The limits of integration are limited by the wrap angle of the

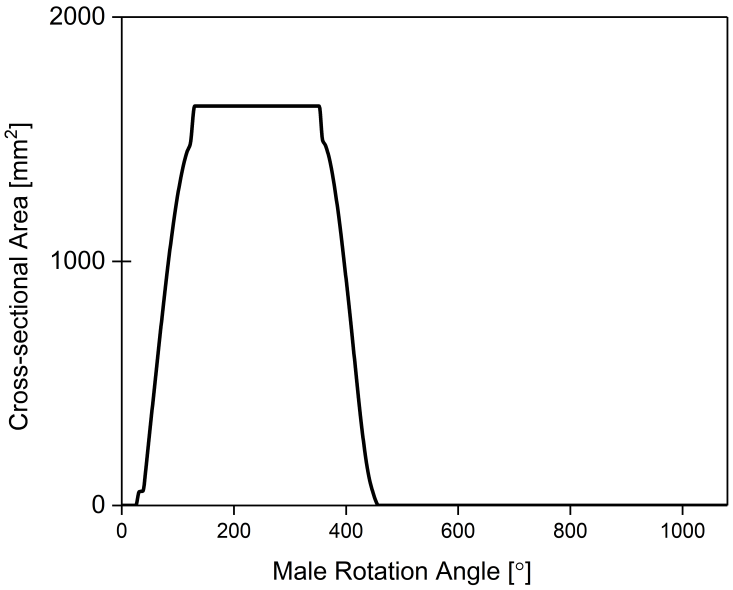

Figure 3.6: Cross-sectional area vs rotational angle

male rotor. The volume versus angle curve is seen in Fig 3.7. The maximum volume occurs when the cavity is completely filled at suction and the minimum is zero upon discharge. The cavity goes from zero to max to zero repeatedly within the full compression cycle.

$$V(\varphi) = h \int f_r(\varphi)\, d\varphi \tag{3.11}$$

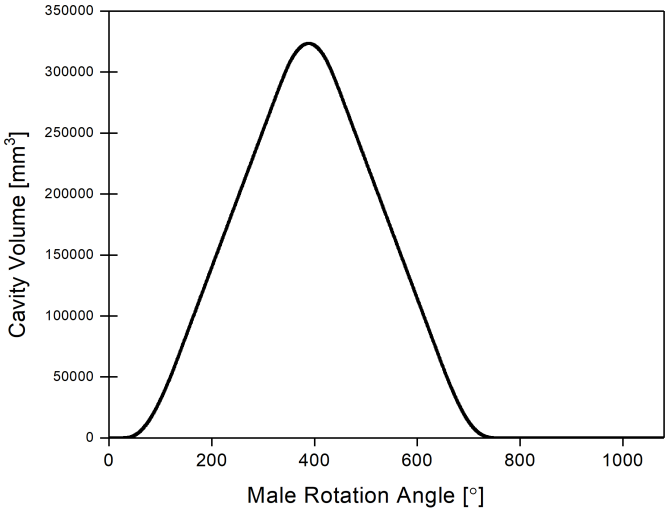

Figure 3.7: Cavity volume vs rotational angle

Alternatively, the volume curve can also be calculated using Eq. (3.12)

$$V(\varphi) = \sum \frac{A(\varphi) L \Delta\tau_1}{\tau_{w1}} \tag{3.12}$$

where

L	Rotor Length
φ_1	Male rotation angle
τ_{w1}	Male wrap angle
τ_1	Twist parameter

3.2.2 Suction and Discharge ports

The suction port is the port at which the gas fills the compressor, and the discharge port is where the gas exits the compressor. Both the suction and discharge port consist of an axial and radial port types. The suction and discharge process are driven by the shape of the port. The axial suction port area is determined theoretically by the meshing line and male rotating angle at the maximum cavity volume [54]. The axial suction area versus the angle curve is seen in Fig. 3.9. The radial suction port increases the port area and is used to reduce the amount of viscous friction drag between rotor tips and housing bores in oil flooded compressors. The suction radial port area is much smaller than the axial suction port, which also reduces the amount of flow resistance. The point at which the suction has to cease is calculated by Eq. (3.13), and any angle less or more than this leads to a decrease in performance.

$$\varphi_2 = \varphi_1 \frac{z_1}{z_2} + \frac{360}{z_2} \tag{3.13}$$

The discharge port consist of axial and radial port types. The axial discharge port shape is seen in Fig 3.10 and is determined by the meshing line and volume ratio design [54]. The radial discharge port changes based on the slide valve position and only used in compressors with small to medium build-in volume ratios. The addition of the radial discharge port reduces the flow resistance

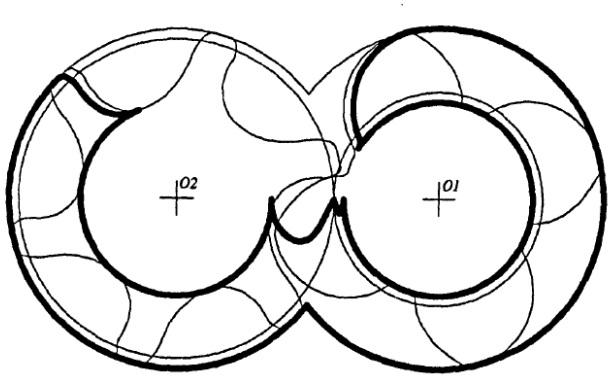

Figure 3.8: Theoretical shape of a suction port (view from the suction end)

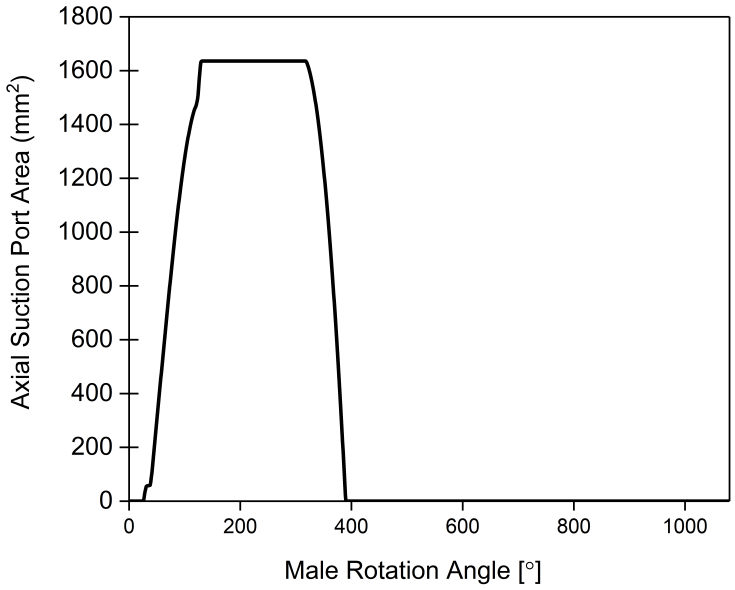

Figure 3.9: Axial Suction Port Area vs. Rotation Angle of Male Rotor

at discharge. Fig 3.11 shows the axial discharge area versus male rotation angle. The axial suction and discharge areas can be calculated by integrating along the port and cavity boundaries.

$$A_{axial} = \oint y dx \tag{3.14}$$

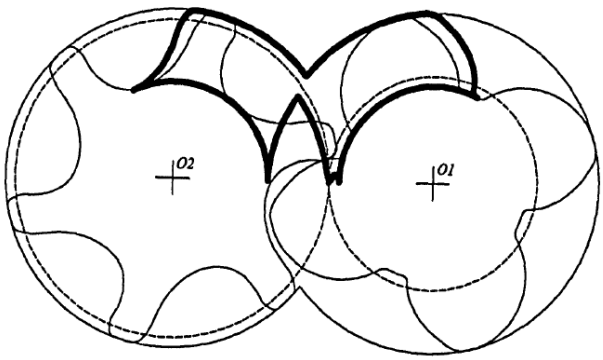

Figure 3.10: Theoretical shape of an axial discharge port (view from the discharge end)

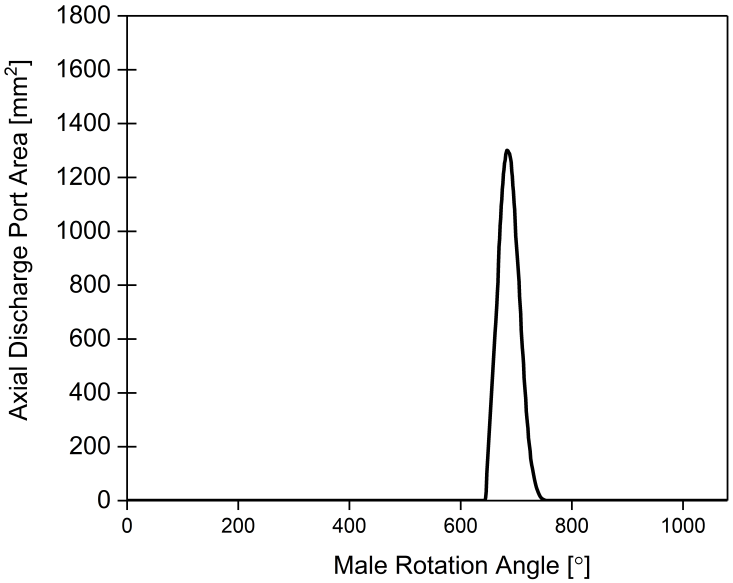

Figure 3.11: Axial discharge port area vs rotational angle

3.2.3 Leakage Curves

Screw compressors consist of leakages from several leakage paths. To gain insight on the impact of each leakage path, geometric curves can be generated for each leakage path. The blowhole and contact line are the only leakage paths used in the 1-D mathematical model due to their large influence on performance. All other leakage paths are not considered within model. The contact line , rotor tip sealing lines, rotor suction end face, and rotor discharge end face flow areas are calculated using the following equation:

$$A = \delta L \tag{3.15}$$

$$L = \int_a^b \sqrt{(x_2 - x_1) + (y_2 - y_1) + (z_2 - z_1)} \tag{3.16}$$

where δ represents the gap clearance in the compressor and L is the length of the leakage. To calculate the sealing length using Eq. (3.16) , start and end position points must be known. With the sealing length the cross section of the area can be calculated using the known measure clearances. If clearances are not known, nominal design clearances are applied. From these equations, these four leakage areas can be plotted versus the male rotational angle. Additionally, the blowhole is calculated using the method presented by Zaytsev [52] adapted from You [55]. The process of calculating the blowhole area begins with defining the coordinates of vertices A,B, and C. Next, the plane ABC equations are defined. Thirdly, the plane and rotor surface intersection is developed for both rotors. Lastly, the blow hole is integrated to find the area. The blowhole shape is constant as the rotor rotates, which produces a constant area seen in Fig. (3.13). This process is the same for both cusp blow hole and compression start blow hole.

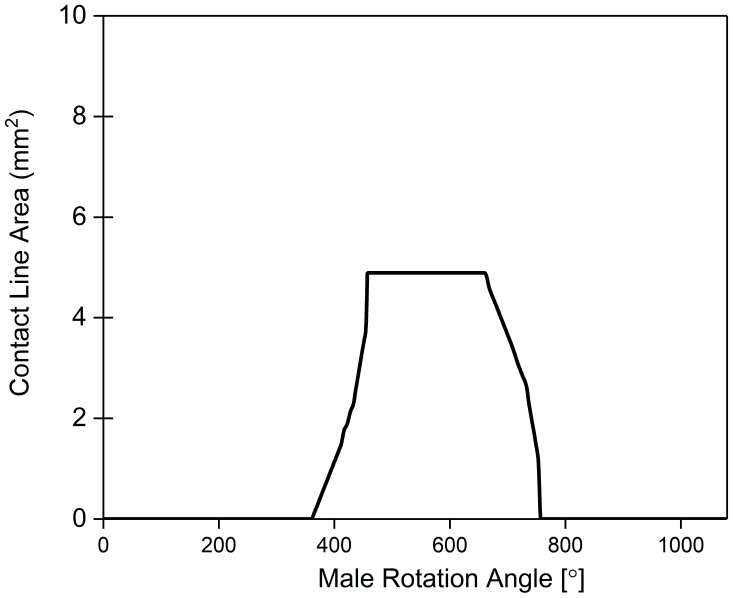

Figure 3.12: Contact line area vs rotational angle

Figure 3.13: Blow hole area vs rotational angle

3.3 1–D Mathematical Model of Working Process

Mathematical models are tools used to reduce the amount of money, time, and resources spent on understanding a process. Various 1-D mathematical models have been developed to better understand and predict the performance of the compressor [28], [56], [57], [15]. Models can be created to understand just one portion of the process, i.e., leakages or the whole process i.e.,(suction, compression, discharge, leakage, etc.). The working process of a screw compressor is typically modeled as an open thermodynamic system and mass flow changes with time or rotational angle. Each process (suction, compression, and discharge) can be defined by its own control volume and conservation equations. The non-steady flow energy equation is used to compute the thermodynamic and flow in terms of rotational angle. Performance predictions are determined using various thermodynamic equations. The volume curve that is attained from the geometrical characteristics is used within several thermodynamic equations along with suction and discharge curves. To determine inefficiencies caused by leakages, compressor leakage information is used as an input within the mathematical model.

Various ordinary differential equations derived from the conservation of mass and energy equa-

tions along with other thermodynamic relations are used to define the compression cycle from suction to discharge with a working fluid and liquid injection. Mathematical models range in complexity; however, several assumptions are used to simplify the model.The objective is to simplify features that have little effect on the overall performance. This allows the program to estimate as close as possible to the real processes. Fujiwara et al, Singh and Patel, Stosic, and other authors developed mathematical models and assumptions varied from researcher to researcher. However, the overall process of developing a model is similar and ultimately used to calculate the isothermal efficiency, volumetric efficiency, and other performance parameters. Experimental results will be used to determine accuracy of the 1-D analysis. After verifying the accuracy of the 1-D analysis, the model can be used for a quick understanding of performance when adjusting various parameters.

For this mathematical model, adopted assumptions are:

- The working fluid through suction, discharge, and leakage paths are modelled as an Ideal gas.
- The pressure within the suction and discharge chamber is constant.
- The heat transfer present in model is between working fluid and oil.
- Working fluid and oil are modeled as separate fluids and both discharge temperatures are calculated.
- Simplified leakage model that only consist of blow hole and contact line leakages.
- Leakages consist of Gas only.
- There is no phase change for helium or oil during simulation cycle.
- Mechanical Equilibrium between gas and oil.
- Oil is an incompressible fluid.
- Work supplied to oil is neglected.

The in-take, compression and expulsion for one cavity is being modeled and is assumed to be the same for the others. The volume is created by the male and female rotors and the compressor housing. The model assumes a control volume seen in Fig. 3.15 that is characterized using a reciprocating compressor with a cylinder, piston, and flows going in and out. This is possibly due to the fact that both the screw and reciprocating compressors are positive displacement machines and a reciprocating compressor is simpler to visualize.

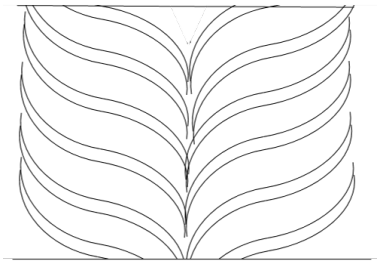

Figure 3.14: Control volume of screw compressor

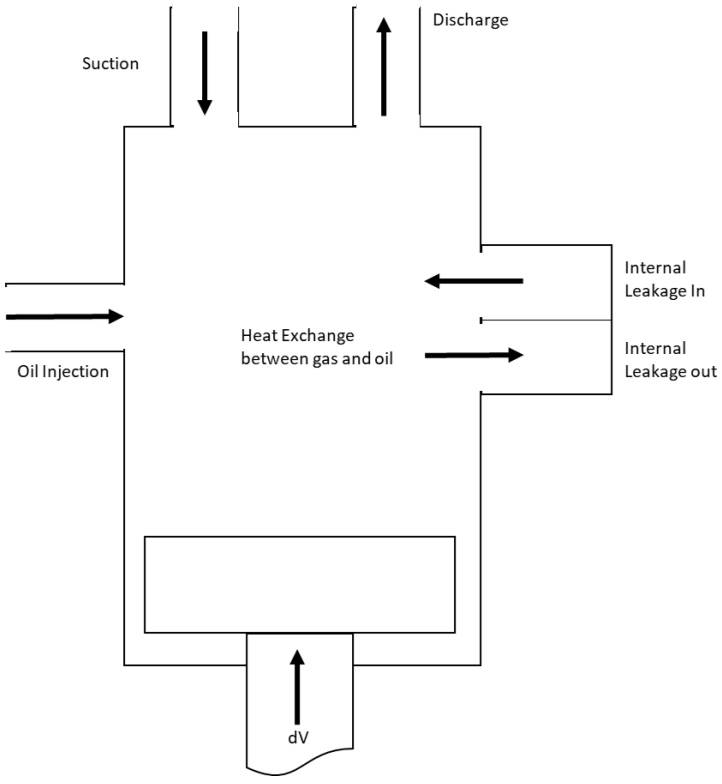

Figure 3.15: Simplified Control volume of screw compressor

3.3.1 Governing Equations of control volume

The mathematical model will begin by defining the conservation of mass equation in terms of rotational angle for the control volume of the screw compressor. The conservation of mass is defined for gas and oil separately in Eq. (3.18) and (3.19). Gas mass entering the compressor includes gas entering through suction port and leakage paths as seen in Eq. (3.20). The mass of gas leaving the control volume consist of gas leaving through the discharge port and leakages as seen in Eq. (3.21). Leakages consist of only gas; therefore, the sum of the oil entering (injected into the compression process) is the amount expelled.

Conservation of Mass

$$\frac{dm_{cv}}{d\varphi} = \frac{dm_{in}}{d\varphi} - \frac{dm_{out}}{d\varphi} \tag{3.17}$$

$$\frac{dm_{g}}{d\varphi} = \frac{dm_{g,in}}{d\varphi} - \frac{dm_{g,out}}{d\varphi} \tag{3.18}$$

$$\frac{dm_{L}}{d\varphi} = \frac{dm_{L,in}}{d\varphi} - \frac{dm_{L,out}}{d\varphi} \tag{3.19}$$

$$\frac{dm_{g,in}}{d\varphi} = \frac{dm_{g,s}}{d\varphi} + \frac{dm_{g,leakin}}{d\varphi} \tag{3.20}$$

$$\frac{dm_{g,out}}{d\varphi} = \frac{dm_{g,d}}{d\varphi} + \frac{dm_{g,leakout}}{d\varphi} \tag{3.21}$$

where

m	Mass
φ	Angle of rotation of the main rotor
Subscripts,	
d	discharge
g	Working fluid
L	Liquid injected
s	suction
in	flow entering cavity
out	flow leaving cavity
leakin	leakage entering control volume
leakout	leakage exiting control volume

The conservation of internal energy in terms of rotation angle is defined for control volume. Similiar to the conservation of mass, the conservation of internal energy can be written in terms of the working gas and oil separately seen in Eqs. (3.23) and (3.24). The contribution of oil compression work is small and therefore neglected.

Conservation of Internal Energy

$$\frac{dU_{cv}}{d\varphi} = \frac{dQ}{d\varphi} - \frac{dW}{d\varphi} + \frac{dm}{d\varphi}h_{in} - \frac{dm}{d\varphi}h_{out} \tag{3.22}$$

$$\frac{dU_g}{d\varphi} = \frac{dQ}{d\varphi} - \frac{dW}{d\varphi} + \frac{dm_{g,in}}{d\varphi}h_{g,in} - \frac{dm_{g,out}}{d\varphi}h_{g,out} \tag{3.23}$$

$$\frac{dU_L}{d\varphi} = -\frac{dQ}{d\varphi} + \frac{dm_{L,in}}{d\varphi}h_{L,in} - \frac{dm_{L,out}}{d\varphi}h_{L,out} \tag{3.24}$$

Ideal Gas Law

$$pv = RT \tag{3.25}$$

where

h	Specific Enthalpy
p	Pressure
Q	Heat Transferred from gas to liquid
R	Gas Constant
T	Temperature
U	Internal Energy
v	Specific Volume
W	Work done on the gas

Using the conservation equations of mass and internal energy in the control volume, the pressure, gas temperature, and oil temperature can be calculated. The pressure and temperature derivations are in Eqs. (3.26) to (3.32). The left-hand side of Eq. (3.22) can be written as

$$\frac{dU}{d\varphi} = m\frac{du}{d\varphi} + u\frac{dm}{d\varphi} \tag{3.26}$$

$$u = C_v T \tag{3.27}$$

$$du = C_v \frac{dT}{d\varphi} \tag{3.28}$$

The specific internal energy of an ideal gas is a function of temperature as seen in Eq. (3.27) where C_v is the specific heat of fluid, however in the numerical model the specific heat is a constant. Combining Eqs. (3.26), (3.27), and (3.28) and inserting back into E1. (3.22) yields the general temperature differential equation.

$$\frac{dT}{d\varphi} = \frac{\frac{dQ}{d\varphi} - \frac{dW}{d\varphi} + \frac{dm_{in}}{d\varphi} h_{in} - \frac{dm_{out}}{d\varphi} h_{out} - u\frac{dm}{d\varphi}}{mC_v} \tag{3.29}$$

Using the ideal gas law, the differential equation for pressure is derived and seen in Eq. (3.30)

$$\frac{dP}{d\varphi} = \frac{m_g R \frac{dT_g}{d\varphi} - p\frac{dV_g}{d\varphi} + RT_g \frac{dm_g}{d\varphi}}{V_g} \tag{3.30}$$

where, V is the volume of gas present in control volume. Using the generic equation of temperature change Eq. (3.29) the temperature for both the working fluid and liquid can be derived seen in Eqs. (3.31) and (3.32).Pressure for the working fluid and injected liquid are the same.

$$\frac{dT_g}{d\varphi} = \frac{\frac{dQ}{d\varphi} - \frac{dW}{d\varphi} + \dot{m}_{g,in} h_{g,in} - \dot{m}_{g,out} h_{g,out} - u_g dm_g}{m_g C_{v_g}} \tag{3.31}$$

$$\frac{dT_L}{d\varphi} = \frac{-\frac{dQ}{d\varphi} + \dot{m}_{L,in} h_{L,in} - \dot{m}_{L,out} h_{L,out} - u_L dm_L}{m_L C_{v_L}} \tag{3.32}$$

3.3.2 Work exchanged by gas in control volume

The working gas and oil are both present within the volume being compressed with the oil being considered an incompressible fluid. The amount of oil within the control volume varies with rotational angle; and as the volume of oil increase, so does the impact it has on the work exchanged in the control volume. In this simulation, the work of compression from the oil is neglected.

Change in work on gas with respect to male rotation angle is calculated using the change in the cavity volume seen in Eq. (3.33).

$$\frac{dW}{d\varphi} = -p\frac{dV}{d\varphi} \tag{3.33}$$

3.3.3 Heat transfer between gas and oil

There are three forms of heat transfer that can be modeled: heat transfer between the gas and the solid, heat transfer between solid to oil, and heat transfer between gas and oil. In this model, the heat transfer between gas to solids and oil to solids is neglected. Previous studies [58,59] concluded that the effect of this form of heat exchange is small in comparison to the internal energy of gas within the cavity. This heat exchange is of particular interest when evaluating thermal distortions in dry compressors. Furthermore, the heat transfer modeled is between the working fluid and oil.

Heat transfer between oil and gas is a very important value that impacts the performance of a compressor using helium. Many models [27, 60–62] have been created to better understand oil-injection, most of which assume that the working fluid and oil are in equilibrium. The oil temperature was seen to follow gas temperatures closely [39] for small droplets of oil. Although an equilbrium assumption is supported in research, this is not assumed in this model. The duration of compression and oil injection position both impact this assumption. Furthermore, it is of importance in this study to better understand the helium and oil temperature relationship during the compression cycle.

Oil injection nozzles' methods can vary greatly and overall complicate the heat transfer model; therefore, oil injection characteristics are assumed. Oil enters the compressor in the form of a droplet with a precise droplet diameter [63, 64]. The most important and difficult parameter to define within the heat transfer equation is the heat transfer coefficient. In order to determine the heat transfer coefficient, an understanding of oil properties, geometry of compressor, and heat transfer relations is needed. The heat transfer model is defined using Eq. (4.4).

$$\frac{dQ}{d\varphi} = \frac{hA(T_{gas} - T_{oil})}{\omega} \tag{3.34}$$

where h is the heat transfer coefficient of the droplet surface and A is the mean Sauter area of all droplets. Ranz [65] defined a formula for this heat transfer mode in Eq. (3.35) .The characteristic length in the Reynolds number is defined using the length of the rotors. After calculating the Nusslet number, the heat transfer coefficient can be obtained using Eq. (3.36), where k is the thermal conductivity of the oil. Area is defined using Eq. (3.37) where r is the particle radius and n is the number of particles. The number of particles is defined using Eq. 3.38 . m_l represents the mass of liquid, ρ_l represents the density of liquid, and D_p is the diameter particle.

$$Nu = 2 + 0.6Re^{0.5}Pr^{0.33} \tag{3.35}$$

$$h = \frac{Nuk}{D_p} \tag{3.36}$$

$$A = 4\pi r^2 n \tag{3.37}$$

$$n = \frac{6m_l}{\rho_l \pi {D_p}^3} \tag{3.38}$$

3.3.4 Gas flow through suction and discharge ports

As shown in Eqs. (3.20) and (3.21) there are several flows that are entering and leaving the cavity. All gas flows within the compressor consist of compressor suction , discharge, and internal leakages. The mass flow rate is calculated using the continuity Eq. (3.39).

$$\frac{dm}{d\varphi} = \frac{c\rho W_f A_{flow}}{\omega} \tag{3.39}$$

where

A_{flow}	Flow Area
c	Flow coefficient
ρ	Density
ω	Angular Velocity
W_f	Fluid Speed

Flow areas are obtained from geometric curves defined earlier in this chapter. The fluid speed is modeled as an converging nozzle using Eq. (3.40). Due to a small Mach number, the flow through the suction port is typically considered as an incompressible fluid. The density is calculated from the downstream conditions. At discharge; under compression, normal compression, and over compression conditions can occur which will affect whether the pressure at discharge is lower, the same, or higher than pressure within control volume. This relationship can cause high pressure difference between the control volume and discharge process leading to increased Mach number. If large Mach numbers are obtained, the gas flow can't be considered incompressible and Eq. (3.41) is used. The speed is calculated using one-dimensional and isentropic energy conservation equation. The flow speed W_f, is negative if flow is going into the control volume, otherwise it is positive.

$$W_f = \sqrt{2 \int_{p_1}^{p_2} v \, dp} \tag{3.40}$$

$$W_f = \sqrt{\frac{v}{\alpha}} \tag{3.41}$$

where α is the isentropic compressibility coefficient. To account for non-isentropic effects, the flow coefficent c must be used. The flow coefficient used is different for each tpe of flow path. Flow coefficients are typically determined from experimentation. This has been done by researchers [40, 66, 67] with varying results. Prins [66] identified flow coefficients for the suction port , discharge port, and leakages as 1, 0.9. and 0.3 respectfully. These coefficients were used in the mathematical model. Others researchers [40, 67] have provided coefficients for suction port flow range from 0.72 to 1, discharge port flow range from 0.6 to 0.85, and leakage flow range from 0.3 to 0.7. As seen, there is a large range of coefficients; and these values are highly dependent on working fluid, injected oil details, and machine type.

3.3.5 Oil Injection

Oil is injected and mixed with working fluid within the control volume of the screw compressor. The benefits of oil injection are the cooling of gas, rotors, and housing; sealing of clearances; and lubrication. Thermal distortions are reduced due to the cooling of rotor parts. Some of the working fluid is dissolved in the oil, reducing the purity of oil being circulated in the compressor. This phenomenon reduces the viscosity oil and sealing of clearances. The volumetric efficiency and overall energy is directly impacted by the solubility of the refrigerant. Helium and oil interactions are unknown and data provided by oil manufacturer were implemented in the model. From the data supplied, the the oil properties incorporated into the model are:

1. Density of oil vs temperature
2. Viscosity of oil vs temperature
3. Thermal conductivity vs temperature

Helium solubility is not considered in this model. Oil specific is treated as a constant due to the minor variation with temperature change. The injected and discharged oil flow rate is constant.

3.3.6 Determining Leakage Flow

Leakage is a significant contributor to the reduction of the efficiency. As stated in earlier section, there are six leakage path's identified by Fleming [43]. The overall leakage is a combination of the six paths. The leakage paths influence will vary with the suction and discharge port position and design of the rotors i.e., length, diameter, and wrap angle. To understand the impact that the leakage will have on the overall performance, a model for the leakage within the working process can was implemented. Each leakage path has unique flow directions and area. The leakage area also changes with the male angle of rotation. The leakage phenomenon includes other factors that are simplified in order to achieve a working mathematical model. Assumptions that are used to simplified the model stated by Fleming [43] are:

1. There is one-dimensional flow through each leakage path

2. Refrigerant gas and oil are separate fluids

3. Only gas leaks through leakage paths

4. Oil remain in the cavity into which they were injected and pass into the discharge process

5. A reversible isentropic calculation modified by use of empirical coefficient is used to determine the vapor flow

The one-dimensional, isentropic, compressible flow energy conservation differential equation is used to calculate the gas flow speed.

$$vdv + dh = 0 \tag{3.42}$$

This equation is used to calculate flow speed through blow hole and compression start blow hole flow areas (path 3 and 4). If the pressure difference is large enough, the maximum fluid flow speed can approach the local sound speed through any leakage path. The following differential equations calculates the local sound speed. The cusp blow hole areas are calculated using the definition of Singh and Patel [26].

$$v = \sqrt{\frac{\delta p}{\delta \rho}} \tag{3.43}$$

where

p gas pressure
ρ fluid density

The continuity equation is used to calculate the mass flow rate through leakage paths.

$$\frac{dm}{d\varphi} = \frac{c\rho v A}{\omega} \tag{3.44}$$

where

A Flow area
c coefficient
m Fluid mass
ω angular speed of the male rotor

For leakage flow defined by Fleming, the coefficient consist of two coefficients, c_1 and c_2. c_1 is the coefficient used to modify the flow area and c_2 is the coefficient used to modify the flow speed of fluid. The flow coefficients c_1 and c_2 account for the area change between the compressor at rest and uniform temperature and the area under load defines coefficient c_1. Coefficient c_1 accounts for three quite distinct physical effects as follows:

1. The tendency of the oil in the compressor to seal the leakage gaps
2. The changes caused to nominal clearances by the cavity pressure under load
3. The changes caused to nominal clearances by the temperature distribution of the rotors and housing under load

Due to the minor effects of the above factors on the blow hole and compression start blow hole areas, the coefficient c_1 is set to 1 for both the blow hole and compression start blow hole areas. On the other hand, the other leakage paths are affected by the above factors. The operating conditions has an effect on each leakage path. At different temperatures and pressures the rotor, bearings, and housing deform to some degree. This deformation causes the internal clearance and leakage mass flow to be altered [42]. Determining the clearances under load is challenging because of the amount of influences involved. Thermal expansion of the rotors and housing, radial and thrust bearing deformations and clearances, etc. are factors that influence the clearance under load. Coefficient c_2 is defined to "account for irreversibility's reducing the flow speed calculated on the basis that the flow is isentropic and one dimensional" [42]. Coefficient c_2 is based on the geometry of the leakage path. This means that each leakage path will consist of a distinct coefficient c_2. Leakage paths can be compared to orifice plates, narrow passages between two parallel plates, and nozzles to estimate coefficients c_2. Another option to determine the coefficient c_2 is to use the

same coefficient for each path and compare the predicted volumetric efficiency with the measured volumetric efficiency. c_1 and c_2 are used as a product and cannot be evaluated individually. The product coefficient $c_1 \cdot c_2$ is influenced by the working fluid and the profile used. Further research on determining the coefficients is recommended for better mathematical model results.

3.3.7 Additional Properties

Additional equations are provided outside of those previously mentioned to define oil and gas properties that are used within the model to determine the gas and oil temperature.

Specific volume of gas

The specific volume is determined by using the cavity volume at particular location divided by the current mass of gas within the cavity seen in Eq. (3.45) .

$$v_g = \frac{V}{m_{gas}} \tag{3.45}$$

Specific internal energy of oil

$$du_L = CdT \tag{3.46}$$

Enthalpy

The specific enthalpy is calculated using Eq. (3.47) where C_p is the specific heat of gas at constant pressure. Oil enthalpy is a function or oil temperature and pressure defined as an incompressible fluid and the change in enthalpy is calculated using Eq. (3.48).

$$h = C_p T \tag{3.47}$$

$$dh_L = CdT + vdP \tag{3.48}$$

Ideal gas assumptions were adopted in this model due to the use of helium; however, when refrigerants are used, real gas properties should be implemented.

3.3.8 Performance

The mathematical model consist of Eqs. (3.17) to (3.39) that are integrated to produce pressure, temperature, and all thermodynamic properties of gas and injected liquid as functions of the male rotation angle. Calculated values gathered from integration can be used further to approximate total compressor power information and performance. Equations to generate performance values are presented below in Eqs. (3.52) to (3.57). The total mass of the compressor is based on the male rotor which implies that the actual mass flow rate would also be based on the male rotor as well.

$$\dot{m} = \frac{mz_1 n}{60} \tag{3.49}$$

where n is the number of revolutions per minute. The volumetric flow rate ($\dot{V}$)is based on the suction conditions and calculated below

$$\dot{V} = \frac{60\dot{m}}{\rho_s} \tag{3.50}$$

The theoretical mass flow ($\dot{m}_t$) is based on the maximum volume of the working chamber

$$\dot{m}_t = \frac{V_{max} n z_1 \rho_s}{60} \tag{3.51}$$

where V_{max} is the maximum volume of compressor and ρ_s is the density at suction.
The volumetric efficiency (η_v) is calculated using Eq. (3.52)

$$\eta_v = \frac{\dot{m}}{\dot{m}_t} \tag{3.52}$$

The area under the PV diagram is defined as the work transferred to the screw rotors during the suction, expansion, and discharge processes [68]. All losses and included phenomena that occur from suction to discharge are encompassed in the indicated work. Furthermore, the specific indicated work can be calculated as well. The power of the compressor can be found using the work in a single compressor working chamber.

Theoretical isothermal work

$$W_t = mRT_s ln\frac{P_d}{P_s} \tag{3.53}$$

Work

$$W = \int V\, dp \tag{3.54}$$

Specific indicated work

$$W_{sind} = \int \frac{V}{m}\, dp \tag{3.55}$$

Indicated power

$$P_{ind} = \frac{W_{ind} z_1 n}{60} \tag{3.56}$$

Isothermal efficiency can be obtained using Eq. (3.57)

$$\eta_{iso} = \frac{W_t}{W_{ind}} \tag{3.57}$$

Bearing Power

Bearings are used within the compressor system. Bearings are used within the compressor to carry the radial and axial loads of the rotors. Significant losses are caused by bearings due to frictional loss. The type of bearing, operating conditions, and compressors impact the amount of bearing power losses. The bearing power loss is modeled using Eq. (3.58) which is obtained from Scorg help manual [69]. Where, D_f is the diameter factor, P_{ind} is the indicated power, w_{tip} is the tip speed, c is a coefficient, and F_{speed} is a speed factor. A diameter factor of 0.01 and speed factor of 1 was used to represent rolling bearings.

$$\frac{D_f P_{ind} w_t ip}{c F_{speed}} \tag{3.58}$$

CHAPTER 4

NUMERICAL MODEL

Numerical models are used when an analytical approach is difficult or not available. Although these models do not provide an exact solution, the approximate solution can be close enough to realistic outputs. A 1-D numerical model was developed in MATLAB to simulate the compression process of a twin screw compressor using helium as the working fluid. The model uses a combination of equations such as the conservation of energy, conservation of mass, and other thermodynamic relations. Although there is commercial modeling software readily available, in this research the model was created to alter models that aren't adjustable in commercial software. Additionally, several authors [52, 54, 70, 71] have provided thermodynamic models in literature and they are used here as a basis.

1-D numerical models can be useful tools that allow one to alter different parameters and gather an understanding of how they affect the performance and other parameters. Geometric terms such as wrap angle, rotor length, rotor combination, etc. can be modified to understand how the rotor geometry affects performance. Likewise, thermodynamic properties such as the mass flow rate of the working fluid, mass flow of oil, suction conditions, oil injection location, etc. can be better understood using a well-developed numerical model. Additionally, modelling can reduce time, energy, and resources used from reducing the amount of testing needed, as well as point you in the right direction for testing by providing strong performance predictions. In this chapter, the steps and details of the model are laid out. The flowchart of the numerical algorithm can be seen in Fig 4.1.

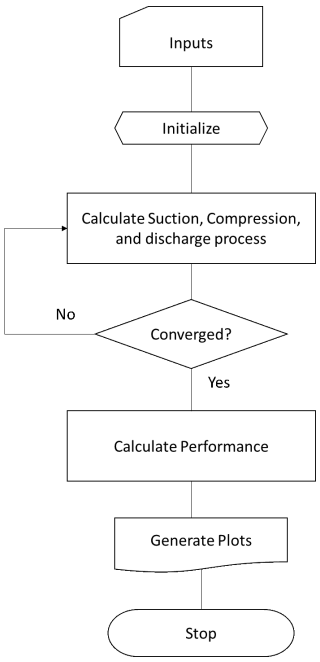

Figure 4.1: Model Flowchart

4.1 Summary of Governing Equations

A summary of the equations derived in Chapter 3 are restated here. Using these equations, the thermodynamic properties during compression and discharge can be determined with respect to the male rotation angle. The pressure and gas temperature during suction is assumed to be held constant. The numerical model illustrates the complete working cycle comprising of suction, compression, and discharge processes. Helium properties such as internal energy and enthalpy are calculated using ideal gas assumptions while oil properties are calculated using incompressible fluid state conditions. Density of helium is calculated using by dividing the mass of gas by volume of gas present in control volume.

Energy Conservation

$$dU = dQ - dW + \dot{m}_{in} h_{in} - \dot{m}_{out} h_{out} \tag{4.1}$$

Mass Conservation

$$dm = \dot{m}_{in} - \dot{m}_{out} \tag{4.2}$$

Mass flow model

$$\frac{dm}{d\varphi} = \frac{c\rho VA}{\omega} \tag{4.3}$$

Heat Transfer

$$\frac{dQ}{d\varphi} = \frac{hA(T_{gas} - T_{oil}}{\omega} \tag{4.4}$$

4.2 Input and Outputs of Thermodynamic Model

The numerical model inputs that are needed contain a mixture of data files and direct inputs. Data files include information that have been generated based on rotor geometries and are held constant for all cases within thermodynamic simulation. These inputs are necessary to begin computation and are found below.

4.2.1 Thermodynamic Model Inputs

- Data files
  - Cavity Volume
  - Axial suction area
  - Axial discharge area
  - Blow hole leakage area
  - Contact line length
- Direct Inputs
  - Suction Pressure
  - Discharge Pressure
  - Suction Temperature
  - Oil Inlet Temperature
  - Oil mass flow rate entering and exiting compressor – assumed constant

- Revolutions per minute (RPM)
- Helium Specific Heat – assumed constant
- Oil Specific Heat
- Oil Density

4.2.2 Thermodynamic Model Outputs

- Discharge pressure
- Discharge temperature
- Leaving oil temperature
- Gas mass
- Gas mass flow rate
- Isothermal Efficiency
- Volumetric Efficiency

The numerical model of the screw compressor outputs calculated thermodynamic properties within the working cycle from suction to discharge along with the performance behavior.

4.3 Functions of Thermodynamic Properties

Several thermodynamic properties are needed in the numerical model. Functions are embedded within the numerical model that calculate each property. Helium is used as the working fluid and this model, and all thermodynamic properties are based on it. The model can be adapted to evaluate other refrigerants easily. Thermodynamic properties are calculated using the functions below.

Fuction1(φ, P_s, P)

This function calculates the mass flow of gas entering the compressor with current pressure and suction pressure as inputs.

Function2(φ, P_d, P)

This function calculates the mass flow of gas leaving the compressor with current pressure and discharge pressure as inputs.

Function3(φ, $\dot{m}_{gas,in}$, $\dot{m}_{gas,out}$)

This function calculates the total mass of gas within the cavity using gas mass flow rates in and out of compressor or cavity as inputs.

Function4(φ, T_{gas}, P, $\dot{m}_{gas,in}$, $\dot{m}_{gas,out}$, m_{gas}, dQ)

This function calculates the gas temperature at the current angle. Pressure, gas mass flows in and out of compressor, heat transfer between gas and oil, and gas temperature are used as inputs.

Function5(φ, T_{gas}, P, dV_{gas}, $\dot{m}_{gas,in}$, $\dot{m}_{gas,out}$, m_{gas})

This function calculates the current pressure with previous pressure, gas mass flows in and out of compressor, change in gas volume, and gas temperature being used as inputs.

Function6(φ, $Toil$, P,$\dot{m}_{oil,in}$,$\dot{m}_{oil,out}$, m_{oil}, dQ)

This function is used to calculate the current temperature of oil. Pressure, oil mass flows in and out of compressor, heat transfer between gas and oil, and oil temperature are used as inputs.

Function7(φ, $Toil$, T_{gas}, m_{oil})

This function is used to calculate the change in heat transfer with inputs of oil temperature, gas temperature, and total mass of oil.

Function8(φ)

This function calculates the change in cavity volume with respect to the male rotor angle

Function9(φ, $Toil$, T_{gas}, m_{oil}, m_{gas}, P, dQ, dV_{gas})

This function calculates the change in internal energy with respect to the male rotor angle. The inputs used in this function are oil temperature, gas temperature, total mass of oil, total mass of gas, pressure within cavity, change in heat transfer, change in cavity volume.

Function10(φ, $dmoil_{in}$, $dmoil_{out}$)

This function is used to calculate the total amount of oil present in cavity using oil mass flow rates in and out of compressor or cavity as inputs.

Function11($Tgas$, P, fluid)

This function calculates the specific volume of helium. The inputs are gas temperature, pressure, and fluid type.

Function12($Toil$, P)

This function calculates the specific volume of oil. The inputs are oil temperature and pressure.

Function13((T_{gas}, P, fluid)

Function calculates the specific gas enthalpy. The inputs are gas temperature, pressure, and fluid type.

Function14($Toil$, P, $C_{p,oil}$)

Function calculates the specific oil enthalpy. The inputs are oil temperature, pressure, and specific heat of oil.

4.4 Procedure for Model Solution

This section will outline the numerical algorithm applied. The numerical model was executed using MATLAB as the programming language. MATLAB is a powerful program that can be used to analyze data, develop algorithms, and create models and applications. Geometry and input data are used to initialize the model. A schematic of the model process is shown in Fig. 4.2. Using the geometrical and operating conditions as inputs, the numerical model integrates over a span of theta the governing equations as presented in section 4.2 which produces valuable output data. A single cavity is observed from the time it encounters suction to the time the cavity disappears at end of discharge. A built-in MATLAB solver was employed to mimic the fifth-order Runge-Kutta method with an adaptive step size to decrease computational time. The ODE solver that is used in the thermodynamic model is 'ode45', which has the ability to solve nonstiff differential equations — medium order method [72].

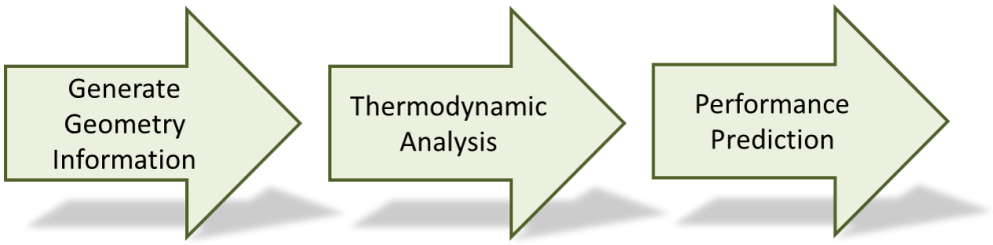

Figure 4.2: Model Schematic

All governing equations and thermodynamic property functions are calculated at each integration step. The thermodynamic properties use temperature and pressure values from the previous step in order to output the needed value to calculate the necessary governing equations at the next step. the suction pressure and temperature at intake are assumed to be provided from an infinite reservoir. Similarly, when the compressor cavity is open to discharge the change in pressure becomes constant as the cavity pressure reaches the discharge pressure boundary condition. All mass flow rates are solved using an isentropic converging nozzle model. The leakages that are accounted for in this program are the blowhole and contact line. These leakages were selected due to the high impact on compressor performance. All other leakages are ignored. The blowhole leaks from the leading cavity to the trailing, and the contact line leakage leaks back to suction from the current cavity. It is important to note that the leakage only account for gas. In order to compute the leakages, the leading cavity pressure must be known. Initially, this is not possible; therefore the model starts with an ideal (without leakages) case and generates a pressure fit with respect to angle. After the pressure fit with respect to male rotational area is attained, the model is evaluated with leakage flows. The iterations' cycle until the convergence criteria is met. When the thermodynamic properties of helium at end of simulation are known, the performance model is used to calculate isothermal and volumetric efficiencies and P-V diagram. A step by step list is found below to illustrate the thermodynamic numerical model.

Steps to calculate thermodynamic outputs

Step 1: Provide model initial conditions, boundary conditions, volume, suction area, discharge area, speed of compressor, and assume no leakages present.

Step 2: Compute mass flow rate of gas entering volume

Step 3: Compute mass flow rate of the gas leaving the control volume

Step 4: Compute total mass flow rate of gas within the control volume

Step 5: Compute mass flow rate of oil entering volume via injection port

Step 6: Compute mass flow rate of oil leaving control volume through discharge

oil mass flow rate entering and exiting is assumed to be constant.

Step 7: Compute total mass flow rate of oil within the control volume

Step 8: Compute volume change of oil

Step 9: Compute volume change of gas

Step 10: Calculate heat transfer rate

Step 11: Calculate the gas temperature derivative

Step 12: Calculate pressure differential

Step 13: Calculate the oil temperature derivative

Step 14: Calculated new state parameters and proceed to next step

4.5 Numerical Model Validation

The numerical model performance prediction code is compared to SCORG performance output in order to confirm the validity of the numerical model. SCORG is a performance prediction software widely used within industry for positive displacement compressors [69]. Scorg has the capability to design rotor profiles, generate geometric curves, predict performance using 1-D thermodynamic simulation, and generate a numerical grid. SCORG 1-D simulation is fast and reliable. For comparison, SCORG generated rotor profile and geometric curves based on specified rotor details. The geometric output was then used to evaluate the performance at various conditions that are compared to the numerical model created in this work.

The compressor capacity, rotor profile, and all geometric curves are kept constant for all evaluated running conditions. The comparison is done by varying several running conditions: suction pressure, discharge pressure, and oil injection temperature. The suction pressure varies

from 1.02 bar to 1.3 bar. The discharge pressure spans from 5 bar to 9 bar. The oil injection temperature goes from 100 °F to 130 °F. The numerical model and SCORG is within reasonable agreement. The maximum performance prediciton difference between the two models is 6% and 13% for volumetric efficiency and isothermal efficiency respectively.

Numerical model vs. SCORG for various discharge pressures

The numerical model and SCORG performance plots are seen in Figs. 4.3 and 4.4 for varying discharge pressure. The accuracy of the volumetric efficiency was higher than the isothermal efficiency. The volumetric efficiency ranged from 1-6%, and the isothermal efficiency ranged from 1-13%. This shows that the model is more sensitive to discharge pressure varitions. Simulated twin screw compressor running conditions:

- Working fluid: Helium
- Speed: 3550 rpm
- Suction pressure: 1.1 bar
- Oil injection temperature: 110°F

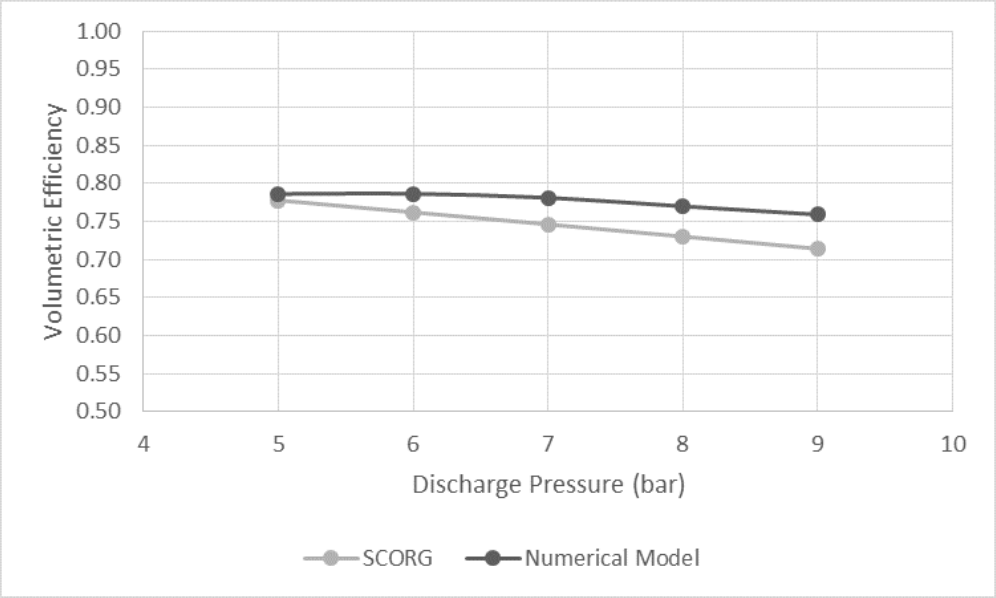

Figure 4.3: SCORG and Numerical Model volumetric comparison for varying discharge pressure

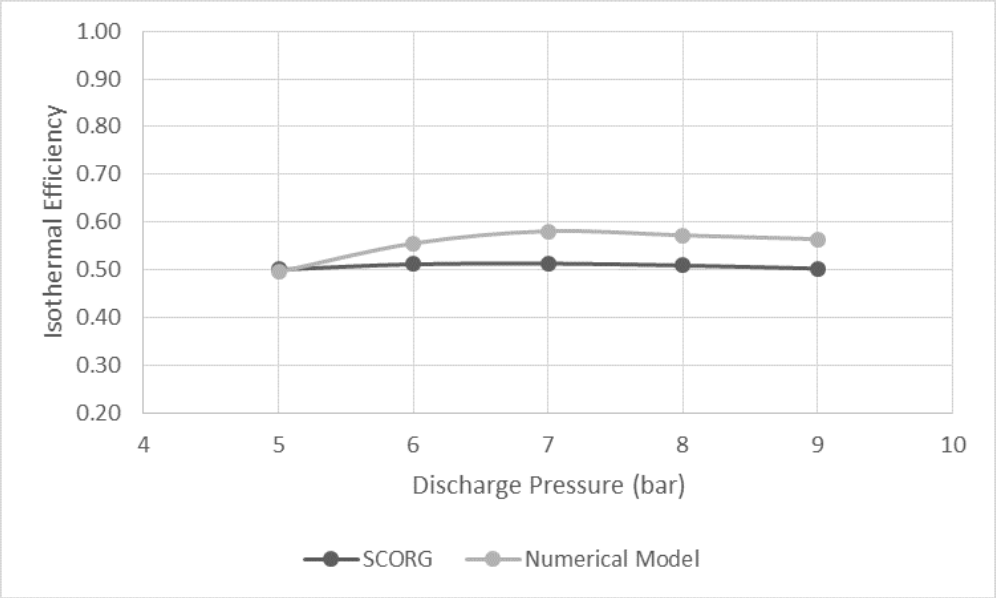

Figure 4.4: Isothermal comparison for varying discharge pressure

Numerical model vs. SCORG for various suction pressures The numerical model and SCORG performance plots are seen in Figs. 4.3 and 4.4 for varying suction pressure. The volumetric efficiency ranged from 4-5% and the isothermal efficiency ranged from 2-3%. The simulated twin screw compressor running conditions are:

- Working fluid: Helium
- Speed: 3550 rpm
- Discharge pressure: 8 bar
- Oil injection temperature: 110°F

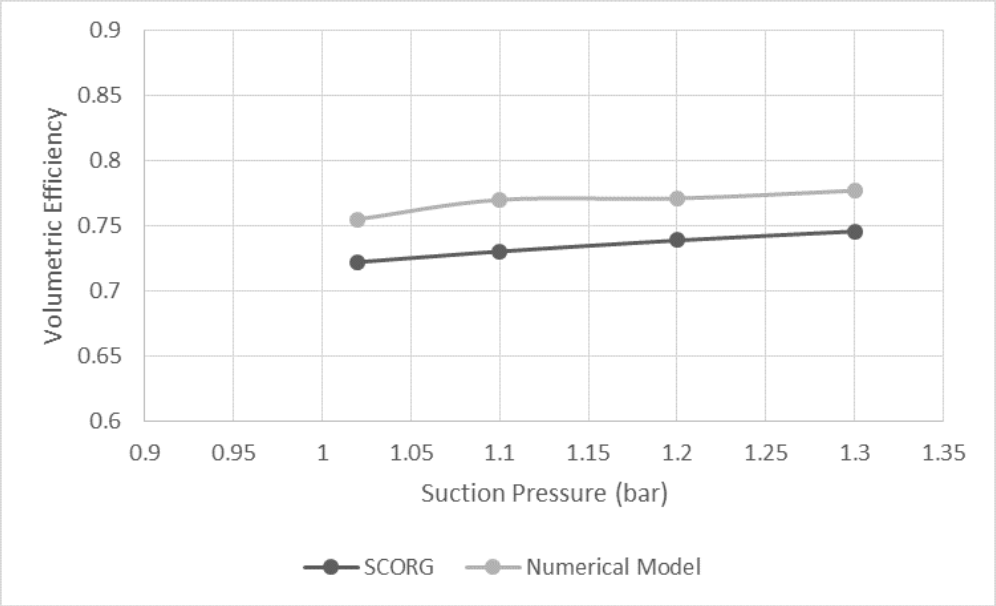

Figure 4.5: Volumetric comparison for varying suction pressure

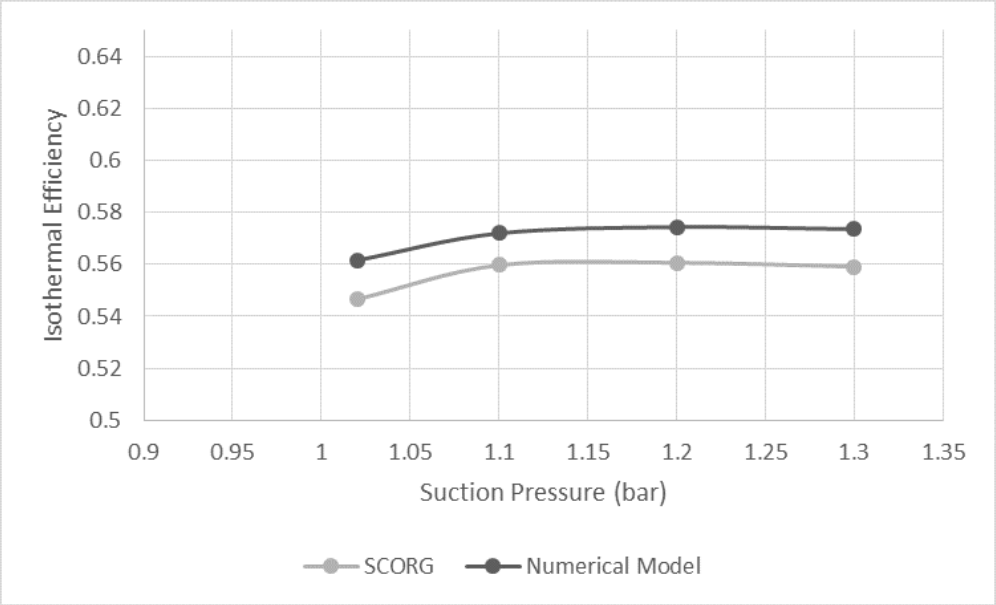

Figure 4.6: Isothermal Efficiency Comparison for Varying Suction Pressure

Numerical model vs. SCORG for various oil injection temperatures The numerical model and SCORG performance plots are seen in Figs. 4.3 and 4.4 for varying discharge pressure. The performance variation is very minimal with the change of oil injection temperature. This model

shows that the performance of the compressor isn't strongly impacted by oil injection temperatures.

Simulated twin screw compressor running conditions:

- Working fluid: Helium
- Speed: 3550 rpm
- Suction pressure: 1.1 bar
- Discharge pressure: 8 bar

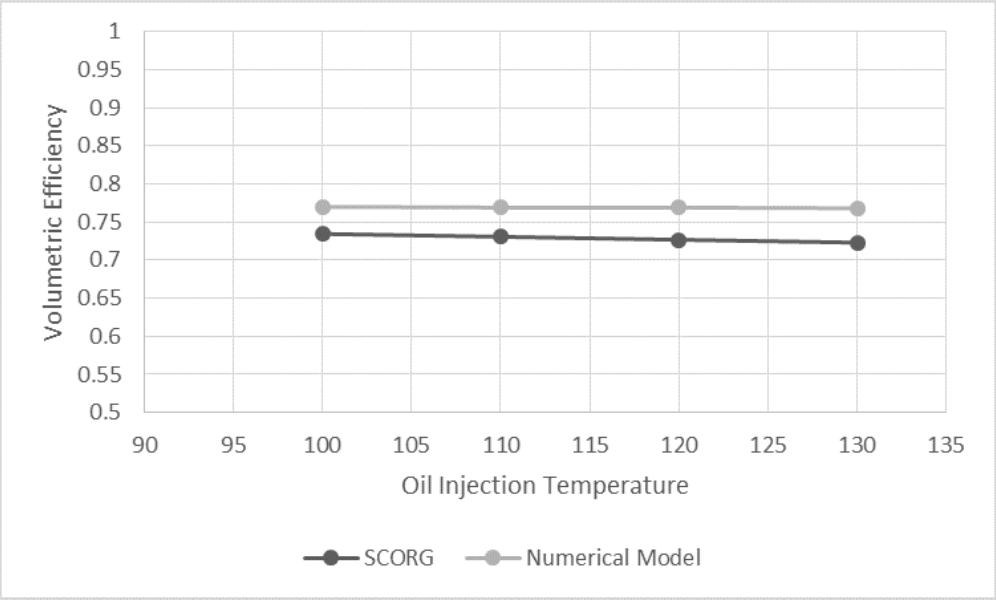

Figure 4.7: Volumetric efficiency comparison for varying oil injection temperature

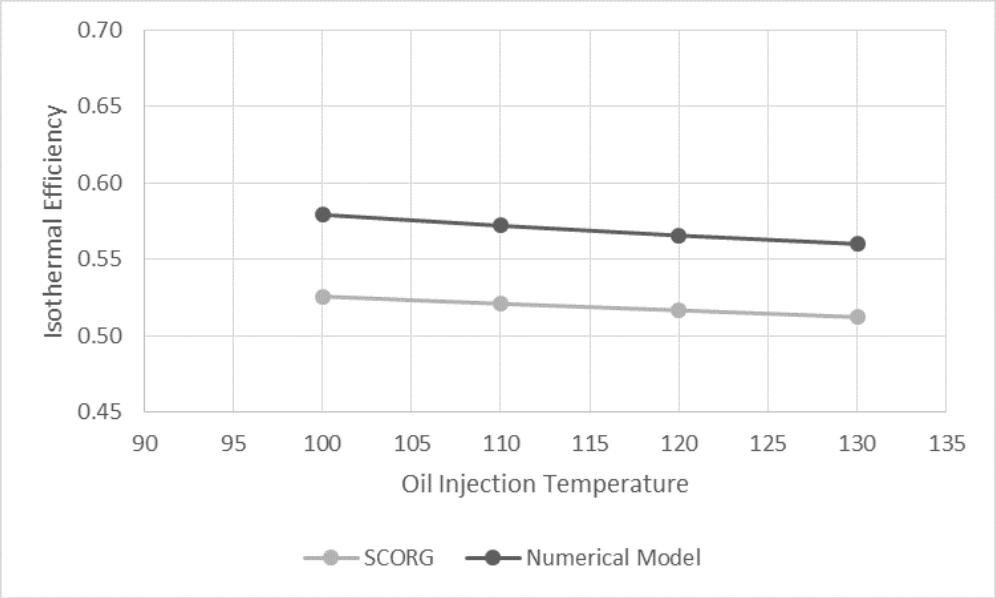

Figure 4.8: Isothermal efficiency comparison for varying oil injection temperature

4.6 Numerical Model Results

An example of the numerical model simulated is presented in this section. The numerical model mimics the suction, compression, and discharge processes that take place in the compressor. Upon completion, several plots are generated to characterize the behavior of the compressor. Additionally, a message box is created to display performance and discharge temperature values. The use of this numerical model output information can help improve compressor design and running conditions. The details of the example simulation and generated plots are provided here.

Compressor Specifications:

- Rotor Profile: 5+6
- Male rotor outer radius: 63.6 mm
- Female rotor outer radius: 50.4 mm
- Male rotor inner radius: 39.6 mm
- Female rotor inner radius: 26.4 mm
- Helix Angle: 46°
- Length of Rotor: 205.9 mm

Running conditions of model:

- Working fluid: Helium
- Speed: 3550 rpm
- Suction pressure: 1.1 bar
- Discharge pressure: 8 bar
- Suction temperature: 62.33°F
- Oil injection temperature: 100°F

Plots generated from numerical model:

- P-V diagram
- Pressure curve
- Gas Temperature curve
- Gas Temperature curve vs. oil temperature plot
- Gas mass within compressor cavity
- All mass of gas flows

The p-V diagram is shown in Fig. 4.9. The p-v diagram is essential in determining performance. From this plot, one can determine whether the working conditions are ideal, over-compressed, or under-compressed for the specific compressor design. In this case, under-compression occurs, which means that the cavity pressure is lower than desired discharge pressure at the end of the compression process. An ideal outcome is desired and can be achieved by changing conditions or increasing built-in volume ratio. Another outcome of the p-V diagram is the indicated power calculation. The indicated work is determined by calculating the area underneath the pressure curve and the indicated power can further be determined from the indicated work.

The pressure within the cavity versus the male rotational angle is shown in Fig. 4.10. The temperature of helium and oil within the cavity versus the male rotational angle is shown in Fig.4.11. The helium temperature is constant until the start of compression. Similarly, the oil temperature is constant until oil is injected into the compressor. The oil is modeled to enter the compressor at the start of compression. The oil gains heat from the helium as the helium temperature increases.At

discharge, the helium and oil are at equilibrium. Fig. 4.12 shows the cavity, suction, discharge, leakage in, and leakage out masses. Due to under-compression at end of compression the mass flow out becomes negative. The volumetric and isothermal efficiencies are displayed in Fig. 4.13 along with the helium and oil discharge temperatures.

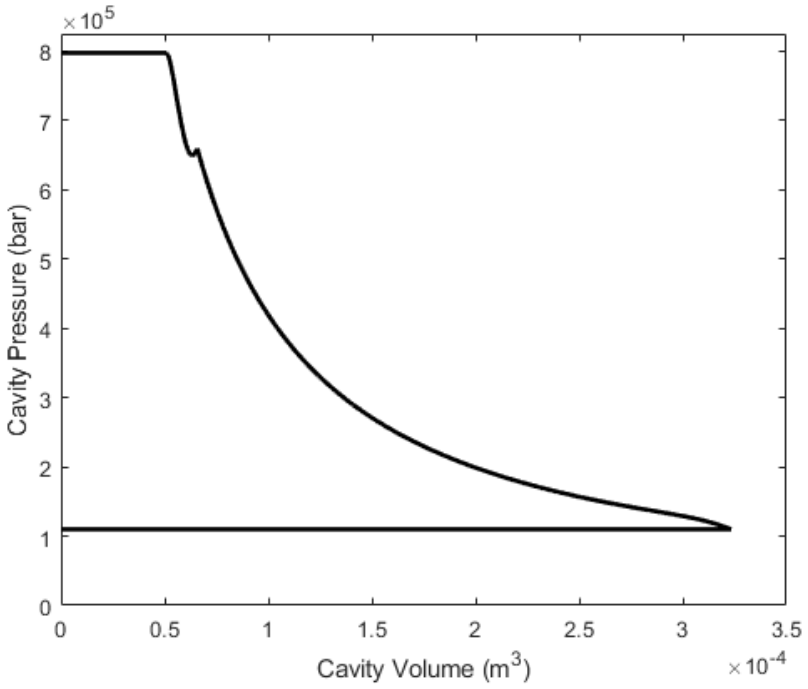

Figure 4.9: p-V diagram

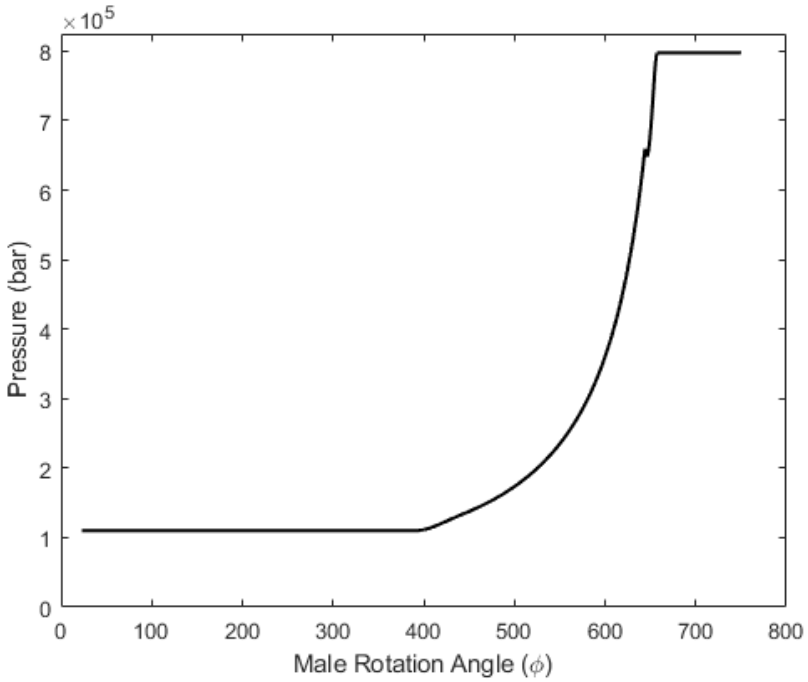

Figure 4.10: Pressure curve vs. male rotation angle

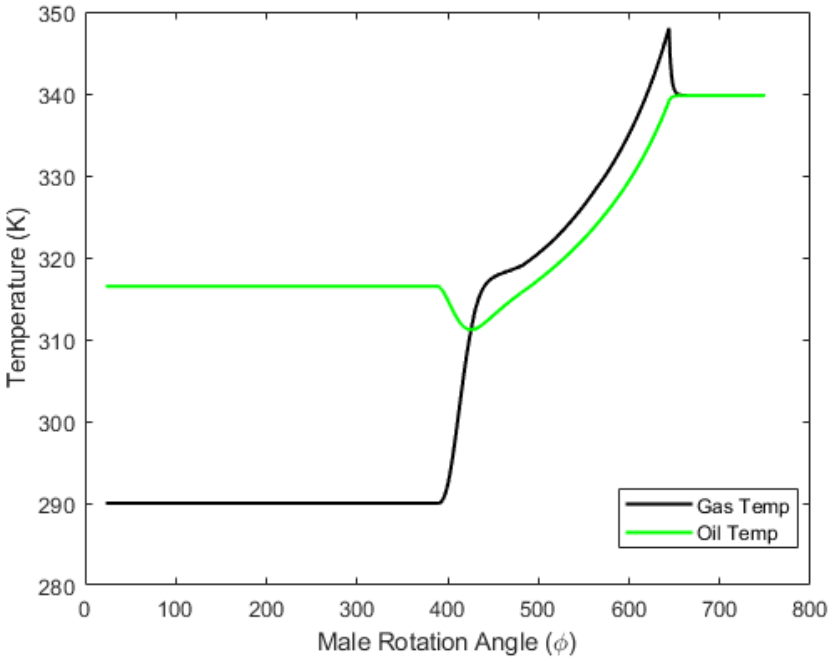

Figure 4.11: Helium vs. Oil Temperature

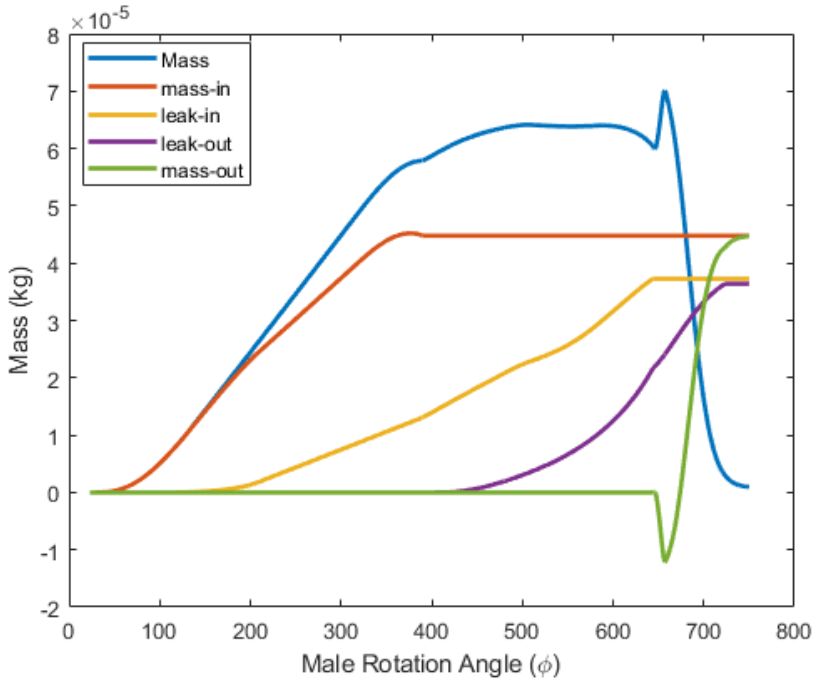

Figure 4.12: Various gas mass flows in cavity vs. male rotation angle

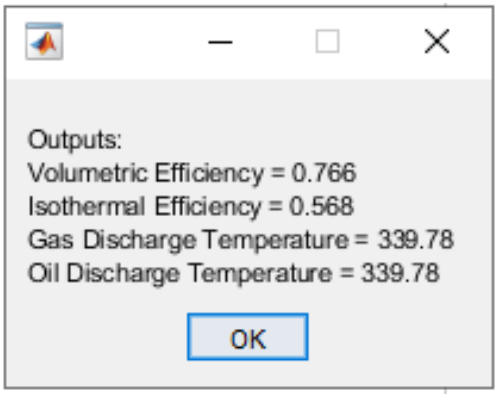

Figure 4.13: Helium vs. Oil Temperature

4.7 Oil injection analysis within screw compressor

In this section,the numerical model is used to study the impact of oil injection on the performance of the compressor. The oil injection location and oil flow rate are the varied parameters. The oil injection location ranges from end of suction (θ = 390°) to just before discharge (θ = 555°). The mass flow rate is altered to keep the discharge temperature between 327K to 363K. The droplet size

of the oil used was 0.1 mm and was kept constant throughout analysis. The discharge temperature and isothermal efficiecy are desired outputs. Since the oil volume is neglected, the volumetric efficiency to remain nearly constant for all changes in oil injection location and oil flow rate. The details of simulation are shown below.

Compressor Specifications:

- Rotor Profile: 5+6
- Male rotor outer radius: 63.6 mm
- Female rotor outer radius: 50.4 mm
- Male rotor inner radius: 39.6 mm
- Female rotor inner radius: 26.4 mm
- Helix Angle: 46°
- Length of Rotor: 205.9 mm

Running conditions of model:

- Working fluid: Helium
- Speed: 3550 rpm
- Suction pressure: 1.1 bar
- Discharge pressure: 8 bar
- Suction temperature: 62.33°F
- Oil injection temperature: 110°F

The results are shown in Figs. 4.16-4.15 where the x-axis is the mass flow rate variation and the y-axis is the output values of discharge temperature or isothermal efficiency. The different lines shown represent the oil injection location in degrees. Fig. 4.16 showed that the discharge temperature decreases as the mass flow rate increases. The increase in discharge is caused by the lack of oil and helium interaction as the oil injection moves further from suction. Also, as the oil injection port moves closer to discharge, the temperature at discharge increases. This is due to the fact that there is less oil within the cavity, which reduces oil's ability to seal and cool. This suggest that the discharge temperature of helium is impacted greatly by the mass flow rate and injection

location of oil. The influence of oil injection on the isothermal efficiency is shown in Fig.4.14 . This shows that the isothermal efficiency increases as oil mass flow rate increases. The results also show that the isothermal efficiency decreases as the oil injection port gets closer to discharge. These outcomes are a direct result of the lower discharge temperatures previously mentioned. Therefore, oil injection location and mass flow rate has a strong impact on the isothermal efficiency. Oil drag forces are neglected within this model, so the true impact of increasing the oil mass flow rate is not observed.

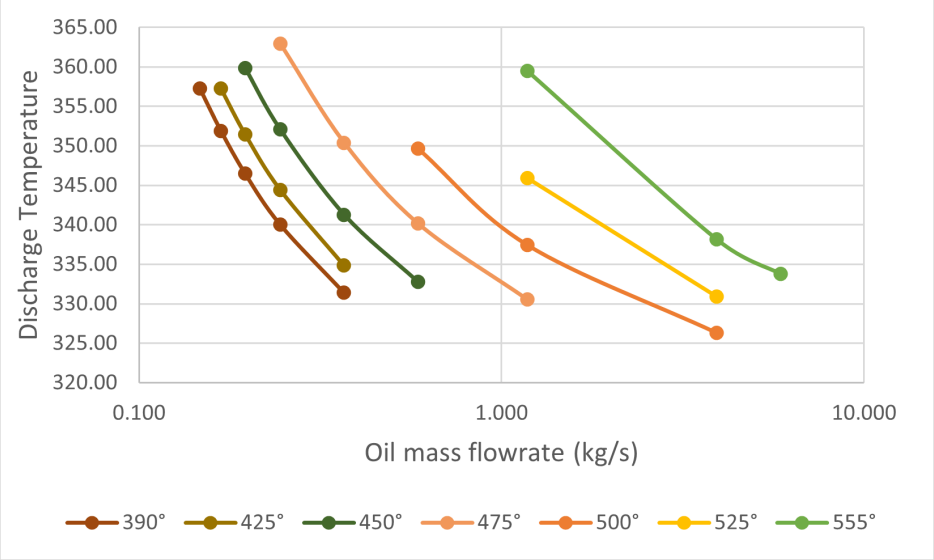

Figure 4.14: Oil injection influence on discharge temperature

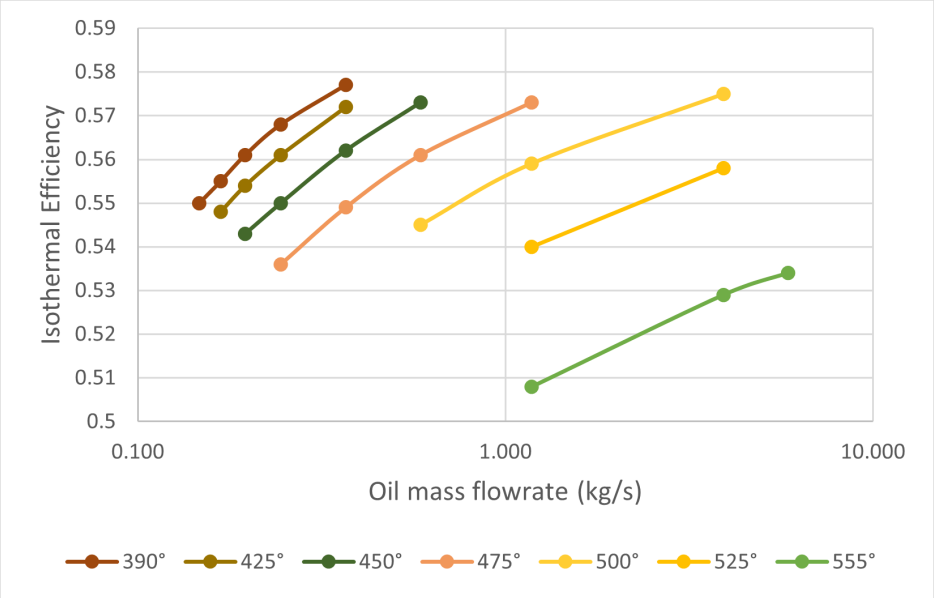

Figure 4.15: Oil injection influence on isothermal efficiency

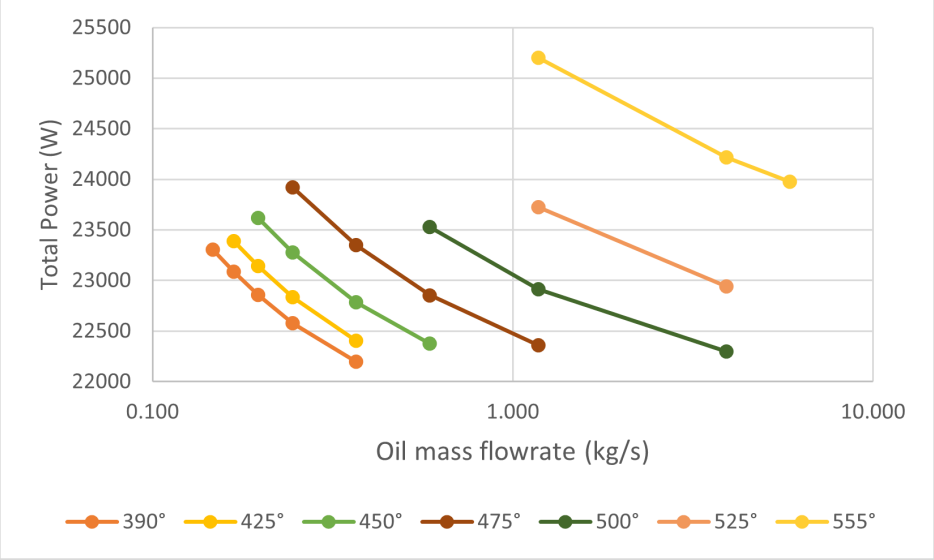

Figure 4.16: Oil injection influence on power

CHAPTER 5

SCREW COMPRESSOR EXPERIMENTAL INVESTIGATION

5.1 Test Screw Compressor rated at 150HP

The power requirement to use a compressor is often the bulk of the energy needed within a system. Since the compressor comprises the largest source of lost input power, understanding these losses and developing improvements and changes to reduces these losses is of primary importance to improve overall system efficiency. The compressor performance is studied observing various aspects of the compressor such as rotor design and operating conditions. Each has a large impact on the compressor performance. In this dissertation, the focus is on understanding the performance fluctuations as the thermodynamic parameters are adjusted. Furthermore, undergoing compressor experimentation is important in comprehending how to reduce the irreversibilities at different operating conditions.

The main objective of conducting compressor testing is to gain insight on how the isothermal and volumetric efficiencies are impacted by various thermodynamic parameters. Different thermodynamic properties are evaluated to understand their effect on oil and helium equilibrium during compression cycle. In this chapter, test setup, instrumentation, and volumetric and isothermal efficiencies measurements are outlined.

5.2 Compressor Test Setup

A 150HP Hartford MSC-127 Series compressor with theoretical capacity of 22g/s is used for testing. This oil- flodded screw compressor is a hermetically sealed compressor using helium as the process fluid. The simplified flow diagram of the compressor skid is shown in Fig. 5.5 and a picture of the physical compressor skid is found in Fig. 5.6

Skid Equipment

Compressor

Make: Hartford

Model: MSC-127

Capacity: 22g/s

Maximum allowable working pressure: 410PSIG

Maximum Discharge: 18atm

Motor: 150 HP, 3600rpm

Helium Cooler

Make: Standard Xchange

Model: BP415-40

Duty: 16.653 kBtu/hr

M.W.A.P: 435psig

Oil Cooler

Make: Standard Xchange

Model: BP415-40

Duty: 237.4 kBtu/hr

M.W.A.P: 435 psig

Relief Valve

Make: Mercer Valve Co., inc

Model: Series 9100

Oil Flow Needle Valve

Make: Deltrol

Model: E3210

Back Pressure Regulator

Make: Parker

Model: Flo-Con

Oil Level Switch

Make: Henry Laboratories

Model:E-9400 Series

Lubricating Oil

Type: CP-4600-48

5.3 Selection of Measurement Device, Equipment, and Probes

There are several measurement devices used during testing to gather temperature, pressure, mass flow, and input power readings at several different locations throughout the compressor skid. The surface temperature measurements were taken using temperature sensors, thermocouples, and a temperature probe. The pressure measurements were taken using a pressure transducer and pressure transmitter. The mass flows for the oil and helium were measured using a Coriolis flow meter and a venturi flow meter. A current and AC voltage transducer along with a analog input card was used to record power measurement. Exact measurement devices are listed below.

Table 5.1: Flow meters

Device	**Details**	**Location**
Coriolis Flow Meter	Make: Micro Motion Inc Model: Elite Coriolis meter	Bypass gas and Oil Injection
Venturi Flow Meter	Make: Primary Flow signal	Bypass gas

Table 5.2: Temperature Measurement Devices

Device	**Details**	**Location**
Temperature Probe	Make: Fluke Model: 80PK-27	Compressor suction, compressor discharge, oil injection, entering water, and leaving water.
Thermocouple	Make:McMaster-Carr Model:9251T94	Compressor suction, compressor discharge, oil injection, oil compressor discharge, entering water, and leaving water
Temperature Sensor	Make: Prosense Model: RTD Bolt-on ring sensors	Compressor discharge and oil injection

Figure 5.1: Temperature Probe

Figure 5.2: Temperature Sensor

Figure 5.3: Installed Thermocouple

Table 5.3: Pressure Measurement Devices

Device	Details	Location
Pressure Transducer	Make: Endress+Hausser Model: Cerabar T PMP131	Compressor suction and compressor discharge.
Pressure Transmitter	Make: Emerson Model:Rosemont 3051	Compressor suction

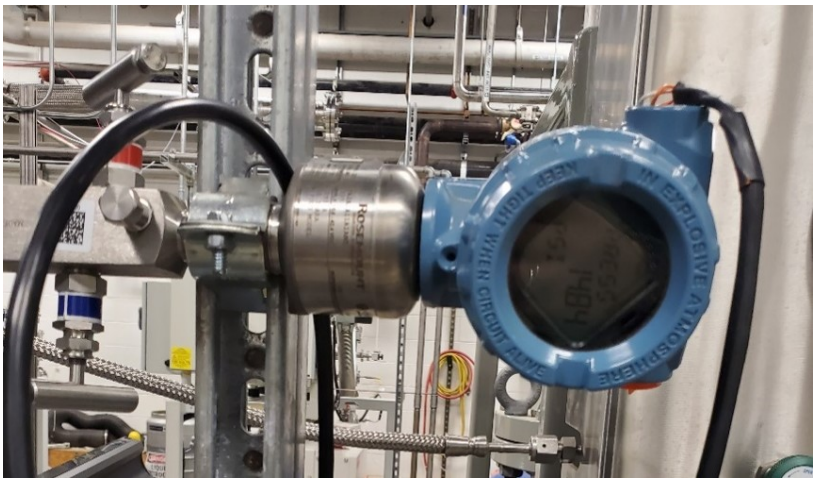

Figure 5.4: Rosemount Pressure Transmitter

Table 5.4: Power Measurement Devices

Device	Details
Current Transducer	Make: Ohio Semitronics Model: ACT-200E2
AC Voltage Transducer	Make:CR Magnetics Inc. Model:CR4580-500
Analog Input Card	Make: Allen-Bradley Model: 1769-IF8
Power Quality Analyzer	Make: Fluke Model: 434

5.4 Defining Measurements Matrix

A combination of suction pressure, discharge pressure, compressor discharge temperature, and oil injection temperature points are evaluated and defined in Table 5.5. Each parameter is is varied, while the other are fixed to understand its effect on the isothermal and volumetric efficiencies. To to vary each parameter while keeping the others fixed there are various, there are various changes

that must be made to the compressor skid. Each adjusted parameter, change to compressor skid, and limitations of changes will be described in this section.

Suction and discharge pressures

The bypass control valve regulates the compressor suction pressure. The discharge pressure is set by the total gas charge since the compressor is being tested in a closed loop. As the total charge increases, the discharge pressure increases as well and vice versa. Adjusting the charge is referred to as massing into and out of the system. The discharge pressure is also limited by the back pressure regulator. The minimum pressure differential for the Hartford compressor is 6 bar. Furthermore, variations in the suction can cause the discharge to vary since the mass flow through the compressor is proportional to it. However, assuming the mass-in and mass-out valves are not leaking, these variations will settle since the gas charge is fixed.

Oil inlet temperature

The oil inlet temperature parameter is controlled by modifying the cooling water flow. The maximum oil injection is 240 °F. The water flow ranges from 4 GPM to 27 GPM, and the water inlet temperature ranges from 24 °C to 32 °C.

Helium discharge temperature

The helium discharge temperature parameter is controlled by adjusting the amount of oil injected into the compressor by using the oil flow needle valve. The max discharge temperature for the compressor is 99 °C.

Table 5.5: Test Matrix

Suction Pressure (bar)	Discharge Pressure (bar)	Compressor Discharge Temperature (ºF)	Oil Injection Temperature (ºF)
1.02	14	150	110
1.1	15	170	120
1.2	16	190	130

5.5 Data Collection and Reduction

Duting testing, the data is collected using CS-Studio8. Upon completion, the data is organized and performance parameters are calculated. Additionally, the mass flow rates and temperatures are calculated using energy balance equation to check for accuracy of measurement devices. Additionally, the performance indicators equations are defined in this section.

Discharge temperature

The discharge temperature is calculated using measured terms to cross-check measured discharge temperature for accuracy.

$$T_2 = \frac{\dot{W}' + \dot{m}'_h C_{p,h} + m'_o C_{p,o} T'_{o,i}}{\dot{m}'_h C_{p,h} + m'_o C_{p,o} T'_{o,i}} \tag{5.1}$$

The measured terms from testing that are used for discharge temperature cross-check calculation are power $\dot{W}$, helium mass flow ($\dot{m}_h$), oil mass flow ($\dot{m}_o$), Helium specific heats($C_{p,h}$), oil specific heat ($C_{p,o}$), Helium inlet temp (T_{h1}), and oil inlet temp ($T_{o,i}$). Oil and helium discharge temperatures are the same, and no oil is being injected at inlet conditions are assumed

Helium Flow Mass Flow Rate

$$\dot{m}_{theo} = \frac{\rho V_c N}{60} \tag{5.2}$$

Oil flow mass flow rate

$$\dot{m}_o = \frac{\dot{W}' - \dot{m}'_h C_{p,h} (T'_{h,d} - T'_{h,s})}{C_{p,h} (T'_{o,D} - T'_{o,i})} \tag{5.3}$$

Isothermal efficiency

The isothermal efficiency is defined as the isothermal work to the actual work as shown in Eq. (5.7). The isothermal work is calculated using Eq. (5.4) where $\dot{m}_h$ is the measured helium flow

rate determined using the Coriolis flow meter at the inlet of the compressor.

$$\dot{W}_{T,rev} = \dot{m}'_h \phi C_{p,h} T'_{h,s} ln(p_r) \tag{5.4}$$

$$p_r = \frac{p'_{h,D}}{p'_{h,s}} \tag{5.5}$$

$$\dot{W}_{iso} = \dot{m}'_h \phi C_{p,h} T'_{h,s} ln(p_r) = 30.28kW \tag{5.6}$$

$$\eta_T = \frac{\dot{W}_{iso}}{\dot{W}_{actual}} \tag{5.7}$$

Volumetric efficiency

The Volumetric efficiency is defined as a ratio of the actual amount of gas to the theoretical amount of gas. The efficiency calculation is specified in Eq. (5.8) . The actual amount of gas is determined by experimental measurement and measured by a Coriolis meter and a venturi and they matched closely within 1%. The theoretical amount of gas is calculated using Eq. (5.2) at suction conditions using suction pressure and helium suction temperature.

$$\eta_v = \frac{\dot{m}_{actual}}{\dot{m}_{theo}} \tag{5.8}$$

where

C_p	Specific heat
$\dot{m}$	Mass
T	Temperature
η_T	Isothermal Work
η_v	Volumetric efficiency
$\dot{W}$	Work

Subscripts

calc	Calculated Value
d	Discharge
h	Helium
i	Injected
iso	Isothermal
o	Oil
s	Suction

Denotation

$'$	Measured value

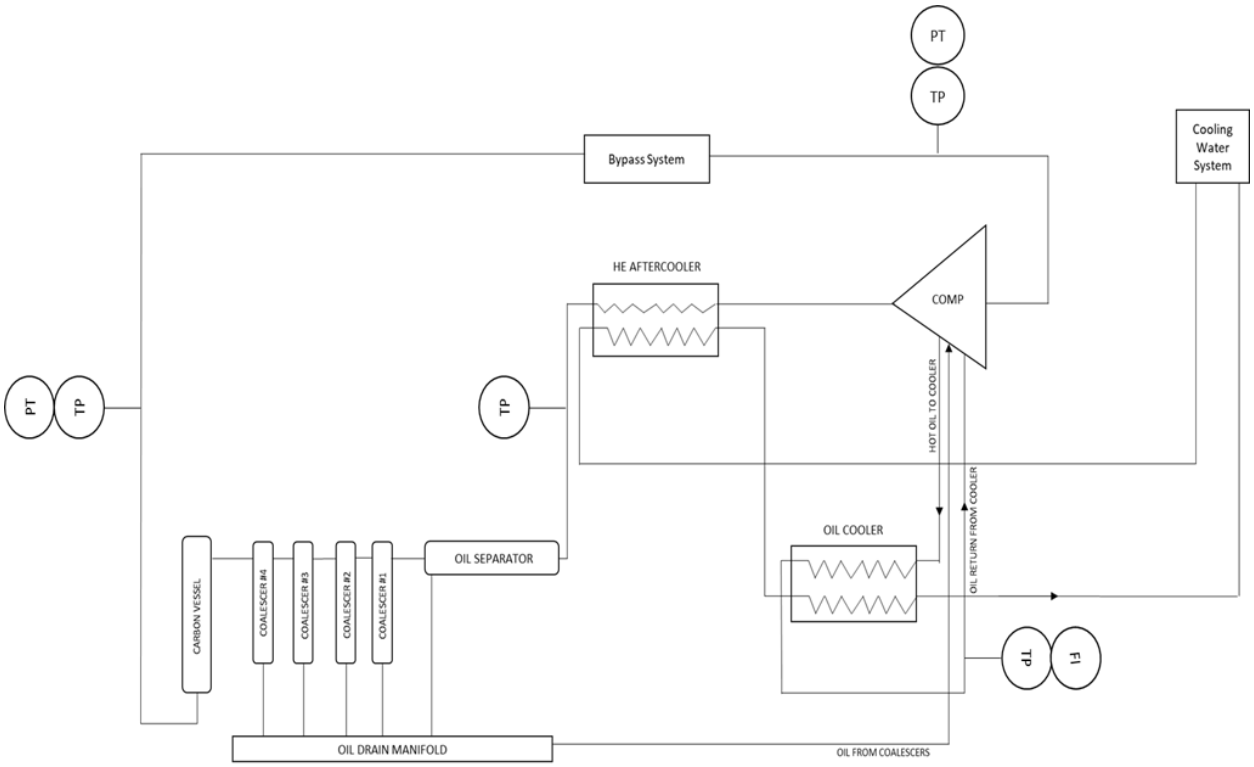

Figure 5.5: Compressor Skid Diagram

Figure 5.6: Compressor Skid

CHAPTER 6

EXPERIMENTAL RESULTS AND DISCUSSIONS

This chapter presents results obtained during testing of the compressor using the set-up described in chapter 5. The isothermal and volumetric efficiencies are observed when changing several parameters. The performance criteria in this study are the volumetric and isothermal efficiency. Volumetric efficiency is defined as the amount of gas displaced to the theoretical amount of gas that should be displaced. The isothermal efficiency is defined as the minimum amount of work to the actual amount of work into the system.

The operating parameters that are tested in this study are:

- Compressor discharge to suction pressure ratio
- Suction pressure
- Discharge temperature
- Oil injection temperature

6.1 Pressure Ratio (PR) vs. Performance at each suction

Pressure ratio is the pressure at discharge divided by the suction pressure. Figs. 6.1 and 6.2 show that the isothermal and volumetric efficiencies decrease with the increased pressure ratio at various oil injection temperature while keeping discharge temperature and suction pressure constant. Both performance parameters are impacted in this way because the leakages increase with higher pressure ratios which decreases the delivered volume flow rate. The pressure ratio, however, has a larger influence on the volumetric efficiency.

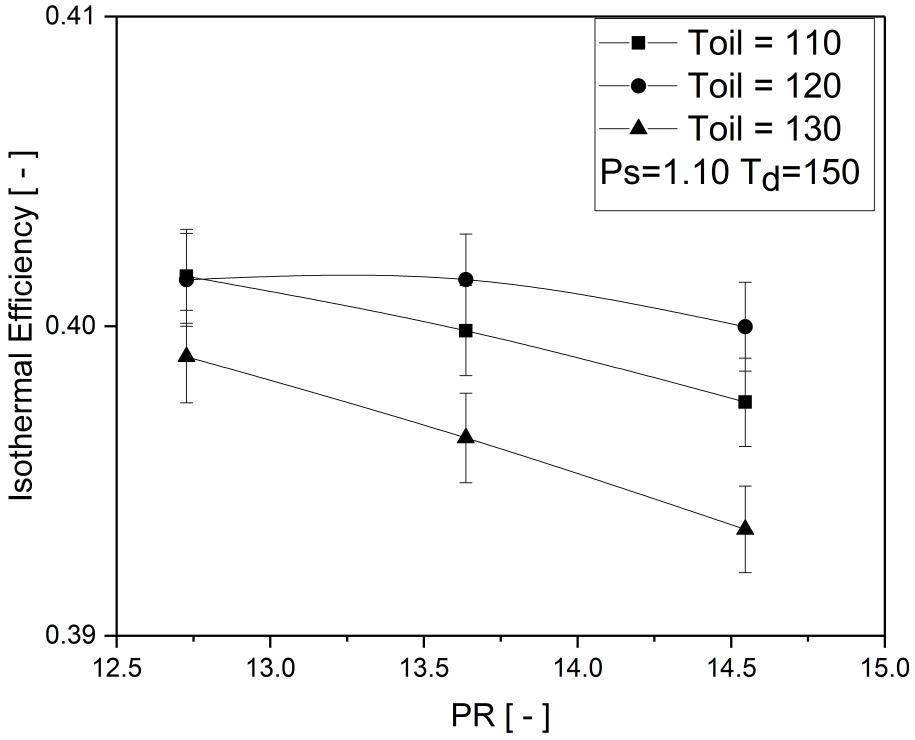

Figure 6.1: Pressure Ratio vs. Isothermal Efficiency

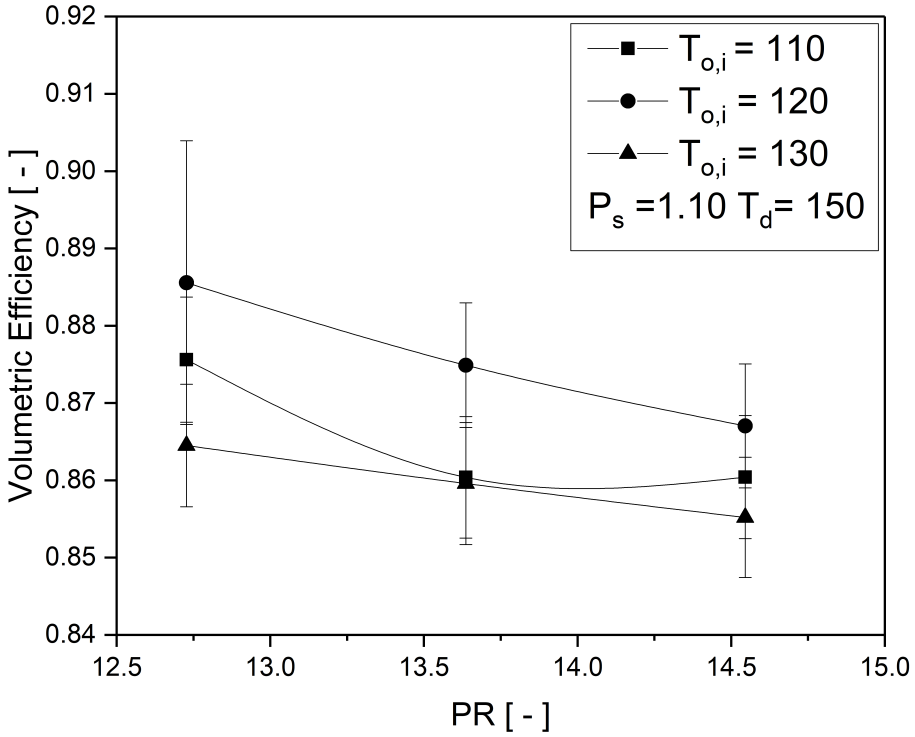

Figure 6.2: Pressure Ratio vs. Volumetric Efficiency

6.2 Suction Pressure Effect on Performance

The suction pressure impact on performance was assessed. Figs. 6.3 and 6.4 shows the suction performance profiles with respect to suction pressure with 3 different oil injections temperatures. As suction increases, the performance also increases. This is best explained by an increase in mass flow. Increased mass flow through suction is known to occur with the increase of suction pressure as seen in literature [3]. Additionally, suction pressure has a proportional relationship with the power of compression. Higher suction pressure results in reduction in leakage losses. As losses are reduced, the performance increases.

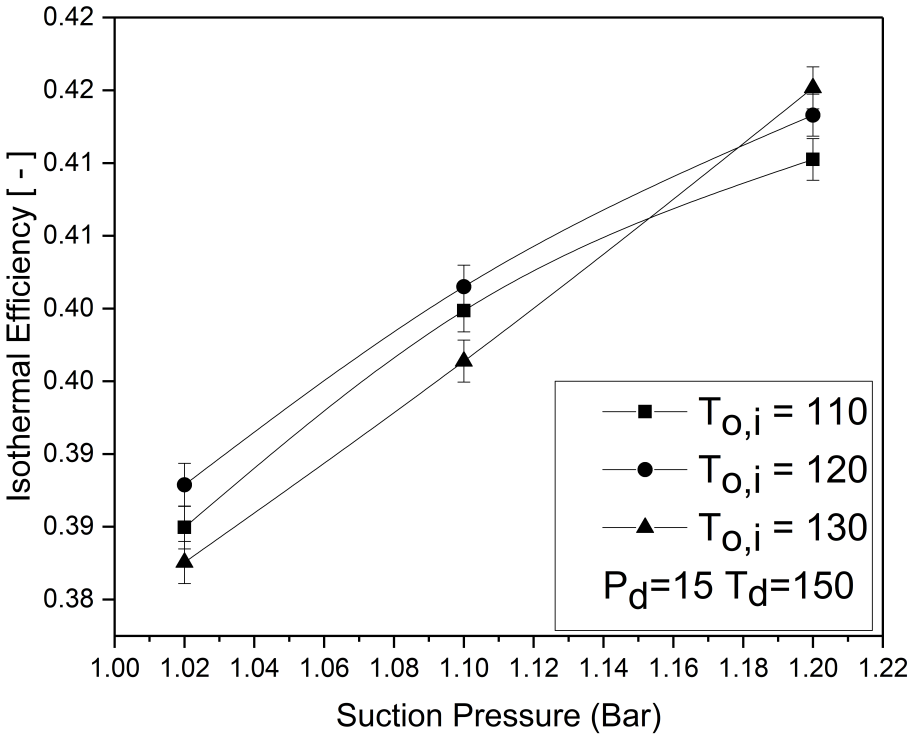

Figure 6.3: Suction Pressure vs. Isothermal Efficiency

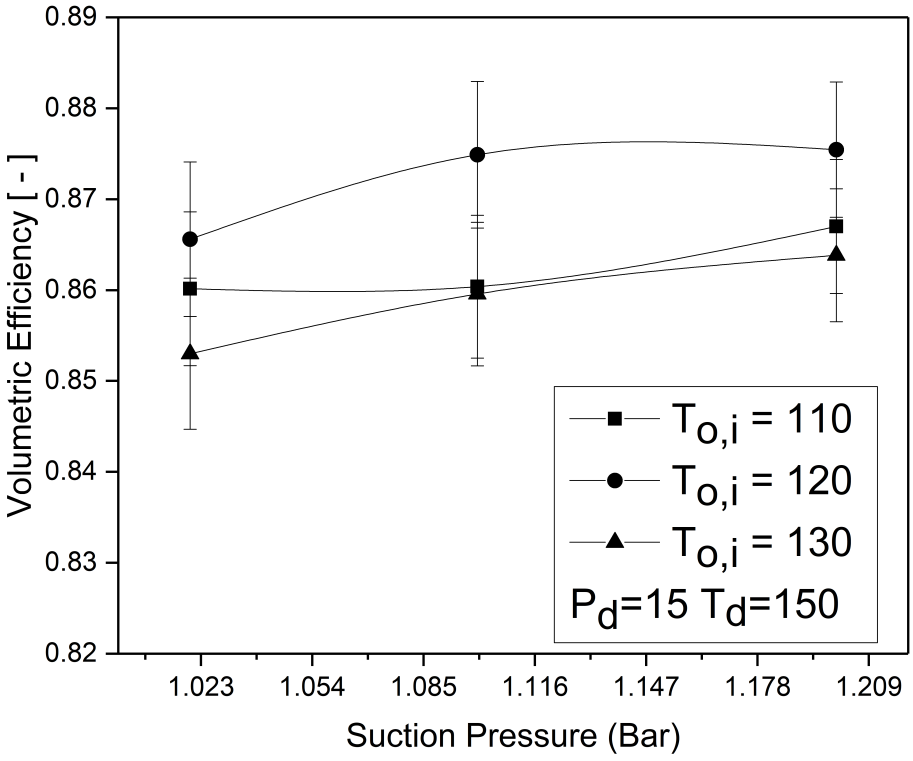

Figure 6.4: Suction Pressure vs. Volumetric Efficiency

6.3 Discharge Temperature Impact on Performance

The effect of the discharge temperature of helium on performance is seen in Figs. 6.5 and 6.6. As the discharge temperature increases, the isothermal and volumetric efficiencies decrease. This is caused by the decrease in helium mass flow with the temperature increase. The reduced mass flow rates occur because of oil viscosity variations. As the temperature increases, the viscosity of oil decreases, resulting in more leakages.

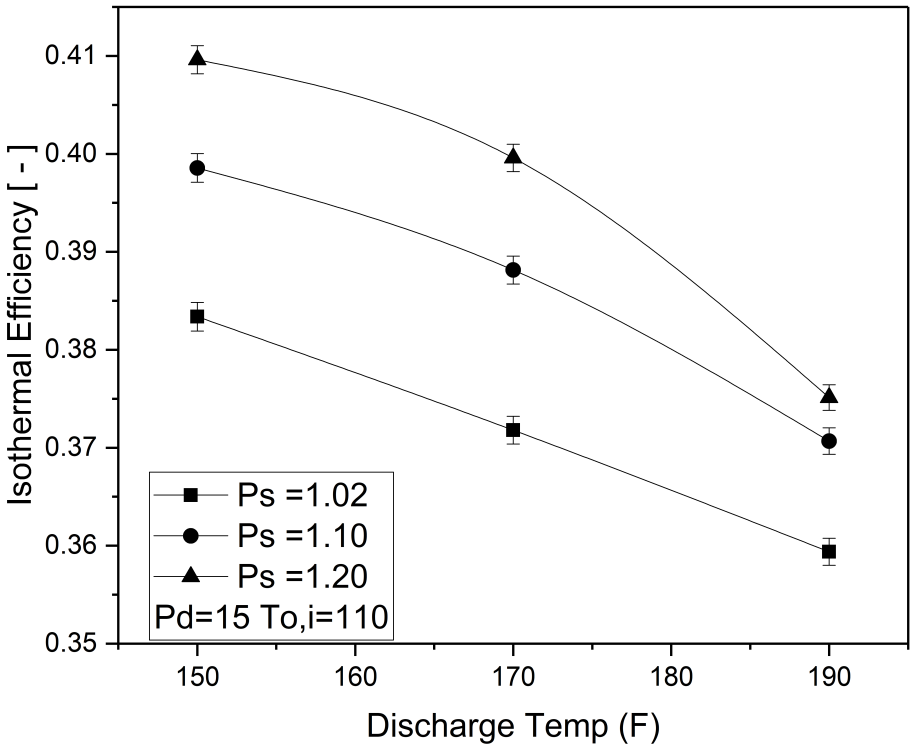

Figure 6.5: Discharge Temp vs. Isothermal Efficiency

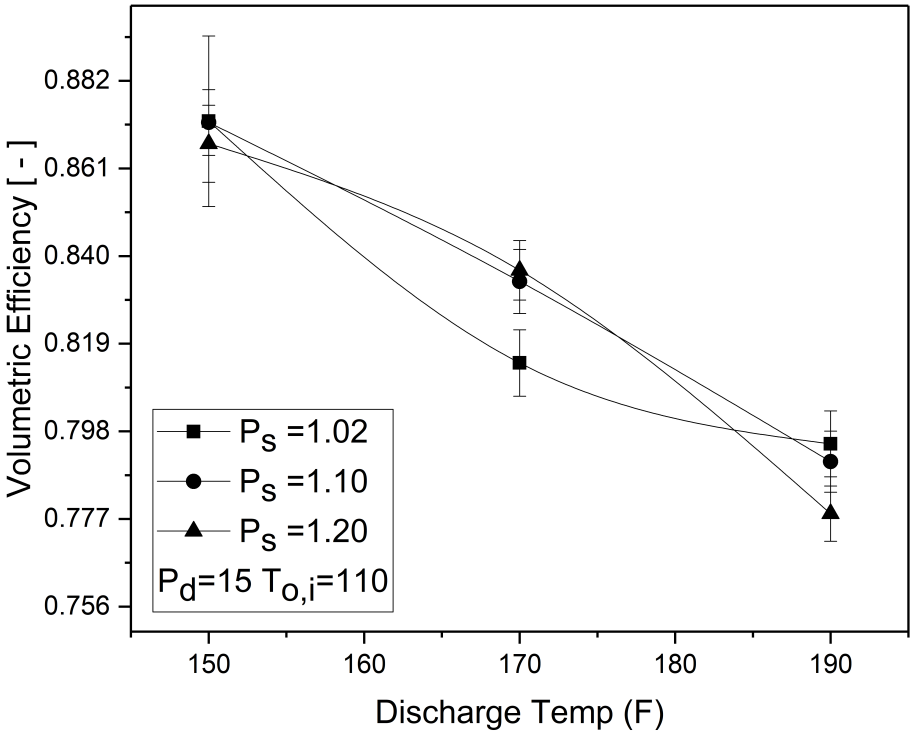

Figure 6.6: Discharge Temp vs. Volumetric Efficiency

6.4 Oil Injection Temperature Impact on Performance

The oil injection change has a small impact on the performance of the compressor. Figs. 6.7 and 6.8 suggest that as the oil temperature increases, the efficiencies increases then decreases. This shows that the oil has an optimum inlet temperature for given conditions, and the compressor can obtain peak performance when the oil injection temperature is optimized for each condition. As oil injection temperature increases, the discharge temperature also increase. The change in isothermal efficiency is caused by the rise in discharge temperature. Oil injection temperature is limited by viscosity and drag forces.

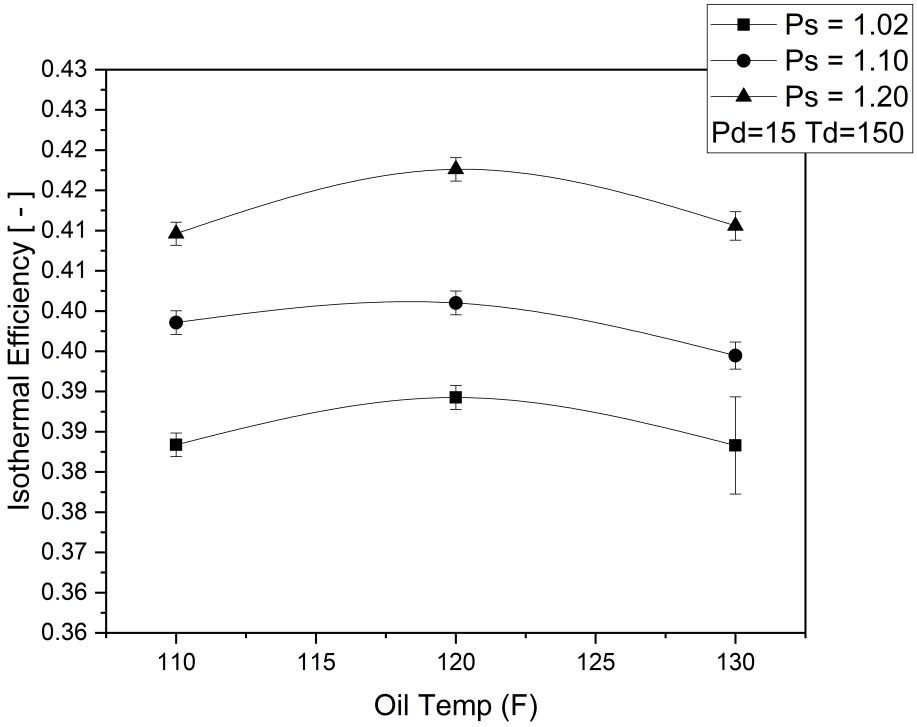

Figure 6.7: Oil injection temp vs. Isothermal Efficiency

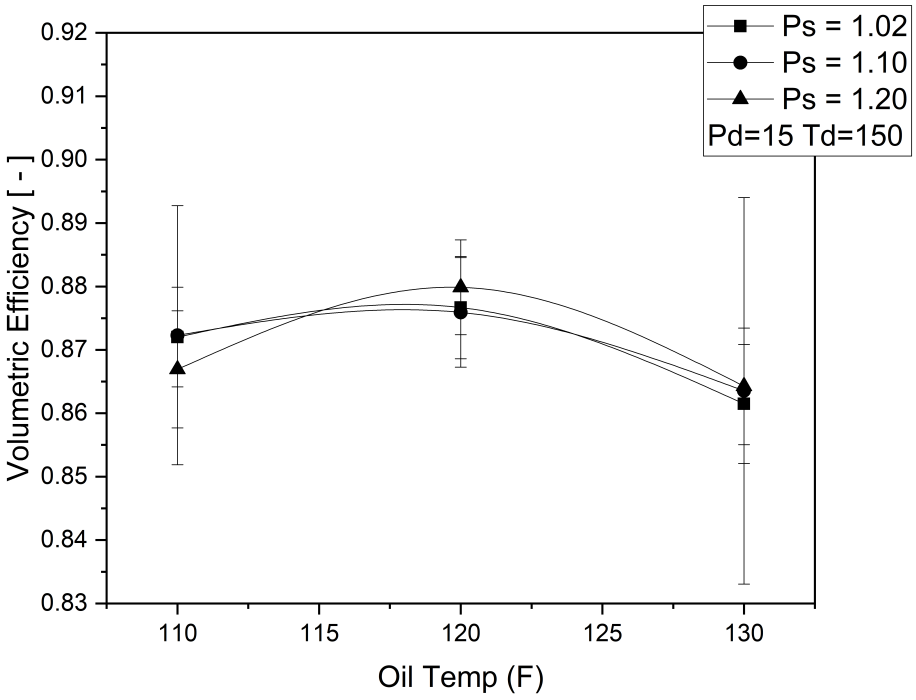

Figure 6.8: Oil injection temp vs. Volumetric Efficiency

6.4.1 Calculations

In order to verify that the collected measurements make sense, the cross-check equations presented in Chapter 5 are used. Here, an example calculating the discharge temperature and oil mass flow theoretical values are shown.

Table 6.1: Example Point

Name	**Value**	**Units**
Suction Pressure	1.02	Bar
Discharge Pressure	14	Bar
Discharge Temperature	150	F
Oil Inlet Temperature	110	F

Discharge Temperature:

$$T_{hd,calc} = \frac{\dot{W}' + \dot{m}'_h C_{p,h} + \dot{m}_o{}' C_{p,o} T'_{o,i}}{\dot{m}'_h C_{p,h} + \dot{m}_o{}' C_{p,o} T'_{o,i}} = 352.67K \tag{6.1}$$

where,

C_p	Specific heat
$\dot{m}$	Mass
T	Temperature
$\dot{W}$	Work
Subscripts	
d	Discharge
calc	Calculated Value
h	Helium
i	Injected
measured	Measured value
o	Oil
s	Suction
Denotation	
$'$	Measured value

$$T_{hd,measured} = 336.75K \tag{6.2}$$

$$T_{hd}\%difference = |\frac{T_{2,measured}}{T_{2,calc}} - 1| = 4.51\% \tag{6.3}$$

Oil Flow Mass Rate:

$$\dot{m}_{o,calc} = \frac{\dot{W}' - \dot{m}'_h C_{p,h}(T'_{h,d} - T'_{h,s})}{C_{p,h}(T'_{o,d} - T'_{o,i})} = 1586.64g/s \tag{6.4}$$

$$\dot{m}_{o,measured} = 954.40g/s \tag{6.5}$$

$$\dot{m}_o\%difference = |\frac{\dot{m}_{o,measured}}{\dot{m}_{o,calc}} - 1| = 38.85\% \tag{6.6}$$

Energy Balance:

$$\dot{W}_{calc} = \dot{m}'_h C_{p,h}(T'_{h,d} - T'_{h,s}) + \dot{m}'_o C_{p,o}(T'_{o,d} - T'_{o,i}) = 58.55kW \tag{6.7}$$

$$\dot{W}_{measured} = 94.78kW \tag{6.8}$$

$$\dot{W}\%difference = |\frac{\dot{W}_{measured}}{\dot{W}_{calc}} - 1| = 38.22\% \tag{6.9}$$

Isothermal Efficiency:

$$\dot{W}_{iso} = \dot{m}'_h \phi C_{p,h} T'_{h,s} ln(p_r) = 30.28kW \tag{6.10}$$

$$p_r = \frac{p'_{h,d}}{p'_{h,s}} = 13.65 \tag{6.11}$$

$$\eta_T = \frac{\dot{W}_{iso}}{\dot{W}_{actual}} = 0.39\% \tag{6.12}$$

Volumetric Efficiency

$$\dot{m}_{theo} = \frac{\rho V_c N}{60} = 21.45g/s \tag{6.13}$$

$$\eta_{vol} = \frac{\dot{m}'_h}{\dot{m}_{theo}} = 0.88 \tag{6.14}$$

where, $\dot{W}_{iso}$ is the isothermal work, ϕ is the ratio of specific heats, η_T is the isothermal efficiency and η_{vol} is the volumetric efficiency. From this cross-check example, it is seen that the difference between the theoretical and measured for the discharge temperature, oil mass flow rate, and work is 4.51%, 38.85%, and 38.22% respectively. A difference of a few percent is reasonable; however, 38.22% energy balance difference provides justification for further investigation. The theoretical calculations are determined using the energy balance equation with measured values as inputs. The theoretical work and work measured should be reasonably close. An analysis has been completed to understand the reason for major difference calculated. The first observation would be to understand the assumptions made in the energy balance and their contributions to the overall result. Adopted energy balance assumptions are equal discharge temperature for oil and helium and no helium is dissolved in oil.

Helium Superheat

At the discharge of the compressor, it is possible for the measured discharge temperature of helium to vary from the bulk helium temperature. This is caused by heat transfer losses through the pipe and oil film. At discharge, the fluid is primarily helium with oil assumed to coat the pipe walls. Therefore the helium temperature could be hotter than the measured helium and oil temperatures. The discharge temperature is measured on the outside of the pipe. Adding a superheat of 50 to the measured superheat only reduces the measured vs. theoretical energy balance by 2%. This shows that the superheat amount does not have a strong impact on the energy balance error.

Helium solubility

In an oil-flooded screw compressor it is common for solubility issues to occur due to the vigorous gas and oil mixing that some of the gas would be dissolved in the oil. The amount of gas dissolved in oil is highly dependent on the components within the mixture as well as the gas temperature. The cooler the working fluid is, the more likely it is for solubility to occur [73]. Within the scope of the study, the exact amount of helium dissolved in the oil is unknown. To gauge the impact of solubility on the calculated energy balance, an assumption of 90% will be applied, although this is highly unlikely. At 90%, the calculated energy balance would reduce by 1.8% and the overall energy balance difference would reduce by roughly 2.6%. This shows that the solubility factor is not the main contributor to the percent difference found. Evaluating the assumptions used in the energy balance equation leaves us with further questions on where the difference in measured and calculated results may be found. What factors are impacting the calculated work? To further understand this, the power factor and specific heat of oil impact will be evaluated.

Power Factor

During initial testing, the power factor was assumed from data provided by the manufacturer. To determine the accuracy of these data, repeat testing was conducted with a power analyzer installed on the skid that provided a power factor measurement. It was shown that the measured power factor was significantly lower than the value provided from the manufacturer. When re-calculating the work for repeat testing (using the power meter), the energy balance difference value reduced

greatly to 14%. This brings the calculated and measured work closer by a substantial amount however a large difference still remains.This leads us to the last point of evaluation, oil specific heat. The specific heat varied slightly in the calculation to understand the impact it has on the overall energy balance calculation. It is seen that a slight increase reduces the difference significantly. For example, when the specific heat increases by 20%, the difference decreases by roughly 11.5%. An oil sample should be taken to confirm if the specific heat is a key contributing factor in the energy balance difference. Furthermore, it is assumed that the the error in the energy balance difference is a culmination of several things. Combining each of these assumptions together would reduce the overall difference in the energy balance to 0.15%.

6.5 Uncertainty Analysis for each Performance

An uncertainty analysis on volumetric and isothermal efficiencies are completed using the measured variables. Human error, instrumentation, environmental conditions, and fluid property calculation all contribute to uncertainty within the experimental system. Several variables are used within the performance calculations. Each measurement has an amount of uncertainty associated with it. The total uncertainty impact the variable has on the volumetric and isothermal efficiencies are calculated. Table 6.2 list the variables, measured values for one test point, absolute and relative uncertainty values.

Flow rate of helium was measured using a Coriolis meter. The meter was calibrated for helium at zero flow. The suction temperature was measured using a handheld temperature probe. Each variable that has an impact on the performance calculation's absolute uncertainty has been implemented and the total uncertainty for volumetric and isothermal efficiencies are calculated.

Table 6.2: Uncertainty

Variable	**Measured value**	**Absolute Uncertainty**	**Relative Uncertainty**
Helium mass flow rate (g/s)	18.75	0.01	0.1%
Suction Temperature (K)	296.95	0.1	0.0%
Suction Pressure (bar)	1.02	0.01	1.0%
Discharge Pressure (bar)	14.03	0.01	0.1%
Input work (W)	75544.42	0.01	0.0%

Measurement of uncertainty

The overall uncertainty and impact that each measurement has on the uncertainty is evaluated using volumetric and isothermal efficiency equations. Illustrating the process:

Calculate all values with added absolute uncertainty

$$\sigma_m = m + \delta m \tag{6.15}$$

$$\sigma_{T_{hs}} = T_{h,s} + \delta T_{h,s} \tag{6.16}$$

$$\sigma_{P_s} = P_s + \delta P_s \tag{6.17}$$

$$\sigma_{P_d} = P_d + \delta P_d \tag{6.18}$$

$$\sigma_W = W + \delta W \tag{6.19}$$

Calculate efficiency at each altered point while holding all other inputs to be unaffected. This should be done one at a time. This will be shown in Eqs. (6.20) to (6.24) using the isothermal efficiency. The same approach is applied to the volumetric efficiency.

$$\sigma_{W_{iso,m}} = \frac{\sigma_m \phi T_{h,s} ln(\frac{p_d}{p_s})}{W} \tag{6.20}$$

$$\sigma_{W_{iso,T}} = \frac{m\phi\sigma_{T_{h,s}} ln(p_r)}{W} \tag{6.21}$$

$$\sigma_{W_{iso,p_d}} = \frac{m\phi T_{h,s} ln(\frac{\sigma_{p_d}}{p_s})}{W} \tag{6.22}$$

$$\sigma_{W_{iso,p_s}} = \frac{m\phi T_{h,s} ln(\frac{p_d}{\sigma p_s})}{W} \tag{6.23}$$

$$\sigma_{W_{iso,W}} = \frac{m\phi T_{h,s} ln(\frac{p_d}{p_s})}{\sigma W} \tag{6.24}$$

Where, σ is the uncertainty. Calculate the difference of the original efficiency and adjusted efficiency then square the difference. The original efficiency is known as the term calculated without taking the uncertainty into account. This determines the amount of uncertainty that the particular adjusted input has on the total output.

$$U_m = (W_{iso} - \sigma_{W_{iso,m}})^2 \tag{6.25}$$

$$U_{T_{h,s}} = (W_t - \sigma_{W_{iso,T}})^2 \tag{6.26}$$

$$U_{p_2} = (W_{iso} - \sigma_{W_{iso,p_d}})^2 \tag{6.27}$$

$$U_{p_1} = (W_{iso} - \sigma_{W_{iso,p_s}})^2 \tag{6.28}$$

$$U_W = (W_{iso} - \sigma_{W_{iso,W}})^2 \tag{6.29}$$

Sum each uncertainty and take the square root to calculate the total uncertainty for the volumetric of isothermal efficiency.

$$U_{\eta_{iso}} = \sqrt{U_m + U_{T_{h,s}} + U_{p_d} + U_{p_s} + U_W} \tag{6.30}$$

The outlined procedure produces the total amount of uncertainty with the isothermal efficiency calculation. The same steps are applied to the volumetric efficiency calculation and a total uncertainty for this individual test point is 0.39% and 0.99% for the isothermal and volumetric efficiencies

respectively. Is it shown through this analysis that the helium flow rate has the largest impact on uncertainty.

CHAPTER 7

CONCLUSION

Oil flooded screw compressors are widely used in many applications such as refrigeration and cryogenics. Although there has been much progress in industry, the information is limited within helium refrigeration. The compressor is the heart of the cryogenic process, while also demanding the most energy within the cycle. Therefore, understanding ways to reduce energy demand is important. In this thesis, the screw compressor has been selected for evaluation, a numerical model has been designed and validated using experimental analysis, and thermodynamic parameters that influence the performance have been observed using helium as a working fluid. The numerical model takes into account two leakage path losses: blowhole and contact line. The thermodynamic state of helium and oil is predicted as a function of male rotation angle and the performance characteristics are produced. The model has been compared with commercial software SCORG and test data with acceptable agreement.

Drawn conclusions of this work in entirety:

- A program was created to generate the necessary geometric characteristics for a 5+6 rotor profile. Each geometric curve that is used within performance prediction model is presented in this work. The geometries generated were used within a numerical model to determine the screw compressor performance at various operating conditions. Ideal-gas-law assumptions were used for simplification of the model. The numerical model takes into account two leakage path losses: blowhole and contact line.

  Parameters such as suction pressure, discharge pressure, suction temperature, oil inlet temperature, oil injection location, and oil mass flow rate can be varied within the model. The thermodynamic simulation can determine mass flow rates through suction, discharge, and leakage paths as well as the thermodynamic states of helium and oil is predicted as a function of male rotation angle. The performance is calculated using the outputs of the thermodynamic

simulation. The performance is characterized by the isothermal and volumetric efficiencies. The numerical model results have been validated against a commercial software SCORG with acceptable agreement. Using the model, the oil injection analysis determined:

  - Oil follows the gas temperature closely throughout the compression cycle and can be assumed to be in thermal equilibrium at discharge
  - The discharge temperature decreases as the oil mass flow rate increases
  - As the oil injection port moves closer to discharge, the temperature at discharge increases
  - As oil mass flow increases, the isothermal efficiency increases
  - Isothermal efficiency decreases as oil injection port gets closer to discharge
  - Oil injection parameters have a strong impact on the performance of the compressor

- A compressor test stand was used to understand how various thermodynamic parameters impact the performance of a screw compressor using helium as the working fluid. Adjusted parameters during testing were the suction pressure, discharge pressure, discharge temperature, and oil injection temperature. Conclusions drawn from testing are as follows:

  - Performance decreases with the increase in pressure ratio
  - As suction pressure increases, the volumetric and isothermal efficiencies increase
  - Increasing discharge temperature has a negative impact on the overall performance
  - Oil Injection temperature should be varied for various operating conditions to yield optimum performance
  - The power factor has a large influence on cross-check calculations

7.1 Future Work

This works builds on our understanding of compressors used within helium refrigeration. However, there is much more work that can be done. Future work suggestions are provided

- Develop a CFD model to understand oil and helium interaction better and how they influence the performance of the compressor
- Measure the oil and helium discharge temperature at discharge to confirm the thermal equilibrium data provided from 1-D models.
- Understand how the relationship of helium and oil behaves at different pressure and temperature conditions.
- Model all leakage paths to better predict performance. In this work, the numerical model only used two leakage paths.
- Model different injection nozzle flows. In this work, the numerical model assumed the oil entering the compressor is in the form of oil droplets.
- Incorporate oil volume work in order to better predict the performance. In this work, the oil volume work was neglected within the numerical model.
- Adopted real gas laws to obtain more accurate results within the numerical model. In this work, the ideal gas law was used.

APPENDICES

APPENDIX A

NUMERICAL MODEL FUNCTIONS

This appendix provides numerical code that was used in Ch. 4 to determine state values. Several functions and equations are found here.

```
%% Screw compressor geometry data
global m PS PD pd Axial_Suc Axial_dis Tsuc Toil_in w dmoi

THETA = AREAS(1,1:1080);
AREA1 = AREAS(4,1:1080)/10^6;
AREA2=AREAS(10,1:1080)/10^6;
AREA7=AREAS(11,1:1080)/10^6;
AREA3=AREAS(12,1:1080)/10^6;
AREA4 = AREAS(6,1:1080)/10^6;
AREA5 = AREAS(3,1:1080)/10^6;
AREA6 = AREAS(9,1:1080)/10^6;
Vol = AREAS(2,1:1080)/10^9; %m^3
Axial_Suc = fit(THETA,AREA1,'linearinterp');
Axial_dis = fit(THETA,AREA4,'linearinterp');
Blowhole=fit(THETA,AREA2,'linearinterp');
Blowhole2=fit(THETA,AREA7,'linearinterp');
ContactLine=fit(THETA,AREA3,'linearinterp');
Oil_inj = fit(THETA,AREA6,'linearinterp');
Area_CS = fit(THETA,AREA5,'linearinterp'); %DV/dtheta
% DV=Area_CS;
V = fit(THETA,Vol,'linearinterp');
```

Figure A.1: Function for geometric curves

```
function dqdt=dqdt(Tgas,Toil,vel,n) %vel is the flow velocity

%%Inputs
% Tgas => Temperature of Gas
% Toil => Temperature of Oil
% vel => Oil Velocity
% n => Number of droplets
w = 3550;
w = w*2*pi;
%%Outputs
% Diameter or Particle
d=0.1; %mm
% Length of Rotors %mm
L=205.9;
% Absolute viscosity %g/mm-s
v=kviso(Toil)*(densityoil(Toil)*10^-6) ;
% Velocity
vel=vel*1000; %mm/s
% Thermal Conductivity %W/mm-K
k=thermalcond(Toil)/1000;
% Reynolds Number %unitless
Re=Reynoldsh(densityoil(Toil)*10^-6,vel,L,v) ;
% Reynolds Number %unitless
Rew=w*d^2;
% specific heat of oil %J/kg-K
Cv=2177;
% Prandtl Number %unitless
Pr=Prandtl(Cv,v,k);
% Nusselt Number %unitless
Nu=2+(0.6*Re^0.5)*(Pr^0.33);
% Heat Transfer Coefficient %W/mm^2-K
h=((Nu*k)/(d));
% h=7000;

% Particle Radius
r=d/2;%mm
% Area %mm^2
A=4*pi*r^2*n;
% Heat transfer %W[J/s]
dqdt=h*A*(Tgas-Toil);

end
```

Figure A.2: Heat transfer function

```
%% Solution function (Ideal)
function dydt = fODE(t,y)

global PS PD Axial_Suc Axial_dis dmoil_in_rate dmoil_out_rate pd

dydt = zeros(16,1);

dydt(1) = fdmg_in(t,PS-pd,y(11),Axial_Suc,y(3));
dydt(2) = fdmg_out(t,PD,y(11),Axial_dis,y(3));
dydt(3) = fdmgas(dydt(1),dydt(2));
dydt(4) = fdmoil_in(t,dmoil_in_rate);
dydt(5) = fdmoil_out(t,dmoil_out_rate);
dydt(6) = fdmoil(t,dmoil_in_rate,dmoil_out_rate);
dydt(7) = fdVoil(t,dydt(4),dydt(5),y(6));
dydt(8)= fdVg(t,dydt(7));
dydt(9)= fdQdt(t, y(10), y(12),y(6),y(11));
dydt(10) = fdTdt(t,y(10),y(11),dydt(1), dydt(2),dydt(8),y(3),y(12),dydt(9));
dydt(11) = fdPdt(t,y(10),y(11),dydt(3),dydt(8),y(3),dydt(10));
dydt(12) = fdToildt(t,y(12),y(6),dydt(4),dydt(5),dydt(9),y(11),dydt(7));
dydt(13)= fdUgdt(t, y(10),y(11),fdVgdt(t),dydt(9));
dydt(14) = specvol(t,y(3),y(11),y(10));
dydt(15) = fdmleak_in(t,PS,PS,y(3),PS);
dydt(16) = fdmleak_out(t,PS,y(3),PS);
end
```

Figure A.3: Numerical Model Layout

```
% This function calculates dm/dtheta
% d(m)/d(theta)=cl*rho*A*W/w
    %cl=flow coefficient
    %rho=density of flow
    %A=Area from geometric analysis
    %W=flow velocity
    %w=angular speed

function dmdt=dmdtheta(v,P1,P2,A,cl)

w=(3550*360)/60; %deg per sec

W=flowvelocity2(v,P1,P2); %velocity downstream

rho=1/v;

dmdt=(cl*rho*A*W)/w;% kg/deg

 end
```

Figure A.4: Mass flow function

```
%Flow velocity function
function W= flowvelocity2(v1,p1,p2) %pressure trail (p1(Pa)) , pressure lead (p2) ,specific vol (v(m^3/kg)),alpha

W1=sqrt(2*v1*abs(p2-p1)); %m/s

W2=sqrt(v1/(alpha(p2)));

if W1>W2
    W=W2;
else
    W=W1;
end
```

Figure A.5: Speed function

APPENDIX B

TEST DATA PLOTS

Experimental test data is included here for various runs to provide understanding of how helium performance changes with suction pressure, discharge temperature, and pressure ratio.

Suction Pressure

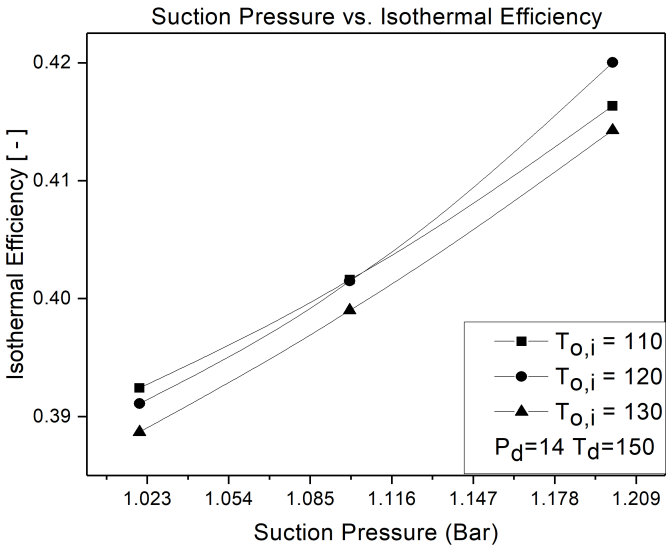

Figure B.1: Suction Pressure vs. Isothermal Efficiency (PD=14bar and TD=150K)

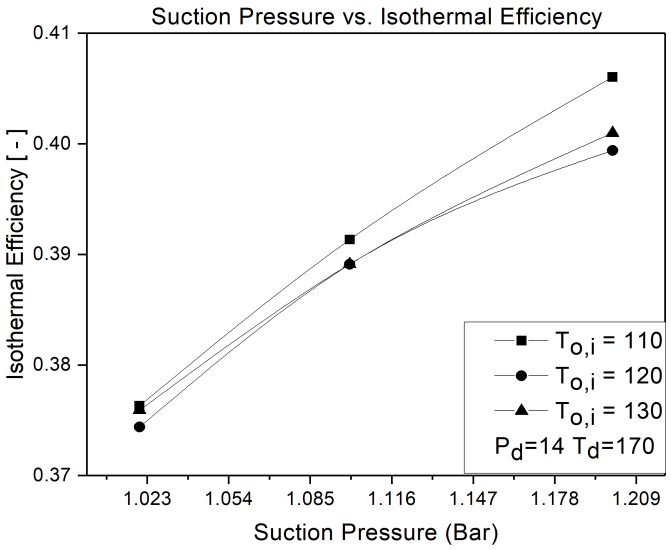

Figure B.2: Suction Pressure vs. Isothermal Efficiency (PD=14bar and TD=170K)

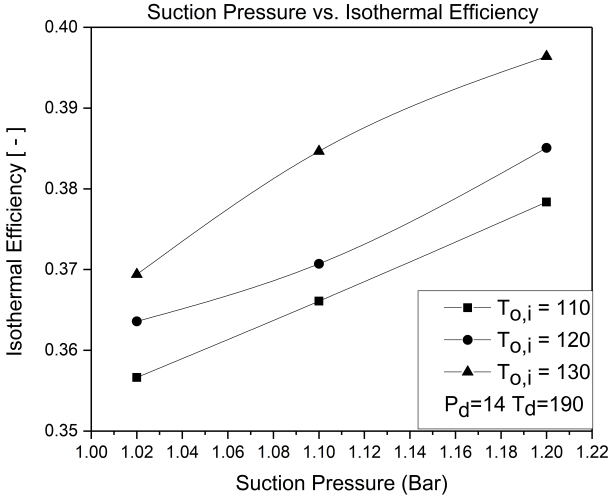

Figure B.3: Suction Pressure vs. Isothermal Efficiency (PD=14bar and TD=190K)

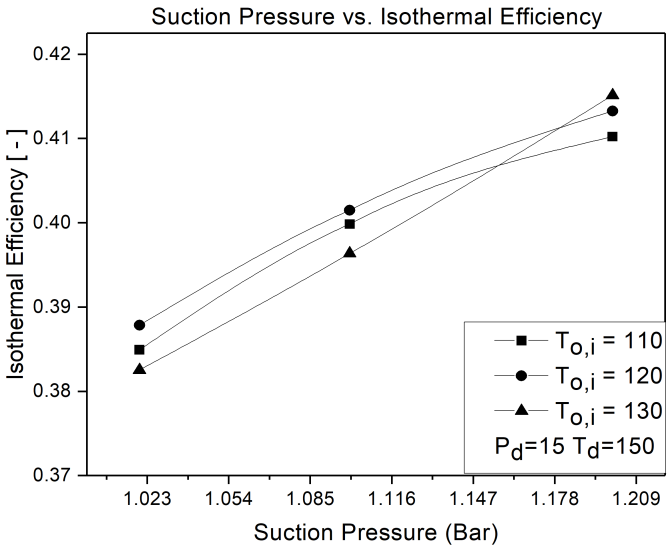

Figure B.4: Suction Pressure vs. Isothermal Efficiency (PD=15bar and TD=150K)

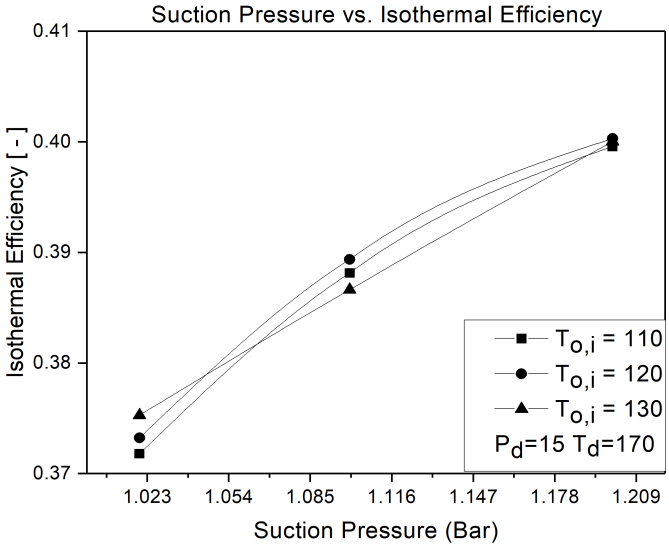

Figure B.5: Suction Pressure vs. Isothermal Efficiency (PD=15bar and TD=170K)

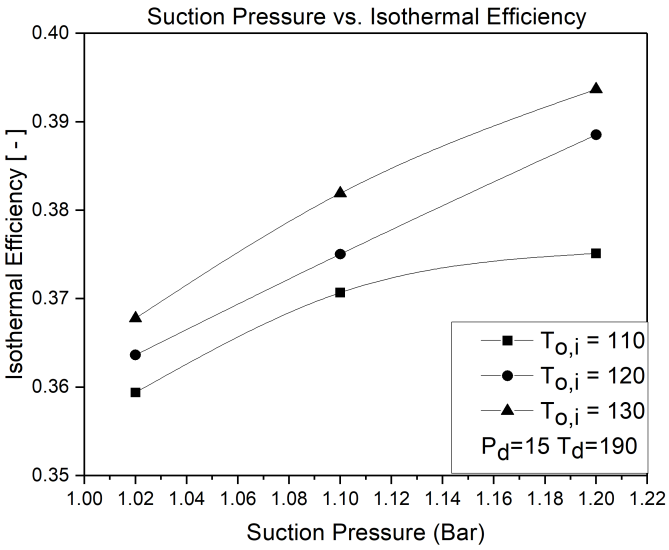

Figure B.6: Suction Pressure vs. Isothermal Efficiency (PD=15bar and TD=190K)

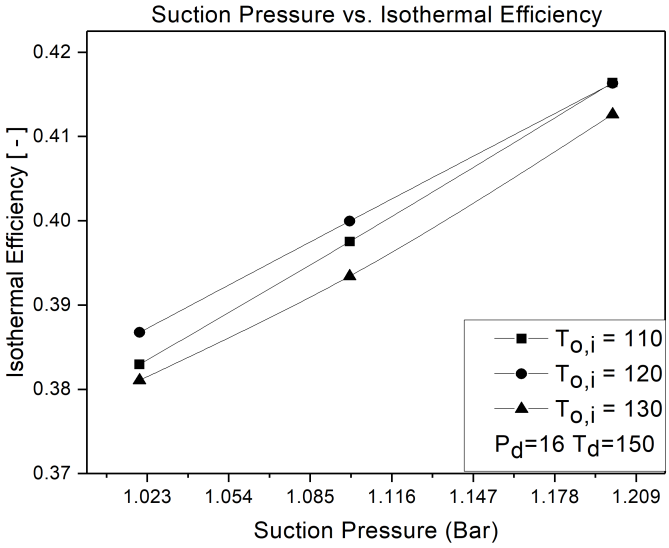

Figure B.7: Suction Pressure vs. Isothermal Efficiency (PD=16bar and TD=150K)

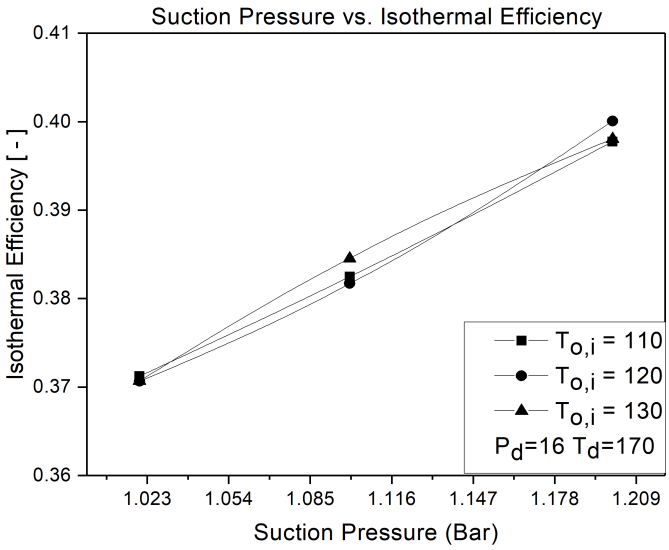

Figure B.8: Suction Pressure vs. Isothermal Efficiency (PD=16bar and TD=170K)

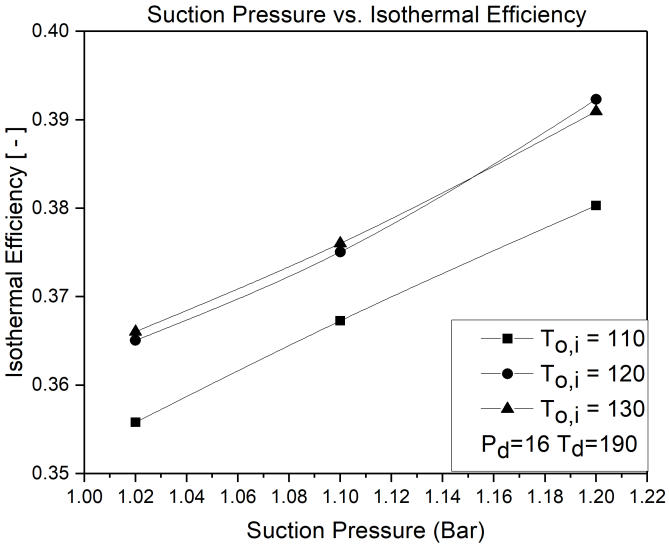

Figure B.9: Suction Pressure vs. Isothermal Efficiency (PD=16bar and TD=190K)

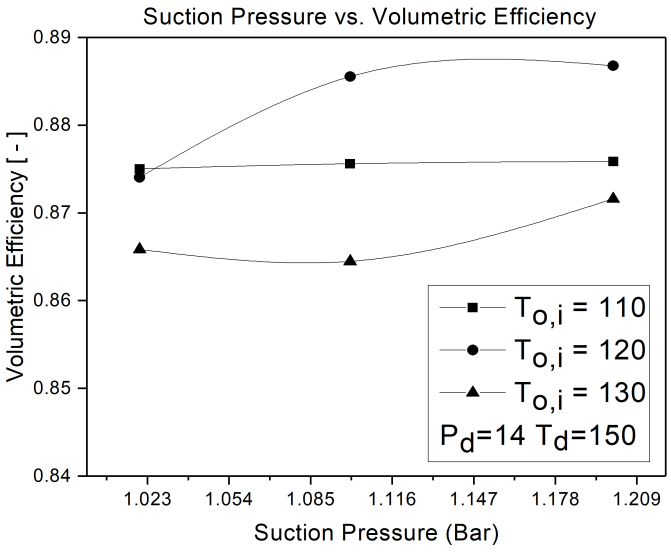

Figure B.10: Suction Pressure vs. Volumetric Efficiency (PD=14bar and TD=150K)

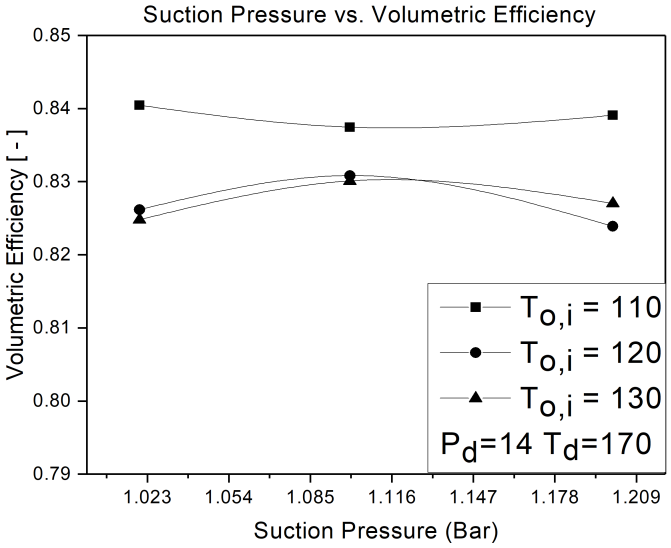

Figure B.11: Suction Pressure vs. Volumetric Efficiency (PD=14bar and TD=170K)

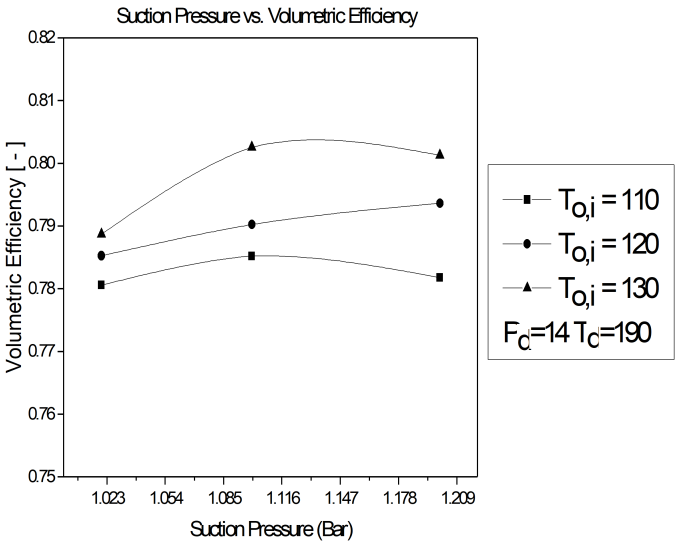

Figure B.12: Suction Pressure vs. Volumetric Efficiency (PD=14bar and TD=190K)

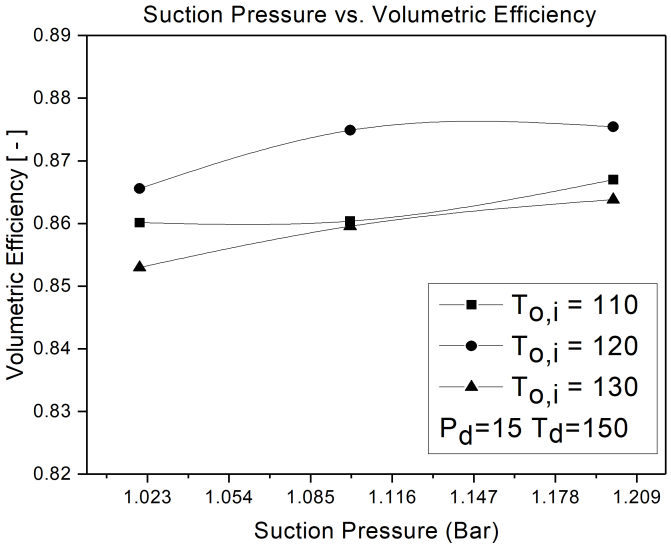

Figure B.13: Suction Pressure vs. Volumetric Efficiency (PD=15bar and TD=150K)

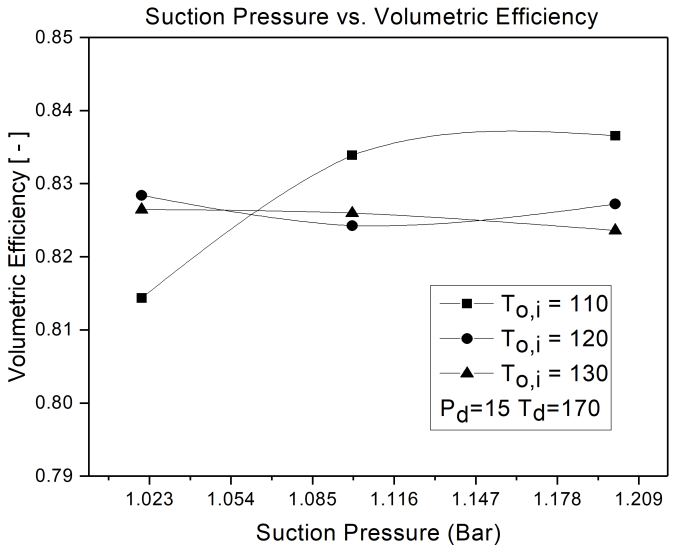

Figure B.14: Suction Pressure vs. Volumetric Efficiency (PD=15bar and TD=170K)

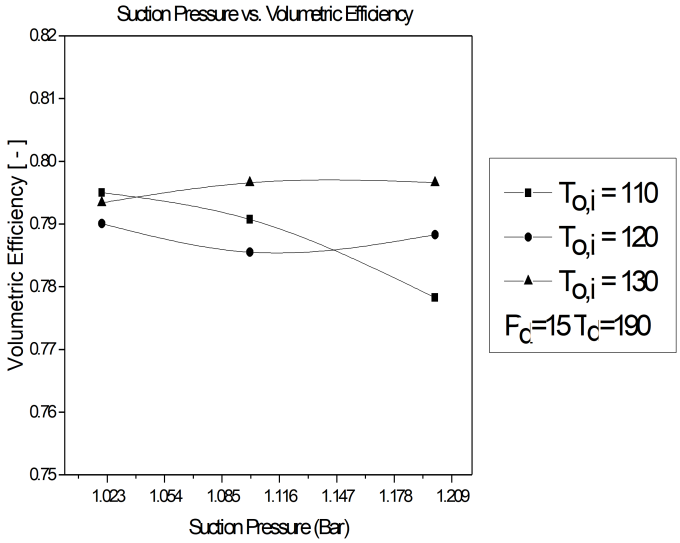

Figure B.15: Suction Pressure vs. Volumetric Efficiency (PD=15bar and TD=190K)

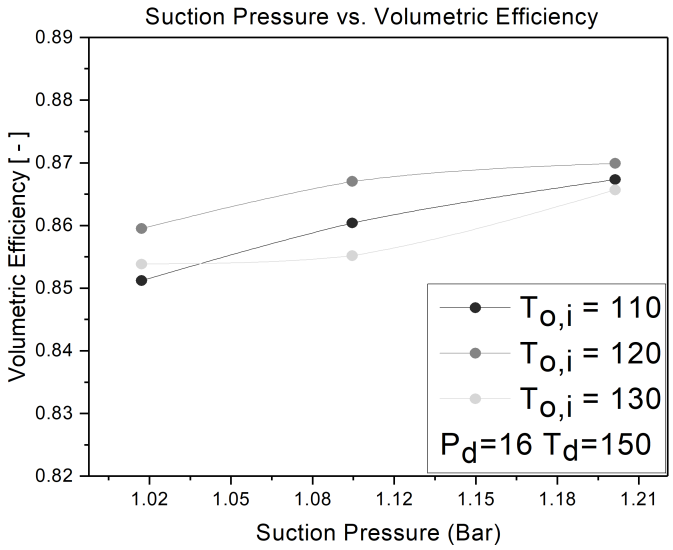

Figure B.16: Suction Pressure vs. Volumetric Efficiency (PD=16bar and TD=150K)

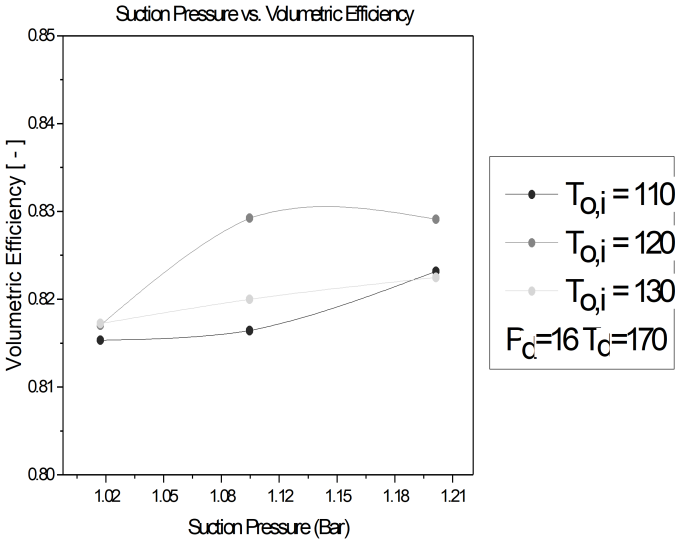

Figure B.17: Suction Pressure vs. Volumetric Efficiency (PD=16bar and TD=170K)

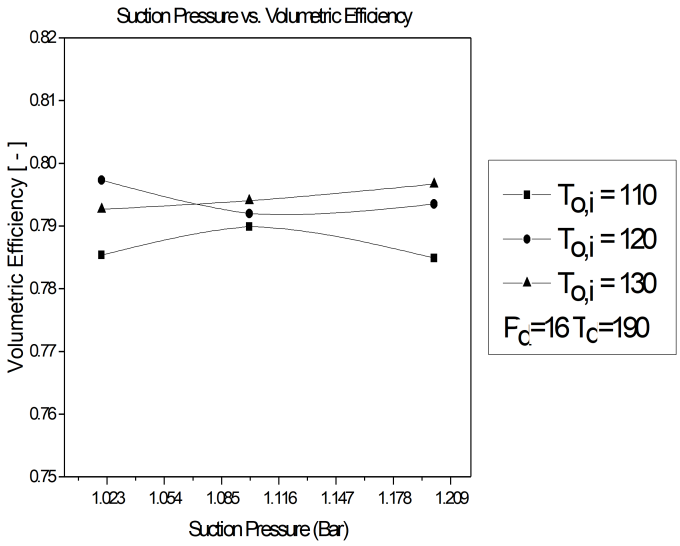

Figure B.18: Suction Pressure vs. Volumetric Efficiency (PD=16bar and TD=190K)

Pressure Ratio

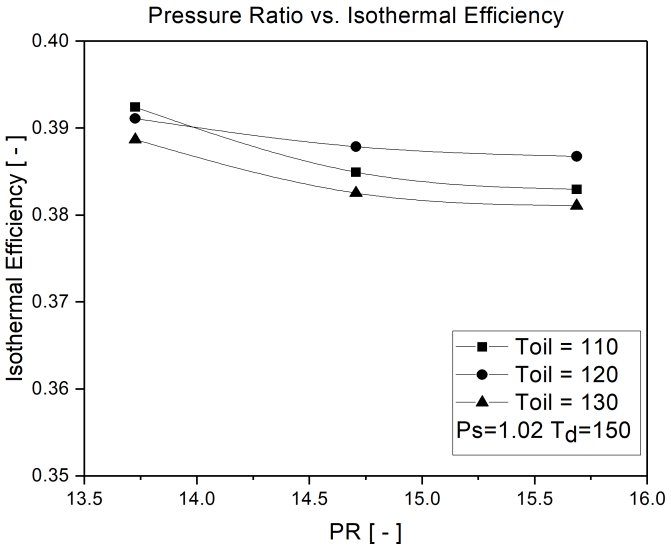

Figure B.19: Pressure Ratio vs. Isothermal Efficiency (Ps=1.02bar and TD=150K)

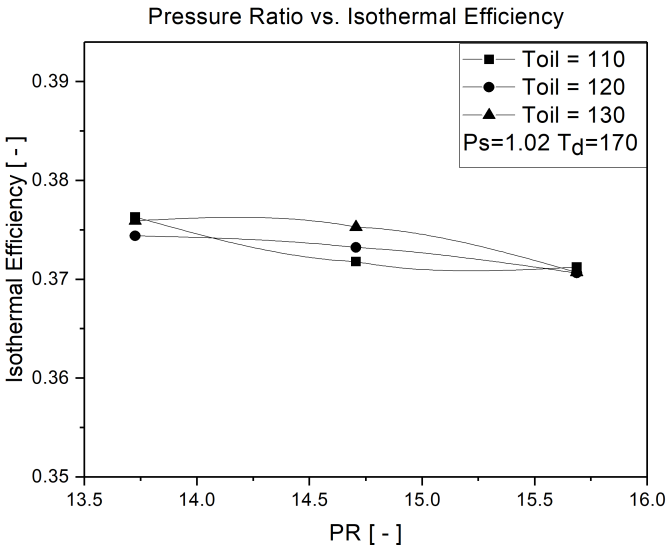

Figure B.20: Pressure Ratio vs. Isothermal Efficiency (Ps=1.02bar and TD=170K)

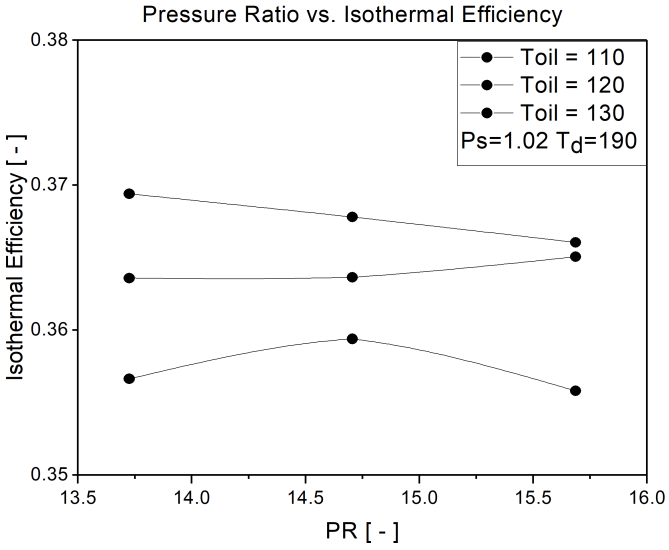

Figure B.21: Pressure Ratio vs. Isothermal Efficiency (Ps=1.02bar and TD=190K)

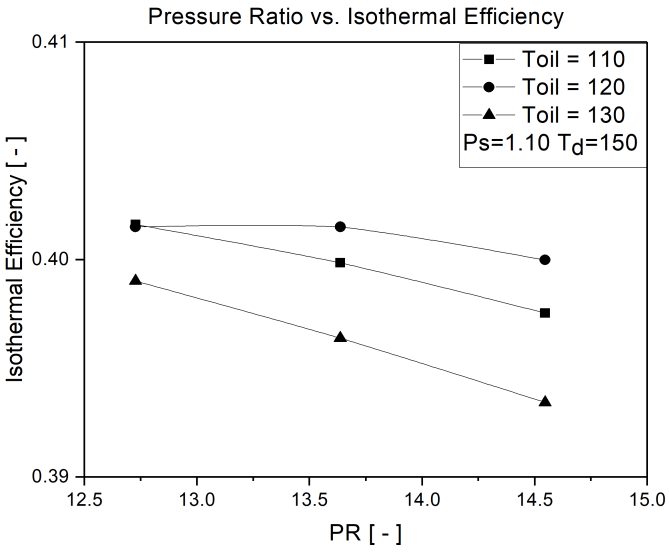

Figure B.22: Pressure Ratio vs. Isothermal Efficiency (Ps=1.1bar and TD=150K)

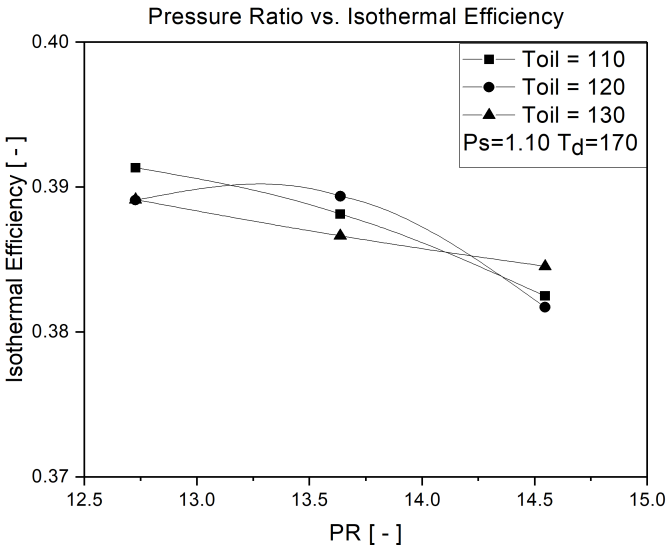

Figure B.23: Pressure Ratio vs. Isothermal Efficiency (Ps=1.bar and TD=170K)

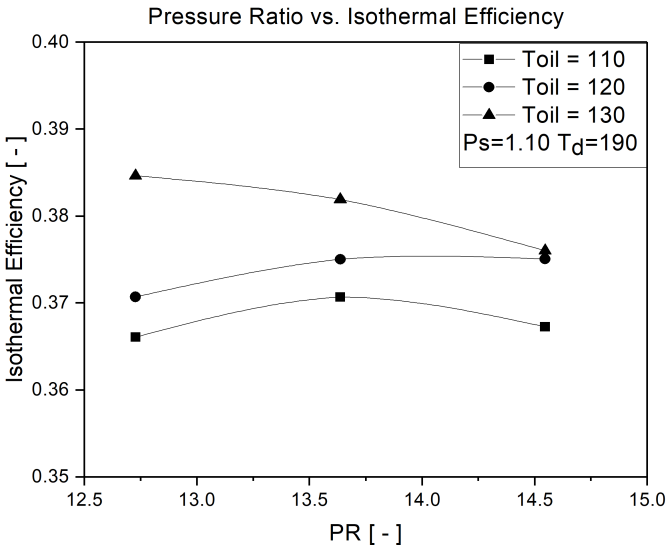

Figure B.24: Pressure Ratio vs. Isothermal Efficiency (Ps=1.1bar and TD=190K)

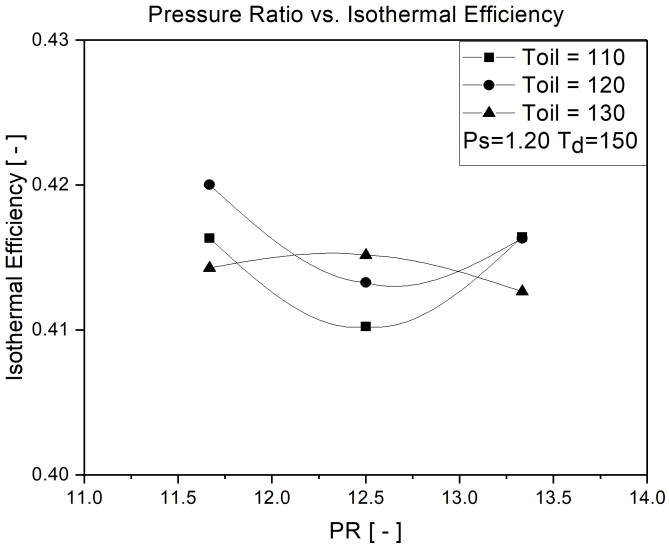

Figure B.25: Pressure Ratio vs. Isothermal Efficiency (Ps=1.2bar and TD=150K)

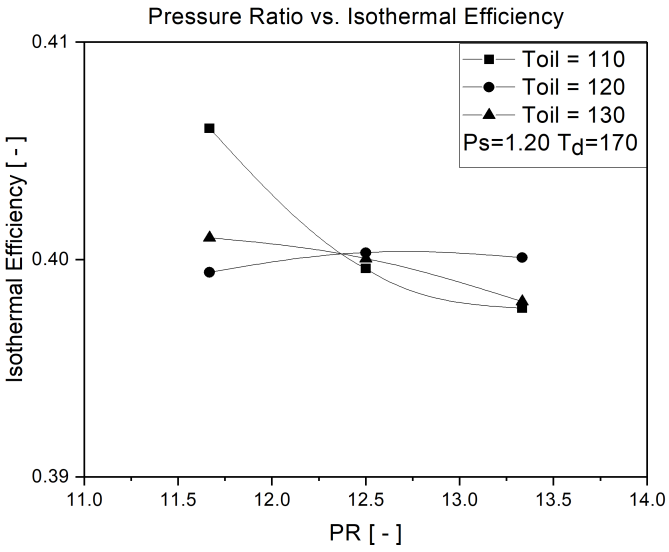

Figure B.26: Pressure Ratio vs. Isothermal Efficiency (Ps=1.2bar and TD=170K)

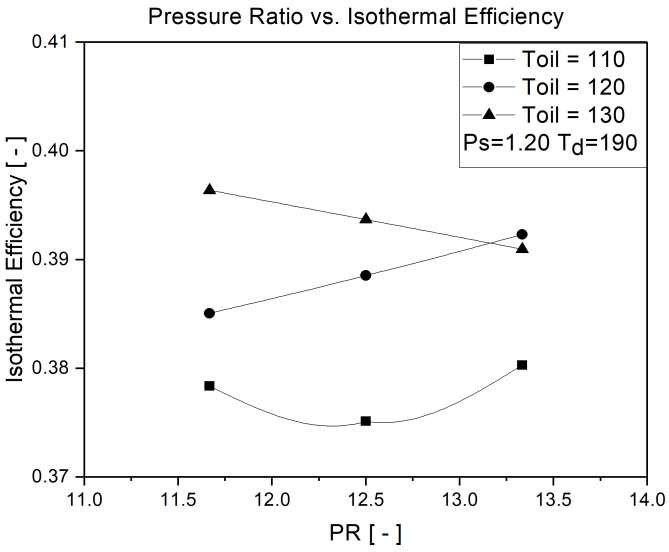

Figure B.27: Pressure Ratio vs. Isothermal Efficiency (Ps=1.2bar and TD=190K)

BIBLIOGRAPHY

BIBLIOGRAPHY

[1] P. Knudsen, V. Ganni, K. Dixon, R. Norton, and J. Creel, "Commissioning and operational results of the 12 gev helium compression system at jlab," *IOP Conference Series: Materials Science and Engineering*, vol. 101, pp. 1–7, 2015.

[2] T. Ohama, Y. Kurioka, H. Tanaka, and T. Koga, "Process gas applications where api 619 screw compressors general manager of sales," 2004.

[3] W. Toscano and L. Hoagland, "Thermodyn perf oil flooded helium screw compressors," pp. 749–759, 1977.

[4] P. Oneill, "Mech design and efficiency of screw compressors," 1966.

[5] J. T. Bruce, "Screw compressors: A comparison of applications and features to conventional types of machines," *GPA Annual Convention Proceedings*, 2000.

[6] N. Stosic, I. K. Smith, A. Kovacevic, and E. Mujic, "Review of mathematical models in performance calculation of screw compressors," *International Journal of Fluid Machinery and Systems*, vol. 4, pp. 271–288, 2011.

[7] U. Sjölin, "History - extended history - extended the history of srm," pp. 6–11, 2011.

[8] Nutz, "A piece of rotary screw history," 2010. [Online]. Available: http://www.airends.com/LysholmArticle.htm.

[9] L. Rinder, *scraubenverdichter*. Springer Verlag, 1979.

[10] V. Ganni, P. Knudsen, J. Creel, D. Arenius, F. Casagrande, and M. Howell, "Screw compressor characteristics for helium refrigeration systems," *AIP Conference Proceedings*, vol. 985, pp. 309–315, 2008.

[11] N. Seshaiah, R. K. Sahoo, and S. K. Sarangi, "Influence of working gas and oil injection rate on efficiency of oil injected twin screw air compressor."

[12] T. Kishi, W. Kudo, H. Iisaka, and N. Ino, "High efficiency high reliability oil injection type helium screw compressor," *Advances in Cryogenic engineering*, vol. 37, 1992.

[13] X. Wu, Z. Xing, Z. He, X. Wang, and W. Chen, "Effects of lubricating oil on the performance of a semi-hermetic twin screw refrigeration compressor," *Applied Thermal Engineering*, vol. 112, pp. 340–351, 2017.

[14] Z. He, T. Wang, X. Wang, X. Peng, and Z. Xing, "Experimental investigation into the effect of oil injection on the performance of a variable speed twin-screw compressor," *Energies*, vol. 11, no. 6, p. 1342, 2018.

[15] N. Stosic, A. Kovacevic, K. Hanjalic, and L. Milutinovic, "Mathematical modelling of the oil influence upon the working cycle of screw compressors," *International Compressor Engineering Conference*, 1988. [Online]. Available: http://docs.lib.purdue.edu/cgi/viewcontent.cgi?article=1644\&context=icec.

[16] K. Hammer, M. Knittl-frank, and L. Rinder, "Modifications in the design of the oil-injection system for screw compressors," *International Compressor Engineering Conference*, pp. 987–994, 2000.

[17] J. Fleming, "Twin helical screw compressor part 2: a mathematical model of the working process," 1998.

[18] N. Stosic and K. Hanjalic, "General method for screw compressor profile generation," *International Compressor Engineering Conference, Purdue University USA, Paper 1099*, 1996.

[19] D. Zaytsev and C. A. Ferreira, "Profile generation method for twin screw compressor rotors based on the meshing line," *International Journal of Refrigeration*, vol. 28, pp. 744–755, 8 2005.

[20] D. Zaytsev and C. I. Ferreira, "Screw compressor rotors profile generation method based on pre-defined meshing line," in *Proceedings of the 3rd international compressor technique conference, August 15-18*. Xian Jiaotong University, 2001, pp. 117–127.

[21] L. Zhang, J. F. Hamilton, and J. F. Hamilton, "Main geometric characteristics of the twin screw compressor," *International Compressor Engineering Conference. Paper 835*, pp. 449–460, 1992.

[22] P. Singh and J. Bowman, "Heat transfer in oil-flooded screw compressors," *International Compressor Engineering Conference*, pp. 135–153, 1986. [Online]. Available: http://docs.lib.purdue.edu/cgi/viewcontent.cgi?article=1520\&context=icec.

[23] Y. Tang and J. S. Fleming, "Obtaining the optimum geometrical parameters of a refrigeration helical screw compressor," 1992.

[24] N. Stosic, "Optimization of screw compressor design," *International Compressor Engineering Conference School*, p. Paper 1592, 2002.

[25] C. X. You, Y. Tang, and J. Fleming, "Optimum rotor geometrical parameters in refrigeration helical twin screw compressors," *International Compressor Engineering Conference School*, 1996. [Online]. Available: http://docs.lib.purdue.edu/icec/1074.

[26] P. J. Singh and A. D. Onuschak, "Comprehensive, computerized method for twin-screw rotor profile generation and analysis." *Proceedings of the Purdue Compressor Technology Conference*, pp. 519–527, 1984.

[27] P. J. Singh and G. C. Patel, "A generalized performance computer program for oil flooded twin-screw compressors," 1984. [Online]. Available: http://docs.lib.purdue.edu/icec/504.

[28] M. Fujiwara, K. Kasuya, T. Matsunaga, and M. Watanabe, "A computer model for calculating screw compressor performance analysis of a rotary screw compressor." 1984.

[29] T. Bruce, "Screw compressors : Misconception or reality."

[30] Z. Zhou, "Computer aided design of a twin rotor screw refrigerant compressor," 1992.

[31] Z. Xing, X. Peng, and P. Shu, "Development and application of a software package for the design of twin screw compressors," 2000.

[32] J. Sauls, "Development of a comprehensive thermodynamic modeling system for refrigerant screw compressors," 1996.

[33] ——, "Application of manufacturing simulation for screw compressor rotors," 2000.

[34] N. Stosic, A. Kovacevic, and I. Smith, "Modelling of screw compressor capacity control," 1998.

[35] P. J. Singh and J. L. Bowman, "Effect of design parameters on oil-flooded screw compressor performance," *International Compressor Engineering Conference*, pp. 71–88, 1986.

[36] N. Sto, L. Milutinovi, K. Hanjali, and A. Kova, "Investigation of the influence of oil injection upon the screw compressor working process * l tude de l ' influence de l ' injection d ' huile sur le fonctionnement d ' un compresseur / t vis," 1991.

[37] X. Peng, Z. Xing, X. Zhang, T. Cui, and P. Shu, "Experimental study of oil injection and its effect on performance of twin screw compressors," 2000.

[38] N. Stosic, L. Milutinovic, K. Hanjalic, and A. Kovacevic, "Experimental investigation of the influence of oil injection upon the screw compressor working process." [Online]. Available: http://docs.lib.purdue.edu/icec/687.

[39] N. Stošic, L. Milutinović, K. Hanjalić, and A. Kovačević, "Investigation of the influence of oil injection upon the screw compressor working process," *International Journal of Refrigeration*, vol. 15, pp. 206–220, 1992.

[40] M. Fujiwara and Y. Osada, "Performance analysis of an oil-injected screw compressor and its application," *International Journal of Refrigeration*, vol. 18, pp. 220–227, 1995.

[41] M. D. Paepe, W. Bogaert, and D. Mertens, "Cooling of oil injected screw compressors by oil atomisation," *Applied Thermal Engineering*, vol. 25, pp. 2764–2779, 2005.

[42] J. Fleming, Y. Tang, and G. Cook, "Twin helical screw compressor - part 1: development, appliations and competitive position," 1998.

[43] J. S. Fleming and Y. Tang, "The analysis of leakage in a twin screw compressor and its application to performance improvement," *Proceedings of the Institution of Mechanical Engineers, Part E: Journal of Process Mechanical Engineering*, vol. 209, pp. 125–136, 1995.

[44] Y. Tang, "Computer aided design of twin screw compressors," p. 287, 1995.

[45] N. Stosic, I. K. Smith, A. Kovacevic, and E. Mujic, "Geometry of screw compressor rotors and their tools," *Journal of Zhejiang University: Science A*, vol. 12, pp. 310–326, 2011.

[46] D. L. Margolis, "Analytical modeling of helical screw turbines for performance prediction," 1978. [Online]. Available: http://www.asme.org/about-asme/terms-of-use.

[47] F. L. Litvin, "Theory of gearing," 1989. [Online]. Available: https://ntrs.nasa.gov/search.jsp?R=19900010277.

[48] L. Rinder, *Schraubenverdichter*. Springer-Verlag, 2013.

[49] I. K. Ahmed Stosic, Nikola; Smith, *Screw Compressors - Mathematical Modeling and Performance Calculation*. Springer, 2017, vol. 8.

[50] N. Stosic and K. Hanjalic, "Development and optimization of screw machines with a simulation model—part i: Profile generation," 1997.

[51] Y. R. Wu and Z. H. Fong, "Optimization design of an explicitly defined rack for the generation of rotors for twin-screw compressors," *Mechanism and Machine Theory*, vol. 44, pp. 66–82, 1 2009.

[52] D. Zaytsev, "Development of wet compressor for application in compression-resorption heat pumps.pdf," 2003.

[53] P. J. Singh and J. R. Schwartz, "Exact analytical representation of screw compressor rotor geometry," pp. 925–937, 1988. [Online]. Available: https://pdfs.semanticscholar.org/95e2/110c9232b01c04994878bcd829ecffa984cc.pdf.

[54] Y. Tang, "Computer aided design of twin screw compressors," p. 287, 1995.

[55] C. X. You, "A theoretical study of rotor forces and torques in helical twin screw compressors," Ph.D. dissertation, University of Strathclyde, 1994.

[56] W. W. Boblitt and J. Moore, "Computer modeling of single-screw oil flooded refrigerant compressors computer modeling of single-screw oil-flooded refrigerant compressors," 1984. [Online]. Available: https://docs.lib.purdue.edu/icec.

[57] B. Sangfors, "Computer simulation of the oil injected twin screw compressor," 1984. [Online]. Available: https://docs.lib.purdue.edu/icec.

[58] A. Kovacevic, N. Stosic, and I. K. Smith, "A numerical study of fluid solid interaction in screw compressors," *International Journal of Computer Applications in Technology*, vol. 21, no. 4, pp. 148 – 158, 2004.

[59] K. Ignatiev, Y. Tang, J. Fleming, and A. Tramschek, "Thermal interaction in a refrigeration twin screw compressor during the compression process," 1994.

[60] M. Fujiwara, H. Y. O. Hitachi, and M. Fujiwara, "Performance analysis of oil-injected screw compressors and its applications," 1990. [Online]. Available: https://docs.lib.purdue.edu/icec.

[61] D. Xiao, Z. Xiong, Y. Yu, and J. F. Hamilton, "The computer simulation of oil-flooded refrigeration twin-screw compressors," in *Proceedings of the Purdue Compressor Technology Conference, Purdue, USA*, vol. 1, 1986, pp. 349–361.

[62] K. Hanjalic and N. Stosic, "Development and optimization of screw machines with a simulation model—part ii: Thermodynamic performance simulation and design optimization," 1997.

[63] J.-G. Persson, "Heat-exchange in liquid-iniected screw-compressors," vol. 640, 1987.

[64] R. Mugele and H. Evans, "Droplet size distribution in sprays," *Industrial & Engineering Chemistry*, vol. 43, no. 6, pp. 1317–1324, 1951.

[65] W. E. Ranz, "Evaporation from drops : Part ii," *Chemical Engineering Progress*, vol. 48, pp. 173–180, 1952.

[66] J. Prins and C. I. Ferreira, "Feasibility and design of leakage experiments on a running twin screw compressor," in *ECOS 2000*, 2000, pp. 869–880.

[67] H. Taniguchi, K. Kudo, W. Giedt, I. Park, and S. Kumazawa, "Analytical and experimental investigation of two-phase flow screw expanders for power generation," 1988.

[68] N. Stosic, I. K. Smith, A. Kovacevic, and E. Mujic, "Review of mathematical models in performance calculation of screw compressors," *International Journal of Fluid Machinery and Systems*, vol. 4, no. 2, pp. 271–288, 2011.

[69] "Scorg, 2016. scorg, user manual, london: City university." [Online]. Available: https://pdmanalysis.co.uk/scorg/.

[70] N. Stosic, A. Kovacevic, K. Hanjalic, and L. Milutinovic, "Mathematical modelling of the oil influence upon the working cycle of screw compressors," *International Compressor Engineering Conference*, 1988. [Online]. Available: http://docs.lib.purdue.edu/cgi/viewcontent.cgi?article=1644&context=icec.

[71] N. Seshaiah, S. K. Ghosh, R. K. Sahoo, and S. K. Sarangi, "Mathematical modeling of the working cycle of oil injected rotary twin screw compressor," *Applied Thermal Engineering*, vol. 27, pp. 145–155, 2007.

[72] MATLAB, *version (R2020b)*. Natick, Massachusetts: The MathWorks Inc., 2020b.

[73] K. N. Marsh and M. E. Kandil, "Review of thermodynamic properties of refrigerants+ lubricant oils," *Fluid Phase Equilibria*, vol. 199, no. 1-2, pp. 319–334, 2002.